3-26-2004

Supramolecular Metal-Organic and Organic Materials

Elisabeth Rather
University of South Florida

Supramolecular Metal-Organic and Organic Materials

by

Elisabeth Rather

A dissertation submitted in partial fulfillment
of the requirements for the degree of
Doctor of Philosophy
Department of Chemistry
College of Arts and Sciences
University of South Florida

Major Professor: Michael J. Zaworotko, Ph.D
Julie P. Harmon, Ph.D
Gregory R. Baker, Ph.D
Anthony W. Coleman, Ph.D

Date of Approval:
March 26, 2004

Keywords: Supramolecular chemistry, crystal engineering, calixarene, metal-organic network, porosity

Dedication

To my mother and my father.

Acknowledgements

I wish to express my sincere appreciation, first and foremost, to my advisor Dr. Michael Zaworotko for his guidance and suggestions throughout the course of this work.

In addition, I would like to thank Dr. Anthony Coleman and his students, in particular Dr. Patrick Shahgaldian and Dr. Eric da Silva, for their collaboration to the work on calixarene compounds. Abuzar Kabir is gratefully acknowledged for his help with the GC experiments.

Finally, I would like to thank Dr. Julie Harmon and Dr. Gregory Baker, members of my supervisory committee, Dr. Victor Kravtsov and Dr. Dwight A. Sweigart, visiting professors at USF; Ashley Mullen, Patrick Healey, Joanna Bis, Jen Medlar, Dr. Jarka Miksovska and Dr. Vasan Kuduva for their helpful comments and encouragements.

I would like to extend my deep appreciation to all that has helped in this research. My sincerest wish is that everyone's hard work and collaboration goes on to help mankind. Thank you again for your support!

Table of Contents

List of Tables

List of Figures

Supramolecular Metal-Organic and Organic Materials

Elisabeth Rather

ABSTRACT

The rational design of functional solids based upon the development of strategies for controlling intermolecular interactions and structural arrangement of simple molecular building units, represents a salient feature in the context of supramolecular chemistry and crystal engineering. Consideration of chemical functionality, geometrical capability and knowledge of the interplay between two or more sets of supramolecular interactions specific of preselected chemical components will facilitate further extension of crystal engineering towards the construction of supramolecular materials possessing valuable properties.

Calixarenes represent excellent building blocks for the design of solid-state architectures, in particular calix-4-arenes crystallize easily and the introduction of a wide range of director functions is relatively simple. For example, amphiphilic and pseudo-amphiphilic calixarenes may be synthesized by selective functionalization at either face of the skeleton and a second functionality may then be introduced at the opposite face. Careful examination of the crystal packing of a series of calix-4-arene derivatives systematically modified with various alkyl chain lengths at the lower rim and selected

functional groups at the upper rim will be considered in the broader perspective of crystal engineering strategies and development of novel materials.

Metal-organic networks are typically based upon the cross-linking of transition metal-based nodes by "spacer" organic ligands. Since there is an inherent control over the chemical nature of the components of such metal-organic structures, it is possible to design infinite architectures that possess well-defined topologies and contain cavities suitable for incorporation of guest molecules. Investigation of metal-organic networks based upon rigid ligands possessing two types of coordination sites (nicotinate and dinicotinate) and conformationally labile ligands possessing saturated fragments (glutarate and adipate) will be addressed in the context of topological approaches to the design of multi-dimensional networks with particular emphasis upon their resulting properties.

Chapter 1

Introduction

1.1. Perspectives

1.1.1. Solid State Chemistry

"Order from Chaos"

K. Eric Drexler

The organization that takes place when, from a saturated solution, randomly moving molecules crystallize into an ordered pattern, involves a complex array of interactions that assemble these molecular entities into crystalline architectures. If the properties of such assemblies are inherently dependant upon the molecular composition of the solid material, they are also affected by the crystal structure and symmetry of the arrangement adopted by the components upon crystal growth. This feature had been discovered long before the first X-ray experiments when Abbé Haüy[1] observed that the cleavage, the property of a crystal to come apart between specific planes, is directly linked to the nature and arrangement of the building blocks in the crystal. Haüy's Law of Rational Indices, the building block law, has led to the essential concept that the knowledge of the symmetry of a crystal prefigures the knowledge of the symmetry of its properties.[2] The discovery of the X-ray in 1895 by W.C. Röntgen and the following

discovery of X-ray diffraction by Max von Laue in 1912 and its subsequent application by W.H. and W.L. Bragg to the determination of the crystal structure of mineral and inorganic substances have provided the means to unequivocally characterize the solid state.[3] The structural determination of crystalline substances has also been of importance for further investigation of the solid state and its properties. In antithetic instances, the highly orderly arrangement of the ionic constituents of inorganic solids results from strong forces, while weaker interactions are involved in the cohesion of crystals purely composed of organic molecules. In the context of natural or synthetic molecular compounds, crystal structure determination has primarily focused upon the identification of the molecular entities themselves; however, further analysis of the crystal packing, arrangement of these molecules within the crystalline lattice, has rapidly afforded precise data on the intermolecular interactions holding them within the regular three-dimensional architectures in which they crystallize.

Specific investigations on crystal nucleation processes, controlled growth and morphology during crystallization towards the generation of materials possessing properties related to the crystal properties constitute an important branch of modern solid state chemistry.[4-18] These approaches, generally inspired from the knowledge acquired from natural or biomineral solid state systems with the purpose of generating the corresponding properties in synthetic materials, have exemplified how a thorough understanding of the crystallization process may lead to the ability to prepare a variety of products with desirable properties. On the other hand, a separate field has been developed based upon principles delineated by major advances in crystallography and structural

determination, which have provided enhanced insight into how molecules interact and assemble within the solid state, with the goal to design materials directly at the molecular level.[19-25] In summary, the generation of synthetic solid state materials, which can afford unique optical, mechanical, magnetic or electronic properties or possess various polymorphs, represents an important aspect towards a wide variety of applications in material or pharmaceutical sciences. Owing to technological advances in both software and hardware, the characterization of these novel materials *via* crystallographic methods has become relatively straightforward and can afford the means to specifically study the arrangement of the molecular constituents and to understand how these building blocks are held together within the solid state.

1.1.2. The Cambridge Structural Database, CSD

The investigation of the solid state towards the generation of novel materials with useful properties can highly benefit from preceding examination of general and reliable trends developed by correlated relevant structures. In this perspective, the Cambridge Structural Database, CSD,[26] constitutes a powerful database possessing exploitable information such as crystal symmetry, atomic coordinates, molecular geometry, interatomic distances and angles, concerning the crystal structures reported in the literature of over 290,000 organic, inorganic, organometallic, coordination and bioorganic compounds, which have been characterized *via* X-ray or neutron diffraction (ConQuest Version 1.5 © CCDC 2002). Accordingly, valuable information can be easily obtained from statistical analysis of the wide range of available data.[27] In the context of the study of 3D arrangement of molecules within the solid state and how molecular

components are held together through intermolecular interactions, early reports from Pauling[28] and Bondi[29] based upon such statistical type of study, albeit they corresponded to the limited range of structural data available at that time, yet have provided results concerning the van der Waals distances that are still widely used. Later in the 1980's and 1990's, structural studies by means of statistical analysis using the CSD with respect to intermolecular interactions sustaining the crystal lattice underlying the molecular arrangement in organic solids have been performed by Desiraju[30-32] and Etter[33] and have afforded significant advances in the field of solid state chemistry and crystal design.

1.2. Supramolecular Chemistry

1.2.1. Scope and Context

"Supramolecular chemistry is the chemistry of the intermolecular bond, covering the structures and function of the entities formed by the association of two or more chemical species."

Jean-Marie Lehn

Supramolecular chemistry,[34,35] defined by Lehn as "*chemistry beyond the molecule*", is based on intermolecular interactions between molecules that form more complex organized assemblies.[23] The concepts delineated by this recent field of research have been initiated by the comprehensive work on inclusion compounds clathrates,[36-39] cyclophanes,[40] crown ethers[41] and cryptands[42] devoted to the generation of synthetic receptors, *hosts*, which can be seen as the artificial counterparts of the binding sites in biomolecules. Indeed, Nature has afforded a wide range of complex and sophisticated examples of self-assemblies based upon non-covalent intermolecular interactions. In a sense, self-organization constitutes the basis of most biological assemblies. Double

stranded DNA perfectly exemplifies this concept since this highly complex system is based upon hydrogen bonding between the two sets of nucleic bases of the complementary helices.[43,44] Countless further examples have also substantiated the importance of intermolecular interactions to sustain various biological systems: from protein folding governed by strong hydrogen bonds[45] to a range of other non-covalent interactions including the amphiphilic self-assemblies of membranes sustained by the hydrophobic effect upon the polymeric region of phospholipids.[46] These biochemical processes occurring at the molecular level have largely inspired chemists to create novel artificial systems,[5,47-54] which offer opportunities to impact areas as diverse as material sciences, physics and pharmaceuticals. Such approaches have consisted in using and applying the knowledge acquired from specific natural systems with the purpose of generating the corresponding properties in novel synthetic materials[55] and they have already lead to important innovations.[56,57]

In the context of supramolecular interactions, the underlying concept of molecular recognition between functional groups interacting *via* non-covalent interactions is particularly relevant towards the idea of exploiting encoded molecules that assemble in a defined manner in the same vein as the coupling of matching biological entities provides specific response in living systems. In this regard, Linus Pauling has early foreseen the importance of complementariness between the functional groups of molecular entities, which, by assembling *via* weak interactions such as hydrogen bonds, generate specific function as disclosed in his volume "The Nature of the Chemical Bond":

"Although the hydrogen bond is not strong it has great significance in determining the properties of substances. Because of its small bond energy and the small activation energy involved in its formation and rupture, the hydrogen bond is especially suited to play a part in reactions occurring at normal temperatures. It has been recognized that hydrogen bonds restrain protein molecules to their native configurations, and I believe that as the methods of structural chemistry are further applied to physiological problems it will be found that the significance of the hydrogen bond for physiology is greater than that of any other single structural feature."

Linus Pauling

That molecular recognition between complementary functions is crucial in the phenomenon of specific organization between molecules has been further conceptualized within the field of supramolecular chemistry and has revealed to possess great opportunities for new generations of chemists.

1.2.2. Supramolecular Interactions

A thorough knowledge of the array of non-covalent interactions that sustain supramolecular assemblies is critical in order to acquire an understanding of the essential mechanisms that govern the self-organization of molecular entities. In this respect, the significance of studying structural patterns *via* the use of extensive databases has already been mentioned. Judicious exploitation of this information can, in turn, afford the means to develop strategies for controlling the self-assembly of molecular components that possess preselected functional groups, which can engage in specific supramolecular interactions: coordination bonds, dipole-dipole interactions, hydrogen bonding, p-p stacking or van der Waals interactions. Table 1.1 presents a non-exhaustive comparative overview of these different types of non-covalent interactions.

Table1.1. Typical supramolecular interactions and their characteristics

Interaction type	Energy (kJ/mol)	Approximative distance range (Å)	Examples
Coordination bond M-L (with M = transition metal, L = electron donor organic ligand)	50-200	d(M-O,N) = 1.7 – 3.5 Variable, dependant on transition metal and donor element	Coordination polymers *cis*-platin
Dipole-Dipole	5-50	Variable	Acetone Nitro-derivatives
Hydrogen bond A···H-D (with A =acceptor, D = donor)	4-120	d(A···D) = 2.2 – 4.0	Carboxylic acid dimer Nucleic bases
p-p stacking	< 50	d(face-to-face) = 2.8 – 3.5 d(edge-to-face) = 2.9 – 3.8	Graphite Nucleic bases stacking
van der Waals	< 5	*ca*. sum of van der Waal radii	Inclusion compounds Saturated alkyl chains

Based upon the knowledge of the interplay between potential interactions in addition to the consideration of accurately selected functional groups within either a single molecular component or multiple complementary molecules, the supramolecular approach represents a method of choice to generate a novel class of functional materials.

1.2.3. Crystal Engineering

In the context of solid state chemistry, supramolecular science provides a successful approach to the self-assembly of simple molecular building blocks preselected for their complementary geometrical and binding capabilities and can directly lead to a wide variety of crystalline structures sustained by intermolecular interactions. In effect, crystal has been described as the *"supermolecule par excellence"*,[24,25] since its formation results from the cohesive arrangement of its constituents *via* more or less strong forces between these building units. Application of the principles delineated by supramolecular chemistry and molecular recognition has resulted in the rational design of crystalline architectures sustained by intermolecular interactions between complementary molecular

components. Accordingly, the field of *crystal engineering*,[19,58] which involves prediction and control of the architecture within crystalline structures, has recently emerged.[59-62] The corresponding strategies are potentially important for designing materials with specific features and chemists have only recently applied the concepts of supramolecular synthesis and crystal engineering to generate new classes of organic solids and coordination polymers with a remarkable degree of success in terms of design.[63-66] In addition, the modular aspect of these supramolecular assemblies provides a range of opportunities for the variation of the elemental components that can be judiciously selected for their potential applications.[67]

In summary, the rational design of organic solids and coordination compounds from building units that allow the introduction of specific functionalities may offer valuable information concerning the interplay between the range of potential interactions and the relative degree of control within the resulting supramolecular architectures. Systematic investigation towards determining the factors that might favor the generation of such self-assemblies is of high interest for further development of functionalized supramolecular materials. In this respect, the work presented herein concerns the development of novel supramolecular organic and metal-organic materials based upon organic macrocycles and coordination networks respectively. This study will provide design strategies that apply to both types of systems and an understanding of the essential mechanisms that control the generation of crystalline structures of these classes of compounds. Applications of these principles will delineate our approach towards the construction of organic architectures and metal-organic networks possessing valuable

properties.

1.3. Supramolecular Organic Materials

1.3.1. Scope and Context

Aiming to the construction of a class of crystalline compounds based upon organic building units that enable the incorporation of variable of functionalities towards a systematic evaluation of the factors controlling the formation of crystal structures, calixarene molecules constitute a particularly suitable starting material. Calixarenes are macrocycles resulting from the condensation, in basic conditions, of *para*-substituted phenol molecules and formaldehyde.[68] In particular, calix-4-arenes consist in four phenolic moieties bridged in a macrocyclic system by four methylene groups connecting the adjacent positions of the phenol groups. They generally adopt a cone-shaped conformation, where all aryl are *syn* to one another. Such characteristic has actually originated the term "*calixarene*" for their resemblance to the Greek vase "*calix crater*".[69] Calix-4-arene derivatives crystallize easily and their selective functionalization is relatively simple so they represent excellent building blocks for the generation of supramolecular solid-state architectures.[70] Figure 1.1 shows the potential for modularity of calix-4-arenes that may be selectively functionalized at the *para*-positions of each aryl moiety, the upper rim of the cone, while a second functional group may also be appended to the hydroxylate sites at the lower rim of calix-4-arene molecules.

Over a thousand of crystal structures containing calixarene molecules have been deposited in the CSD to date. For the most part, they involve calix-4-arenes derivatives

illustrating their general aptitude to crystallize. In this context, the systematic study of the arrangement adopted by this type of molecules within the solid state with respect to specified variables, substituents, conformation, etc., has been largely overlooked in the relevant literature; nonetheless such structural analyses[71,72] can provide valuable information concerning the supramolecular interactions that control the self-assembly of these systems in order to develop an understanding of the factors inherent in such supramolecular control, with the goal of ultimately affording the means to generate materials with required properties for practical applications.

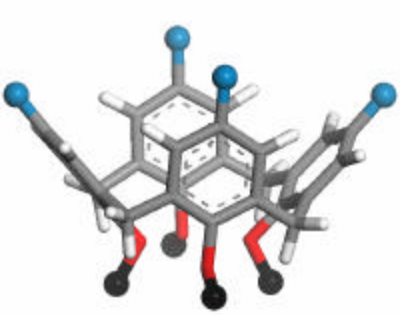

Figure 1.1. Representation of a calix-4-arene molecule in the cone conformation showing the sites at the upper and lower rims that can sustain functional substitution

1.3.2. Properties

The characteristic cone conformation that can be adopted by calixarene derivatives qualifies them as members of a major group of macrocyclic host compounds in supramolecular chemistry. In this regard, their complexation with respect to a range of ions and small organic molecules has been widely studied.[68,73-77] In particular, studies on the inclusion capability of calixarenes, initiated by J. Rebek and V. Böhmer, have revealed that appropriately functionalized calixarenes derivatives, when in presence of guest molecules, can self-assemble to form dimeric units, host capsules, suitable for the

inclusion of these small organic molecules,[76,78-80] Figure 1.2. It should be noted that rational chemical modification of calixarene building units has subsequently led to the generation of much larger supramolecular hosts corresponding to the self-assembly of multiple calixarene derivatives based upon numerous intermolecular interactions,[47,81,82] Figure 1.3.

Another aspect of calixarenes is that they can inherently act as amphiphilic species. In effect, they possess both hydrophobic and hydrophilic groups at the opposite calixarene rims so they are usually suitable for the formation of bilayer arrangements involving head-to-head and tail-to-tail interactions.[75,83] For example, many bilayer structures have been reported for *para-tert*-butyl-calix-4-arenes, in which the presence of hydrophilic phenolic rim and hydrophobic core and upper rim has resulted in the antiparallel alignment of adjacent calixarene molecules,[84-87] Figure 1.4.

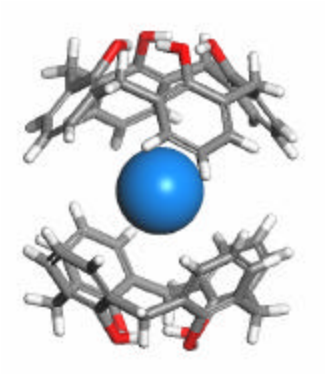

Figure 1.2. Self-assembly of two calixarenes providing host capsule for small guest molecules

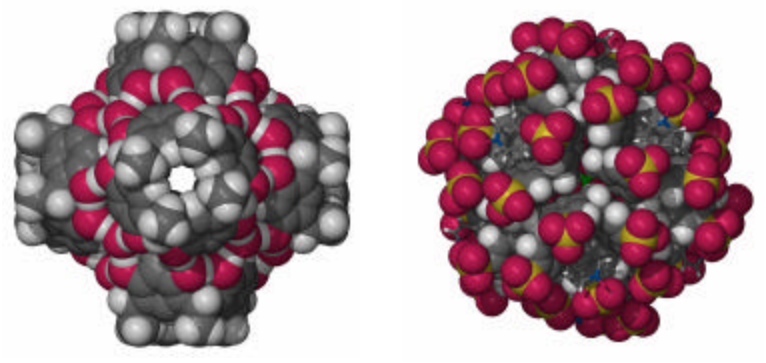

Figure 1.3. Space filling representation of the supramolecular arrangement of calixarene complexes of resorcinarenes and *para*-sulfonatocalixarenes generating large host compounds

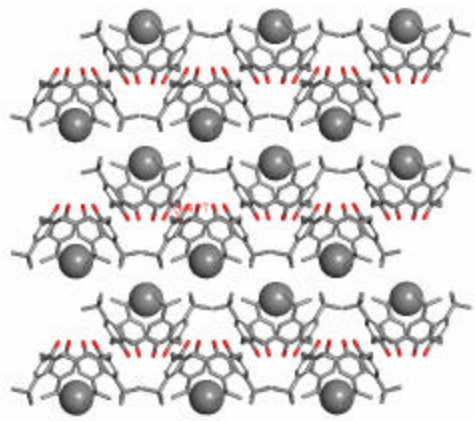

Figure 1.4. Crystal structure of the supramolecular arrangement in bilayers of amphiphilic *para-tert*-butyl-calix-4-arenes

1.4. Supramolecular Metal-Organic Materials

1.4.1. Scope and Context

Metal-organic networks or coordination polymers are organic-inorganic hybrid infinite structures based upon coordination bonds between a transition metal and the heteroatom of an organic molecule called ligand or spacer. Coordination bonds involve the donation of electron density from the donor atom of a ligand to a metal ion.[88] Considering the large variety of possible organic ligands and coordination geometries of transition metals that can afford a wide range of metal-organic compounds, an

understanding of how complementary shapes of molecular building units can be exploited and the selection of appropriate nodes (metal coordination geometries) and spacers enable the specific synthesis of predictable networks.

The first examples of the rational design of supramolecular architectures based upon the coordination between nodes and multi-functional organic ligands have afforded coordination polymers with predictable network architectures in the early 1990's.[60,66] Such an approach has lead to the rapid development of controlled metal-organic network composition and topology, inspired in part by the concepts delineated in crystal engineering. Prototypical examples of infinite networks based upon the linkage between 4-connected nodes and linear bifunctional linkers are shown in Figure 1.5. 2D square grid and 3D diamondoid topologies directly result from square planar and tetrahedral node geometries. The corresponding structures have been generated from commonly available building blocks transition metal ions Co(II), Ni(II), Cu(II) or Zn(II) and 4,4'-bipyridine and a variety of guest molecules,[89-92] Figure 1.6.

In the context of the description of metal-organic networks in terms of the corresponding topologies, it is important to note that both networks possess the same stoichiometry node: linker (1:2) so the corresponding architectures or superstructures exemplify the phenomenon of structural supramolecular isomerism, highly relevant for crystal engineering.[93] In this regard, the importance to develop an understanding of the factors inherent in the supramolecular control of network topologies is evident. Accordingly, the systematic study of recurrent motifs adopted by relevant chromophores, coordination metal geometries and environment configurations, and specific organic

ligands by means of critical analysis of a broad range of known structures constitutes an asset towards the design of new metal-organic structures with desirable properties.

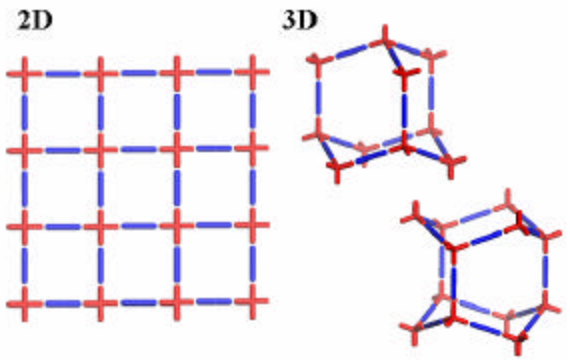

Figure 1.5. Schematic representation of the 2D square grid and 3D diamondoid (hexagonal and cubic) networks that can be generated by linking transition metal nodes by linear bifunctional spacers ligands

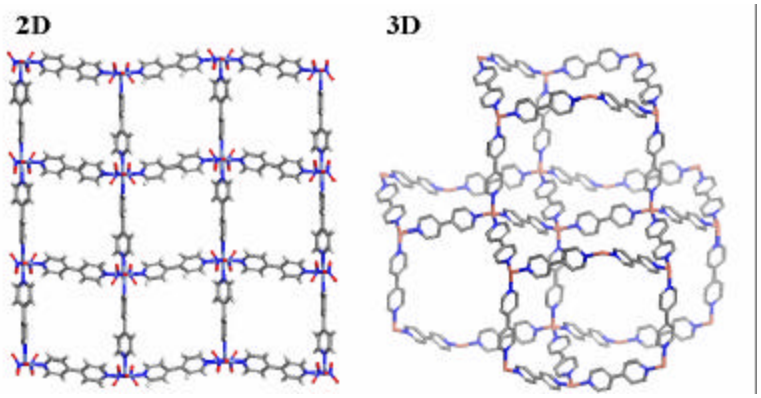

Figure 1.6. Crystal structures of the 2D $[Ni(4,4'\text{-bipyridine})_2(NO_3)_2]_n$ and 3D $[Cu(4,4'\text{-bipyridine})_2]_n$ metal-organic networks, organic and anionic guests are omitted for clarity

1.4.2. Properties

The modular nature of crystal engineered metal-organic networks, which can be generated from a diverse array of complementary building units,[67,94-96] coupled with the structural diversity represented by the range of supramolecular isomers that can be generated from each set of molecular components,[93,97] are of particular interest in the context of fine-tuning the chemical or physical properties.

Furthermore, the presence of channels or cavities, which are controllable in size by the variation in length of the organic spacer, within the supramolecular structures can afford porous materials. In this context, rigid linkers have been widely exploited in the design of network topologies corresponding to such anticipated property. Indeed, if one were to just focus upon linear N,N'-donor spacers, there already exist numerous examples of 2D[66,90-92,97-113] and 3D infinite networks,[89,113-120] many of which have no precedent in minerals. In particular, metal-organic square grids possess cavities that are suitable for interpenetration[90-92,110-113] or enclathration[66,98-103] of a range of guest molecules. In a sense, they have structural features that compare to both clays and zeolites since they are inherently lamellar[109,121] and they can also be porous.[94,103,113] In 3D networks, the presence of large pores may lead to the phenomenon of interpenetration,[122,123] which can be overcome *via* the use of bulky linkers[124] or the presence of guest molecules or ions[60] in order to fill the cavities. On the other hand, recent results have demonstrated that interpenetrated structures can also be porous.[125,126]

1.5. Supramolecular Materials: Tunable Properties towards Useful Applications

There is currently intense research in the nanosciences, which merge the basic experimental sciences towards the controlled manipulation of molecules in order to build nanostructured materials, as illustrated in Figure 1.7. In this context, supramolecular chemistry provides a straightforward method to generate a wide variety of functional nanoscale structures.[127]

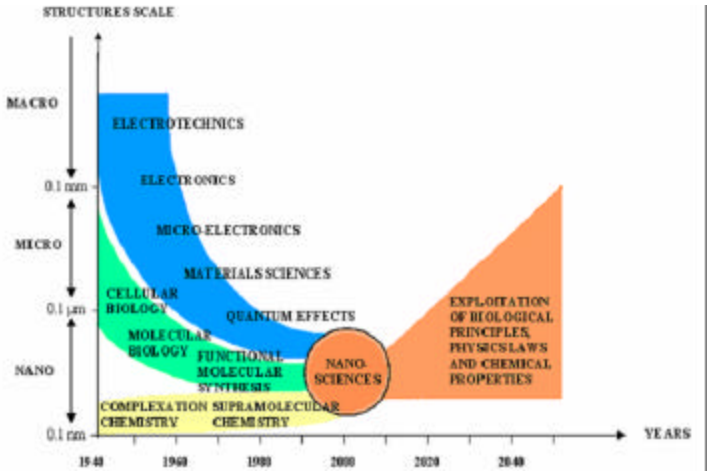

Figure 1.7. The convergence of experimental sciences towards the field of nanosciences (adapted from the review "*Pour la Science*" 290, 2001, p.134)

In addition to their inherent inclusion capability, qualifying them as potential "nanoscale containers",[128] the variety of properties of functionalized calixarenes coupled with their low cost and non-toxicity may allow their exploitation through multidisciplary areas of research as catalysts, extractants, semi-conductors materials, switchable systems for data storage and sensors or bioactive compounds.[73,128-136] In particular, the ability of amphiphilic systems based upon calixarene derivatives to self-assemble in a reminiscent manner as phospholipids in biological membranes makes them an attractive target towards the construction of a wide range of materials such as sensors,[137] microporous membranes[138,139] or bio-active molecules carriers.[140,141]

Nanoporous supramolecular metal-organic materials present various potential applications as adsorbents, sensors, catalysts or in separation and ion exchange.[96,142-145] They constitute an alternative to zeolites that is of interest for its simplicity in generation and functionalization. One can also find interesting advantages of these materials, which can possess intrinsic properties due to the presence of metal ions allowing the

incorporation of additional properties such as luminescence, redox behavior or magnetism.

In summary, the application of supramolecular synthesis and crystal engineering strategies towards the generation of metal-organic and organic materials in the context of a multidisciplinary approach can afford *"the goods: not only smart crystalline materials with useful properties chosen by the crystal engineer and implanted into the molecular building blocks"*.[146]

Chapter 2

Supramolecular Organic Materials based upon pseudo-amphiphilic calixarenes

2.1. Introduction

With a view to the rapid growth of both the biological[73,135,136,147] and material science[73,82,130,137,148-150] applications of calixarenes, recent advances have resulted in the development of simple routes to generate derivatives suitable for coupling to macromolecules such as DNA[151] and proteins[152-155] or for assembly at interfaces towards the production of calixarene thin films.[149,156,157] In this context, amphiphilic calixarenes, bearing both hydrophobic and hydrophilic groups at the opposite calixarene rims, have been shown to be suitable for the formation of self-assembled mono- and multi-layers at the surface of solid supports.[158,159] These films can be generated from calixarene derivatives through a variety of techniques.[160-164] Such materials consist in multi-dimensional supramolecular assemblies and hence their properties may vary from these of individual molecules in solution. In this regard, the study of the spatial arrangement adopted by selected amphiphilic calixarenes within the solid state is clearly relevant.

Amphiphilic molecules or surfactants are well known for their essential roles in biological membranes or detergents. They are commonly defined as molecules possessing both hydrophilic polar functions and lipophilic moieties. Depending on their

molecular geometry, they are capable of self-organization into different phases such as bilayers, corresponding to lamellar systems, or colloidal systems including micelles and inverse micelles.[165] Extending the limits of the definition of the nature of the polar head group, this study will be based upon the so-called "pseudo-amphiphilic" calix-4-arenes in which various alkyl groups are coupled to the phenolic oxygen atoms, introducing van der Waals interactions at one face, while different functionalities, not necessarily hydrophilic, are present at the upper rim of the calixarenes, thereby affecting the intermolecular interactions occurring at this face, Figure 2.1. In this context, the rational design of organic solids based upon the principles of self-assembly *via* hydrogen bonding, stacking interactions, hydrophobic interactions and electrostatics represents a salient aspect of crystal engineering. Considering the modular aspect of calixarene molecular building blocks, there are many opportunities for variation of the functional elements that can be judiciously selected for their potential in terms of intermolecular interactions. Examples of these interactions include face-to-face and edge-to-face aromatic stacking in *para*-H systems, van der Waals repulsions due to the steric effects of bulky groups such as *tert*-butyl and induced dipole-dipole forces in bromo-substituted calixarene systems. Knowledge of the interplay between two or more sets of interactions will facilitate further extension of crystal engineering. In this respect, systematic investigation of the structural features and general trends concerning the spatial arrangement of calixarene derivatives with respect to the specifics of the molecular components may reveal important towards rational application of principles delineated by supramolecular chemistry and crystal engineering to the design of novel supramolecular

architectures.

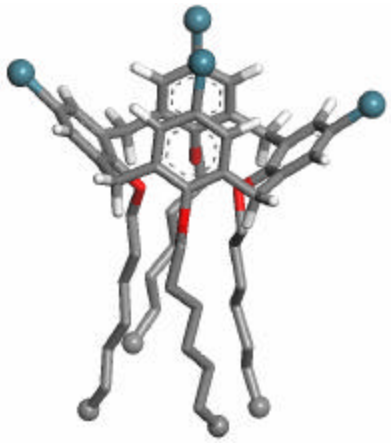

Figure 2.1. Representation of the pseudo-amphiphilic calix-4-arene building block possessing alkyl substituents at the lower rim and variable functionalities at the upper rim

2.2. Calixarenes Crystal Packing: a Database Review

2.2.1. Scope and Limitations

Calixarenes have been widely studied in solid state chemistry: at this time, more than 850 structures involving calix-4-arene derivatives have been deposited in the CSD. The examination of these crystal structures, which exclude resorcinarenes, homocalixarenes and other pyrole calixarenes, with regard to the spatial arrangement of calix-4-arenes within the solid state has afforded relevant information concerning the factors that can influence the crystal packing. Thiacalixarenes were included in this review since they revealed to adopt comparable trends as these of calixarene molecules. It should also be noted that this study was purely based upon crystalline architectures and excluded dynamic properties related to solution phenomena. There exist several potential variables that can affect the supramolecular organization of calixarenes building units. In

particular, chemical composition, shape, position of the functional groups and presence of guest or template molecules may be specifically screened.

Considering the substantial amount of data, a primary classification based upon the chemical composition has revealed proportionate division between molecular and metal-organic structures. In effect, 53% of the data consisted in purely organic compounds, while the remaining 47% corresponded to metal-, alkaline- or mixte coordination compounds. The metal-organic structures were generally coordinated through the phenolic oxygen atoms at the lower rim, which may also be bridged or capped by one metal ion, or *via* specific substituents at the *para*-position such as sulfonate groups that allow coordination chemistry at these sites. The strong propensity of calix-4-arenes to adopt a cone or flattened cone conformation in the solid state is effectively exhibited in 75% of the crystal structures. The other possible conformations are partial cone (6.5%), 1,2-alternate (2.5%) and 1,3-alternate (16%). Figure 2.2 illustrates the four common conformations observed in calix-4-arene macrocycles. The proportion between the different conformations is consistent in both classes of organic and metal-organic structures. Another important trait resulting from the exploitation of these raw data concerns the repartition according to the substituents that have been used to functionalize the upper rim of calix-4-arene molecules. Interestingly, the structures of *para-tert*-butyl-calix-4-arenes derivatives markedly outnumber all other derivatives for 60% of the whole data set. This feature can be explained by the relative simplicity and high yield resulting from the condensation of *para-tert*-butylphenol and formaldehyde in basic conditions with respect to the use of other *para*-substituted phenols.[68,166] The other

main derivatives that have been studied are *para*-hydrogen- and *para*-sulfonato-calix-4-arenes in relative proportions of 16% and 6% respectively. However, the wide diversity of substituents found to functionalize the lower rim, which can also be partially substituted, did not allow delineating specific trends. Finally, the presence of additional guest or solvent molecules as part of the crystal structure corresponded to *ca.* 65% of the cases. A detailed classification of the structures and packing adopted by calix-4-arene derivatives deposited in the CSD can be found in the electronic supplementary data. Tables 2.1 and 2.2 represent simplified categorization corresponding to the most relevant structural motifs discussed throughout this review.

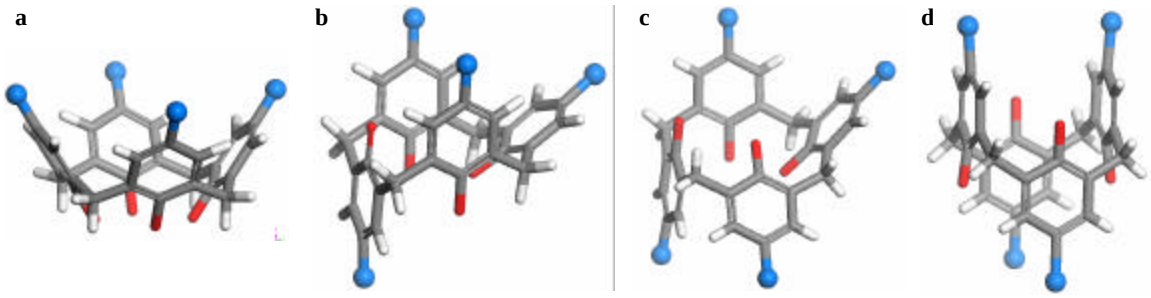

Figure 2.2. Cone (a), partial cone (b), 1,2-alternate (c) and 1,3-alternate conformations adopted by calix-4-arenes

In the context of this study, the available data concerning the molecular structures of calixarenes in the cone conformation that possess four hydrophobic *para*-substituents, hydrogen and *tert*-butyl, have been analyzed with respect to the influence of the lower rim functionality, which can induce, *inter alia*, hydrophilicity or hydrophobicity, over the spatial arrangement of these molecules in the solid state. It should be noted that the guest specifics have been accounted as a secondary variable.

2.2.2. Crystal packing of amphiphilic calixarenes

The model molecule of non-substituted calix-4-arene has only resulted in 19 crystal structures essentially differing by the solvent incorporated in the crystalline architecture. In effect, in the vast majority of the cases, with small solvent hydrophilic and hydrophilic molecules, these simple building blocks have afforded a cyclic trimeric arrangement sustained by p-p edge-to-face aromatic interactions between the mutually partially included calixarene rings, Figure 2.3a. The spatial arrangement of these trimeric subunits in hexagonal close-packing is sustained by van der Waals interactions and generates two types of channels. Further study of the crystal packing and inclusion properties of these subunits has recently been reported by Atwood's group.[167] In the presence of larger guest molecules capable of hydrogen bonding, calix-4-arenes self-assemble in tetrameric subunits resulting from guest inclusion.

For calix-4-arenes possessing bulky substituents *tert*-butyl at the upper rim, the prevailing crystal packing consists into the formation of bilayer structures,[84-87] whether the included hydrophobic guest is a small solvent molecule, *e.g.* CH_3CN, or a larger organic molecule, *e.g.* tetradecane. As illustrated in Figure 2.3b, these bilayers are generated from the antiparallel alignment of adjacent calixarene molecules that divide the space in two distinct regions: a hydrophilic layer composed of the hydroxyl groups of the lower rims orientated towards the same direction and a hydrophobic layer formed by the aromatic rings and *tert*-butyl substituants of the calixarenes including the organic guest molecules.[148] In only few exceptions, for 4 out of 23 structures, a different crystal packing was observed. The absence of included solvent has resulted in the mutual

inclusion of two *tert*-butyl substituents forming dimeric units of *para-tert*-butyl-calix-4-arenes. On the other hand, the presence of highly sterically hindered guest molecules has resulted in the self-assembly of tetramer units similarly to the case of non-substituted calix-4-arenes.

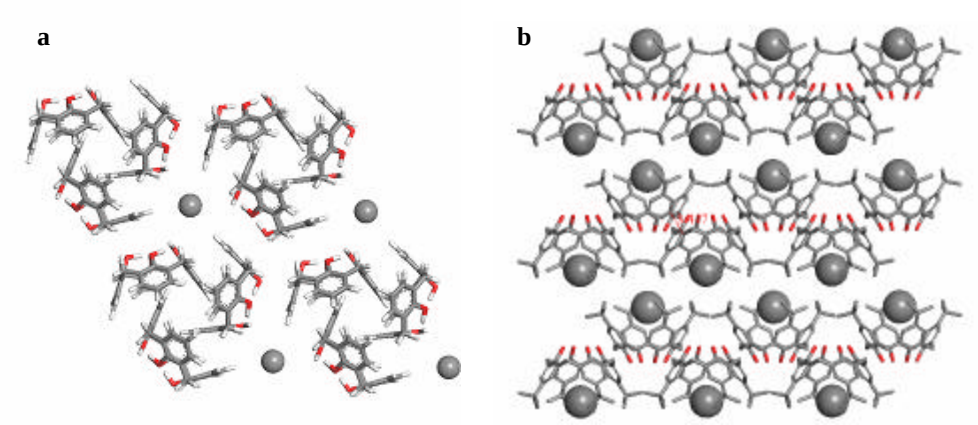

Figure 2.3. Dominant crystal packing observed for calix-4-arenes (a) and *para-tert*-butyl-calix-4-arenes (b)

Of special interest in the context of this review, the class of bipolar amphiphilic molecules, *para*-sulfonato-calix-4-arenes, in which the presence of two hydrophilic rims separated by a hydrophobic core, has been specifically studied in terms of spatial arrangement that is adopted by the macrocycles in the solid state in a recent review by Atwood and Raston.[75] One consequence of their chemical composition is a strong propensity to form bilayer structures involving head-to-head and tail-to-tail interactions. Such bilayers can incorporate hydrophilic guests and the overall arrangement is generally controlled by strong interactions, hydrogen bonds or coordination, involving the sulfonate groups, the guest molecules and the phenolic groups. In this regard, many reports have described the inclusion of various guests[83,168-170] including small biomolecules[171-174] and their effects upon the bilayer motif. *Para*-sulfonato-calix-4-arenes have also been shown

to induce three other significant types of crystal packing: capsules that can incorporate hydrophobic molecules such as crown ether[175-177] and azacrown;[178] or spheres and tubules, Figure 2.4, nanostructures resulting from the controlled self-assembly of three components calixarene, metal ion and organic ligand in specific stoichiometries.[82]

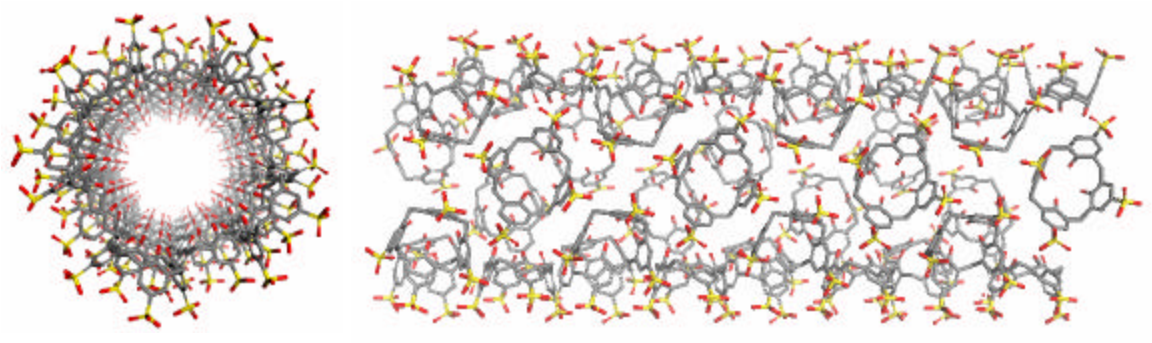

Figure 2.4. Tubular self-assembly of *para*-sulfonato-calix-4-arenes, hydrogen atoms, metal ions and organic ligands are omitted for clarity

2.2.3. Crystal packing of pseudo-amphiphilic calixarenes

Examination of the crystal structures of calix-4-arenes and *para-tert*-butyl-calix-4-arenes that possess various functionalities at the lower rim has allowed delineating some general trends concerning the factors that govern the crystal packing of this class of macrocycles.

First considering the calix-4-arenes with hydrogen atoms at the *para* positions, three cases can be distinguished according to the degree of substitution at the opposite rim. When the lower rim is tetra-substituted by organic moieties that are not bridging or capping this face, the calix-4-arenes primarily adopt a bilayer motif, in which a "rigid" region results from the head-to-head arrangement of anti-parallel calixarene aromatic cores pointing towards each other and a "soft" region consists in the self-assembly of the

various substituents that can interact *via* hydrogen bonding, aromatic stacking or van der Waals forces between the included functionalities, Figure 2.5a. When the lower rim is di-substituted at the two opposite phenolic positions, the almost exclusive tendency of the calixarenes is to form head-to-head dimers held together by face-to-face p-p stacking. In absence of additional components capable of influencing the self-assembly within the crystal lattice,[179] these dimeric subunits may then arrange in a herringbone-type organization, which affords high three dimensional packing efficiency, Figure 2.5b.

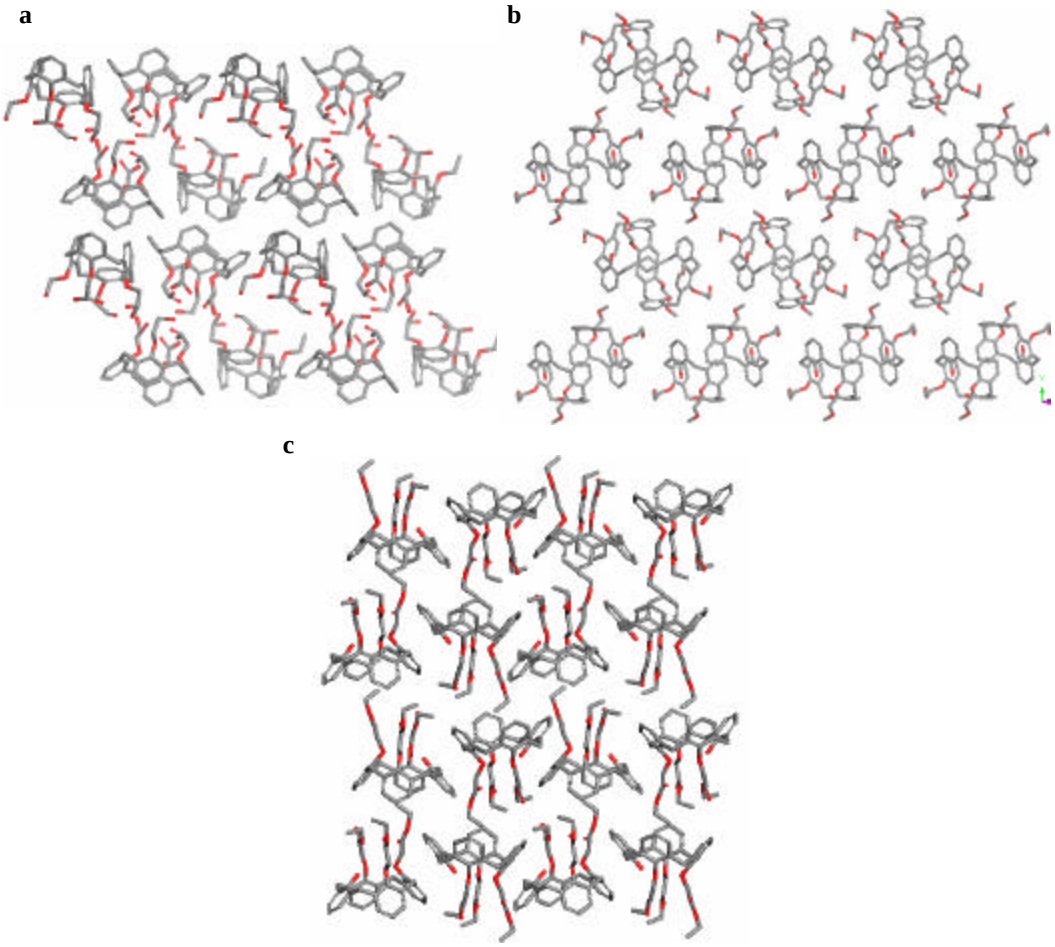

Figure 2.5. Main crystal packing motifs observed for pseudo-amphiphilic calix-4-arene derivatives that can self-assemble in bilayer (a), herringbone of dimers (b) and column (c) modes

When the lower rim is tri-substituted or possesses four substituents capping this face, calixarenes form columnar-type crystal packing *via* partial inclusion of the non-symmetrical substituent or the capped face within the upper rim of a calixarene situated below. These columns of consecutive included calixarenes generally alternate with respect to their directionality to afford efficient three-dimensional packing. It should be noted that this motif only occurs in absence of included guest molecule, Figure 2.5c.

Secondly, the study of the spatial arrangement adopted by *para-tert*-butyl-calix-4-arene derivatives has revealed similar trends with differences attributable to the introduction of a supplementary variable as the presence of bulky substituents at the upper rim. When the phenolic substituents induce a degree of asymmetry within the molecular structure of *para-tert*-butyl-calix-4-arenes, for example mono-substitution or tetra-substitution of the lower rim by three equivalent moieties and an additional distinct group, the columnar-type motif described above is obtained. In the remaining majority of the cases, the specifics of the substituents in terms of shape and functionality constitute the triggers of the crystalline arrangement. From a general perspective, three major situations can be distinguished. In the case of large substituents that possess functional groups susceptible to afford supramolecular interactions with each other such as hydrogen bonds or aromatic stacking, the bilayer-type crystal packing described above prevails, Figure 2.6a. The presence or absence of guest/solvent molecules does not essentially affect the overall supramolecular arrangement. In fact, such small additional components, when non-included in the macrocycles, usually lie between the bilayers; whereas guest inclusion may increase the width of the aromatic layer. When the lower

rim is functionalized with small groups, the presence of included guest molecules within the cavities of the calixarenes generates the formation of capsules. The spatial organization of these capsules can be described as an "anti-bilayer" situation where rigid and soft parts regularly alternate in order to optimize the packing efficiency, Figure 2.6b. Finally, the presence of bulky groups at the lower position of the molecules of *para-tert*-butyl-calix-4-arene induces a different packing mode that is principally governed by van der Waals repulsion of the two sterically hindered faces of the macrocycles. The oblique orientation of adjacent molecules generates a herringbone pattern as illustrated in Figure 2.6c, which offers the closest and most compact crystal packing for these characteristic shapes. Interestingly, this type of motif is recurrent throughout the structures of all calix-4-arene derivatives. Notable instances are constituted by dimeric units, in particular tail-to-tail sub-assemblies generated from strong interactions such as coordination or hydrogen bonds between the lower faces of two calix-4-arenes. These dimers present symmetrical hindered opposite faces formed by both upper rims and hence self-assemble in a similar manner as a single building unit that contain two opposite bulky faces.

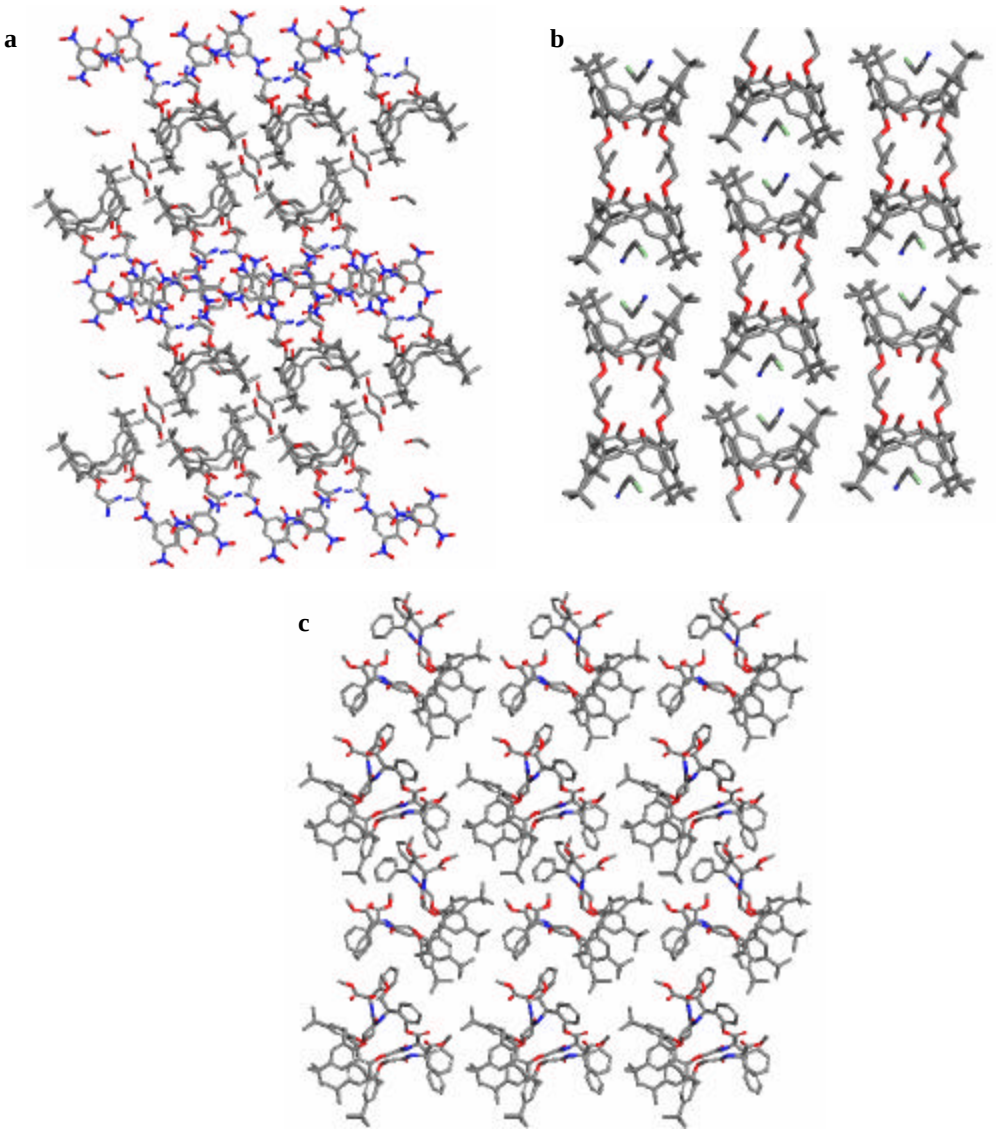

Figure 2.6. Main crystal packing motifs observed for pseudo-amphiphilic *para-tert*-butyl-calix-4-arene derivatives that can self-assemble in bilayer (a), capsule (b) and herringbone (c) modes

In the context of the crystallographic study of pseudo-amphiphilic building units possessing lipophilic substituents, only a small number of calixarenes bearing exclusively alkyl chains at the lower rim have been synthesized and investigated by X-ray crystallography.[180-183] The corresponding crystalline arrangements are essentially governed by the substituent particulars, nitro groups or large multi-aromatic components,

used to functionalize the upper rim. In the case of amphiphilic calixarenes possessing long alkyl chains, *para*-octanoyl-calixarene constitutes a rare and recent example in which the crystal packing is sustained by van der Waals interactions between alkyl chains and by the presence of a hydrophilic layer between two layers of calixarenes.[184] This behavior in the solid state is very similar to those observed for amphiphilic molecules in liquid crystal phase and typical phospholipids in lyoptropic phase.[185]

Finally, with regard towards the study of specific modification of the upper rim of pseudo-amphiphilic compounds by halogen groups and the influence of the resulting induced dipole over the supramolecular organization, for example in the case of brominated calixarenes, the extremely scarce number of these types of functionalized macrocycles[180,186-189] has not allowed the extraction of any particular trend or preferential behavior of such type of halogenated calix-4-arenes.

In summary, some general trends have been delineated concerning the different variables that may affect the supramolecular organization of amphiphilic and pseudo-amphiphilic classes of calix-4-arenes. In the context of this review, several points deserve to be emphasized. First, the extremely large spectrum of functionalities found to modify the lower rim of calix-4-arene derivatives has limited this study from a thorough examination of the systematic variation of the potential supramolecular interactions that can be incorporated to this face. Second, the influence of specifically designed substituents for their strong tendency to generate well-known supramolecular patterns such as the chiral motif resulting from assembly of calix-4-arene possessing melamine substituents and barbituric acid derivatives[190] has been considered as special cases in the

context of this study since these instances are not representative of the crystal packing of calixarene molecules. Finally, the scarcity of crystal structures containing calixarenes possessing more or less long alkyl chains represents an interesting opportunity towards the rational study of such class of pseudo-amphiphilic synthetic compounds through systematic variation of the hydrophobic part. Moreover, further examination of the effect of the modification of the upper rim by bromine substituents and their comparison with other frequent derivatives may reveal of interest towards the generation of supramolecular organic materials based upon the control over the structural motifs resulting from more than one type of intermolecular interactions.

Careful examination of the crystal structures of a series of calix-4-arene derivatives systematically modified at the lower rim with various alkyl chain lengths, and successively systematic modification of the upper rim by three types of functional groups, hydrogen, *tert*-butyl and bromine, which can induce the corresponding sets of weak interactions, aromatic stacking, van der Waals and halogen or induced dipole forces, sustaining the crystal packing, will be discussed in the broader perspective of crystal engineering strategies and development of novel materials.

Table 2.1. Structural analysis of the crystal packing observed in calix-4-arenes

Lower Rim Substituents	CSD Refcode	Space Group	Structural Motif
4 OH	HUVBEF	P-3	Trimers
	WUVKAZ	P-3	
	PEZBIF	P63	
	BALHOM	P63/m	
	DACMAV	P63/m	
	PEZBEB	P63/m	
	PEZWIA	P63/m	
	WUVKED	P63/m	
	WUVKON	P63/m	
	WUVKUT	P63/m	
	WUVLAA	P63/m	
	WUVLEE	P63/m	
	WUVLII	P63/m	
	WUVLOO	P63/m	
	NUNJUB	P-1	Tetramers
	HAZJAT	P4/nnc	
	DACLUO	Pnma	Bilayers
1OH+3OR	QEKMIC	P21/c	Bilayers
	WIWLOD	P21/c	Columns
2OH+2OR (Opposite Rings)	KEVYAL	P21/c	Columns
	TIWHEM	P21/c	Dimers
	PAWTOW	R-3	
	RUWGOF	P21/n	
	LASDEO	P1121/n	
	NEMTUU	P-1	
	WOHJEI	P21/a	
	YAKGIA	P-1	
	VIRXAF	P21/n	Herringbone
2OH+2OR (Opposite rings bridged)	GODWEB	P21/c	Bilayers
	NUVMEW	P-1	Dimers
	NUVMIA	P21/a	Columns
4 OR	JOYHEK	P21/a	Bilayers
	WILNOU	P-1	
	RADSAQ	P21/n	
	NEDDUV	C2/c	
	HILVAZ	C2/c	Columns
	HUBMEW	P-1	Herringbone
4 OR (Adjacent rings bridged)	LINLID	P2/c	Columns
	NEMMUN	C2/c	Bilayers
4 OR (Opposite rings bridged)	TADCOQ	P21/c	Dimers
4 OR (All rings capped)	HEMHUC	P-1	Columns

Table 2.2. Structural analysis of relevant crystal packing observed in para-tBu-calix-4-arenes

Lower Rim Substituents	CSD Refcode	Space Group	Structural Motif
4 OH	BHPMYC	P4/n	Bilayers
	BOCZUO	P4/n	
	CUPWAL	P4/n	
	GOKPEB	P4/n	
	GOKQUS	P4/n	
	LODNOH	P4/n	
	NAPCIQ	P4/n	
	NILCEQ	P4/n	
	NILCIU	P4/n	
	NILCOA	P4/n	
	VEGPIG	P4/n	
	ZAHMOK	P4/n	
	NILCAM	P4/n	
	QIGBAJ	P-1	
	BHPMYC01	P112/a	
	NAPCEM	Pc21n	
3OH+1OR	FAQDUW	P21/n	Columns
	LOMGUP	P-1	
2OH+2OR (Opposite Rings)	KEVXIS	P21/n	Capsules
	SUYXIT	P-1	
	QIKTEJ	P-1	
	KEQYEK	P212121	Columns
	IBOKAL	P-1	Bilayers
	BOWFOI	P-1	
1OH+3OR	WESGIK	P21/a	Bilayer/Herringbone Hybrid
	WEHJEY	P-1	Bilayers
	ABOYAR	C2/c	
	QIFHOC	P-1	
	NECWAT	C2/c	
	ZOJWEA	Pnma	
4 OR	PAMTIG	P21/n	Bilayers
	RADRUJ	P21/n	
	JEGQOB	P21/a	
	DAKSEN	P-1	Capsules
	GIYTOX	P-1	
	KEQYAG	P21	Herringbone
	JOYHAG	P21/c	
3OR+1OR'	NICDOS	P-1	Columns
	KOCQIC	Pbca	

2.3. Experimental

2.3.1. Syntheses

Two series of pseudo-amphiphilic calixarenes were synthesized. A first set of bromo-substituted calix-4-arenes at the *para* position through systematic variation of the chain length of the four alkylated phenolic oxygen atoms of the lower rim resulted in the following compounds: *para*-Br-tetra-O-alkyl-calix-4-arene, with alkyl = butyl, **1**; pentyl, **2**; hexyl, **3**; heptyl, **4**; octyl, **5**; nonyl, **6**; decyl, **7**; undecyl, **8**; dodecyl, **9**. The second series of calixarenes resulted from variation of the substituent at the upper rim while all phenolic oxygen atoms were alkylated by hexyl groups: (*para*-H)$_2$-(*para*-Br)$_2$-tetra-O-hexyl-calix-4-arene, **10**; *para*-H-tetra-O-hexyl-calix-4-arene, **11** and *para*-*t*Bu-tetra-O-hexyl-calix-4-arene, **12**. Syntheses were achieved using appropriately modified procedures of syntheses described in the literature.[191,192] Recrystallization of all compounds was achieved at room temperature *via* slow diffusion in mixtures of organic solvents selected for their ability towards solubilization of calixarene derivatives.

2.3.2. X-ray Crystallography

Single crystals suitable for x-ray crystallographic analysis were selected following examination under a microscope. Single-crystal x-ray diffraction data for compounds **1-5** and **9-12**, and all subsequent compounds described along this dissertation, were collected on a Bruker SMART-APEX diffractometer using Mo$_{?a}$ radiation (*?* = 0.7107 Å). Lorentz and polarization corrections were applied and diffracted data for bromo derivatives and all metal-organic compounds presented further in this work were also corrected for

absorption using the SADABS v.2.02 area-detector absorption correction program (Siemens Industrial Automation, Inc., © 1996). The structures were solved by direct methods and Fourier techniques. Structure solution and refinement were based on $|F|^2$. Unless specified, all non-hydrogen atoms were refined anisotropically and hydrogen atoms of the C-H groups were placed in geometrically calculated positions and refined with temperature factors 1.2 times those of their bonded atoms. All crystallographic calculations were conducted with the SHELXTL 6.10 program package (Bruker AXS Inc., © 2001). Table 2.3 reveals crystallographic data and structure refinement parameters of the compounds presented in this chapter. Full crystallographic data can be found in the electronic supplementary data.

Compound **10** was observed to present two different crystalline phases at 200K and at room temperature corresponding to the structures of **10a** and **10b** respectively. In crystal structures of **1**, **2**, **4**, **5**, **11** and **12** several carbon atoms of the alkyl chains were disordered around 2-fold positions and each corresponding group of atoms was refined with two equally occupied sets of coordinates. In crystal structures of **3** and **10a** the carbon atoms of several alkyl chains of the calixarene molecules in the asymmetric unit occupied several general positions and were refined with fixed site occupation factors (s.o.f.) for occupancies of 0.5 (0.6 and 0.4 for 4 atoms of **3**) for each carbon. All non-hydrogen atoms were refined with anisotropic displacement parameters except for several carbon atoms of the alkyl chains in compound **3**, **5** and **10a**, which were observed to exhibit high thermal motion. The H atoms of the C-H groups were fixed in calculated positions except for the H atoms of the disordered aliphatic chains in compounds **3**, **4**, **5**

and **10a**. The relatively high values for the residual electronic density in **5** and **10a** were due to the non-attribution of these hydrogen atoms. Structure of **3** was badly disordered and presented very low proportion of significant diffraction intensities at higher Bragg angle so a shortage of high-angle data with significant intensity was used to determine a valid solution. The crystal of compound **10a**, was a racemic twin as highlighted by the value of the Flack parameter (0.47). Although the structure was recollected for different crystals and resolved several times; in every case, a comparable Flack parameter was obtained, such results are indicative of the natural tendency of this particular compound with respect to crystal growth. Recrystallization of compounds **6**, **7** and **8** afforded needle-shaped microcrystals. Due to the poor quality of these crystals, diffraction of **6-8** was very weak and it was not possible to obtain acceptable structure solutions. However it was possible to determine their unit cells as means of comparison with the series studied herein. Furthermore, data set collected for **6** and **8** provided the possibility to elucidate the main elements of the crystal packing of these compounds, which was found to be analogous to that of **4** and **5**.

Table 2.3. Crystallographic data for compounds 1-5 and 9-12

Compound	**1**	**2**	**3**	**4**	**5**
Chemical formula	$C_{44}H_{52}Br_4O_4$	$C_{48}H_{60}Br_4O_4$	$C_{52}H_{68}Br_4O_4$	$C_{56}H_{76}Br_4O_4$	$C_{60}H_{84}Br_4O_4$
Formula weight	964.50	1020.60	1076.70	1132.81	1188.91
Temperature, K	200(2)	200(2)	200(2)	200(2)	100(2)
Crystal system	Triclinic	Triclinic	Triclinic	Monoclinic	Monoclinic
Space group	P-1	P-1	P-1	P2/c	P2/c
a, Å	12.2468(12)	13.0107(8)	18.018(4)	28.095(5)	27.628(2)
b, Å	19.0095(19)	18.5940(12)	21.980(4)	16.485(3)	17.4376(15)
c, Å	19.0772(19)	19.8009(12)	23.168(5)	18.384(4)	18.4703(16)
a, deg	102.245(2)	101.3780(10)	113.40(3)	90	90
ß, deg	91.880(2)	91.8250(10)	95.32(3)	98.359(4)	96.874(2)
γ, deg	93.842(2)	94.3990(10)	109.24(3)	90	90
V, $Å^3$	4325.4(7)	4676.9(5)	7681(3)	8424(3)	8834.3(13)
Z	4	4	6	6	6
ρ_{calcd}, $g.cm^{-3}$	1.481	1.449	1.397	1.340	1.341
μ, mm^{-1}	3.761	3.483	3.185	2.907	2.776
F(000)	1952	2080	3312	3504	3696
Crystal size, mm	0.30x0.15x0.10	0.30x0.20x0.10	0.20x0.05x0.01	0.10x0.01x0.01	0.30x0.15x0.05
θ range for data collection, deg	1.09 to 25.06	1.57 to 24.71	0.99 to 21.87	1.24 to 24.71	1.17 to 26.37
Limiting indices	-14<=h<=14 -22<=k<=22 -22<=l<=22	-14<=h<=15 -21<=k<=20 -23<=l<=22	-17<=h<=18 -11<=k<=21 -22<=l<=21	-32<=h<=33 -19<=k<=18 -21<=l<=17	-31<=h<=34 -12<=k<=21 -22<=l<=23
Reflections collected	31517	24047	14807	40470	49331
Unique reflections	15178	15772	13120	14361	18071
R(int)	0.0335	0.0334	0.0252	0.1116	0.0826
Completeness to θ, %	98.9	98.9	70.8	100	99.9
Absorption correction	SADABS	SADABS	SADABS	SADABS	SADABS
Max. and min. transmission	1.000 and 0.825	1.000 and 0.639	1.000 and 0.795	1.000 and 0.714	1.000 and 0.618
Data / restraints / parameters	15178 / 0 / 1032	15772 / 0 / 1037	13120 / 0 / 1633	14361 / 78 / 918	18070 / 37 / 943
Goodness-of-fit on F^2	1.021	0.992	1.056	0.962	1.002
Final R indices [I>2sigma(I)]	R1 = 0.0433, wR2 = 0.1024	R1 = 0.0479, wR2 = 0.1060	R1 = 0.0567, wR2 = 0.1360	R1 = 0.0631, wR2 = 0.1240	R1 = 0.0716, wR2 = 0.1850
R indices (all data)	R1 = 0.0723, wR2 = 0.1202	R1 = 0.0809, wR2 = 0.1209	R1 = 0.1012, wR2 = 0.1666	R1 = 0.1517, wR2 = 0.1601	R1 = 0.1573, wR2 = 0.2280
Largest diff. peak and hole, $e.Å^{-3}$	0.730 and -0.631	0.922 and -0.745	0.507 and -0.344	0.717 and -0.589	1.004 and -0.708

Table 2.3. (continued)

Compound	**9**	**10a**	**10b**	**11**	**12**
Chemical formula	$C_{79}H_{122}Br_4O_5$	$C_{52}H_{70}Br_2O_4$	$C_{52}H_{70}Br_2O_4$	$C_{52}H_{72}O_4$	$C_{68}H_{104}O_4$
Formula weight	1471.41	918.90	918.90	761.10	985.51
Temperature, K	200(2)	200(2)	298(2)	200(2)	200(2)
Crystal system	Monoclinic	Monoclinic	Monoclinic	Orthorhombic	Monoclinic
Space group	P2(1)/c	P2(1)	P2(1)/c	Pbca	P2(1)/n
a, Å	a = 23.725(3)	21.973(3)	19.049(2)	19.3314(15)	19.5064(12)
b, Å	b = 15.6770(17)	16.135(2)	16.623(2)	19.2886(15)	16.9184(10)
c, Å	c = 21.102(2)	27.137(4)	16.059(2)	50.653(4)	38.139(2)
a, deg	90	90	90	90	90
ß, deg	103.075(2)	99.472(2)	97.898(3)	90	92.6920(10)
γ, deg	90	90	90	90	90
V, $Å^3$	7645.3(15)	9490(2)	5036.9(11)	18887(3)	12572.5(13)
Z	4	8	4	16	8
ρ_{calcd}, $g.cm^{-3}$	1.278	1.286	1.212	1.071	1.041
μ, mm^{-1}	2.153	1.751	1.650	0.065	0.062
F(000)	3104	3872	1936	6656	4352
Crystal size, mm	0.50x0.10x0.05	0.30x0.10x0.02	0.20x0.10x0.05	0.60x0.30x0.10	0.30x0.25x0.05
θ range for data collection, deg	1.63 to 27.10	0.94 to 25.11	1.63 to 24.71	1.54 to 24.04	1.07 to 26.43
Limiting indices	-30<=h<=30 -20<=k<=12 -25<=l<=27	-26<=h<=15 -19<=k<=19 -32<=l<=32	-15<=h<=22 -19<=k<=19 -18<=l<=18	-22<=h<=22 -22<=k<=21 -44<=l<=58	-24<=h<=24 -18<=k<=21 -47<=l<=39
Reflections collected	45337	50439	24921	86022	71190
Unique reflections	16842	33327	8588	14864	25748
R(int)	0.0884	0.0721	0.1125	0.0734	0.1179
Completeness to θ, %	99.9	99.2	99.9	99.8	99.4
Absorption correction	SADABS	SADABS	SADABS	None	None
Max. and min. transmission	1.000 and 0.676	1.000 and 0.735	1.000 and 0.903	N/A	N/A
Data / restraints / parameters	16842 / 0 / 799	33327 / 161 / 1914	8588 / 57 / 477	14864 / 0 / 1027	25748 / 3 / 1347
Goodness-of-fit on F^2	0.940	1.022	0.859	1.023	0.955
Final R indices [I>2sigma(I)]	R1 = 0.0557, wR2 = 0.1094	R1 = 0.1085, wR2 = 0.2585	R1 = 0.0700, wR2 = 0.1676	R1 = 0.0810, wR2 = 0.1819	R1 = 0.0823, wR2 = 0.1725
R indices (all data)	R1 = 0.1354, wR2 = 0.1360	R1 = 0.2061, wR2 = 0.3248	R1 = 0.2578, wR2 = 0.2498	R1 = 0.1385, wR2 = 0.2129	R1 = 0.2208, wR2 = 0.2287
Absolute structure parameter	N/A	0.466(16)	N/A	N/A	N/A
Largest diff. peak and hole, $e.Å^{-3}$	0.778 and -0.589	1.580 and -1.240	0.369 and -0.253	0.361 and -0.194	0.513 and -0.399

2.4. Results and Discussion

2.4.1. Influence upon the crystal packing through variation at the lower rim

The first part of this study consists in the systematic evaluation of the effect of the substitution by increasing length chains of alkyl groups, C_nH_{2n+1} (n = 4-12), at the lower rim on the crystal structures of a series of pseudo-amphiphilic tetrabrominated calix-4-arenes. Careful examination of the crystal structures with particular attention to the overall arrangement of the calixarene molecules reveals a clear tendency towards to formation of bilayer-type packing while the chain length increases.

In all compounds, the macrocycles exhibit a C_2 symmetrical, flattened-cone, conformation. The distortions in the orientation of the aryl units corresponding to the symmetry reduction with respect to the four-fold symmetry of the ideal cone conformation are attributed to repulsive van der Waals contacts between adjacent O-alkyl groups at the lower rim of the calixarene molecules.[180,193] The ring inclination angles and corresponding distances between opposite aryl groups are presented in Figure 2.7 and Table 2.4. These values are consistent with the corresponding values of flattened conformations observed *para*-H-tetra-O-alkyl-calix-4-arene derivatives, when the alkyl chain possesses more than 3 carbon atoms.[180] It should be noted that the relatively high inclination of the two opposite closest rims in tetrabrominated calixarene derivatives is also favorized by halogen-halogen interactions, with d(Br···Br) in a range of 3.85 to 3.95 Å and corresponding angles ?(C-Br···Br) = 89.5-96.9° and 97.3-103.5° for compounds **1**-**5**.

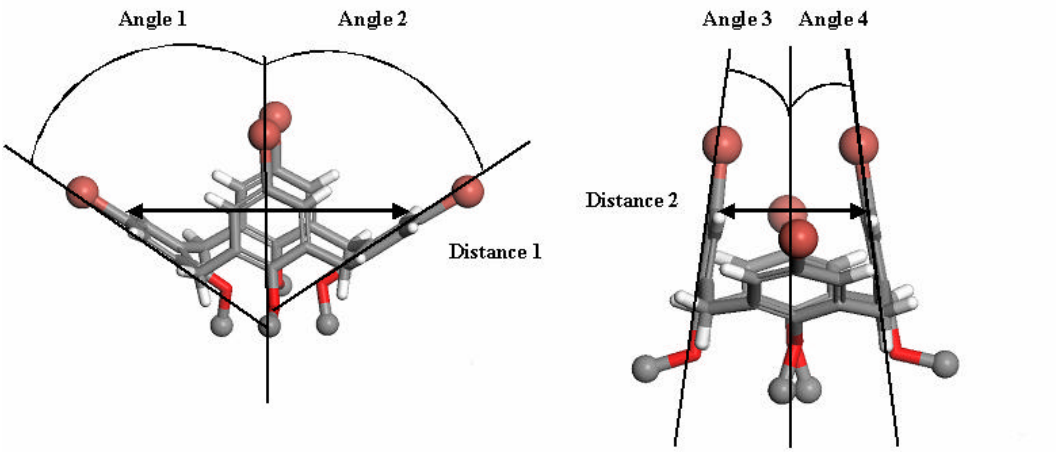

Figure 2.7. Representation of the flattened cone conformation observed in *para*-bromo-calix-4-arenes and designation of the distances and angles used to describe their geometry

Table 2.4. Ring inclination angles and corresponding distances between opposite aryl groups in the crystal structures of compounds 1-5 and 9

Compound	Angle 1 (°)	Angle 2 (°)	Angle 3 (°)	Angle 4 (°)	Distance 1 (Å)	Distance 2 (Å)
1	60.7	52.7	-9.78	-8.00	10.0	4.43
2	63.1	50.3	-9.04	-7.15	10.1	4.45
3	61.6	52.7	-14.7	-5.47	10.1	4.32
4	54.6	48.9	-11.4	-6.55	9.85	4.36
5	56.5	50.5	-11.9	-5.97	9.83	4.41
9	65.1	40.6	-6.63	-4.3	9.89	4.70

The structures of **1** and **2** present analogous crystal packing where the calixarene organization within the solid-state affords higher packing efficiency relative to the other compounds presented herein as illustrated by the corresponding densities, Table 2.3. Figure 2.8 shows that **1** and **2** form two types of layers repeating down [010]. Each layer consists in the arrangement of calixarene molecules in the typical herringbone pattern presented above. Within the layers, one of the alkyl chains of each calixarene pointing in the same direction is partially included in the adjacent macrocycle thus forming columns,

Figure 2.9. Every two columns in the same layer possess opposite orientations related by inversion center and, in **1**, they interact with adjacent layers *via* bromine-bromine interactions with d(Br···Br) = 3.92 Å, Figure 2.9. Considering this type of halogen-halogen supramolecular interactions, Desiraju and Parthasarathy have demonstrated their attractive nature in the solid state.[194] These interactions are directional and present two favorable geometries, when the angles formed by C_1-X_1···X_2-C_2 are noted $?_1(C_1\text{-}X_1\cdots X_2)$ and $?_2(X_1\cdots X_2\text{-}C_2)$, the two preferred geometries of halogen-halogen contacts correspond to $?_1 = ?_2$ (Type I) and $?_1$=180, $?_2$=90° (Type II).[195] In compound **1** both angles are equal, ?(C-Br···Br) = 69.6°, since they are related by an inversion center situated between the two bromine atoms. The distance between the two bromine atoms is slightly higher than the sum of van der Waals radii (3.70 Å)[29,196] allowing the interaction between two layers of calixarenes across the interlayer plane. In compound **2** the presence of an additional methylene in the included aliphatic chain precludes further halogen interactions and adjacent layers essentially self-assemble *via* van der Waals interactions affording similar packing efficiency as in **1**.

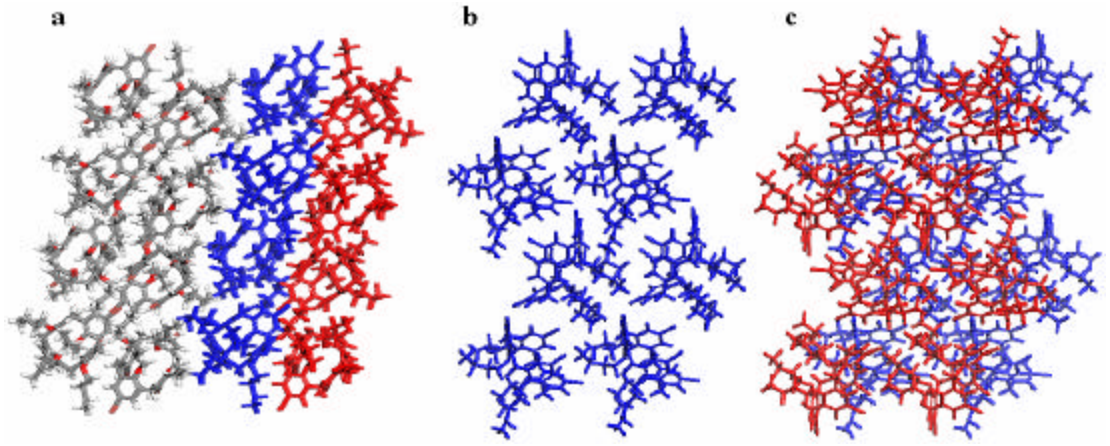

Figure 2.8. Representation of the crystal packing of compounds 1 and 2 down [001] (a) and view of one layer (b) and their superimposition (c) down [010]

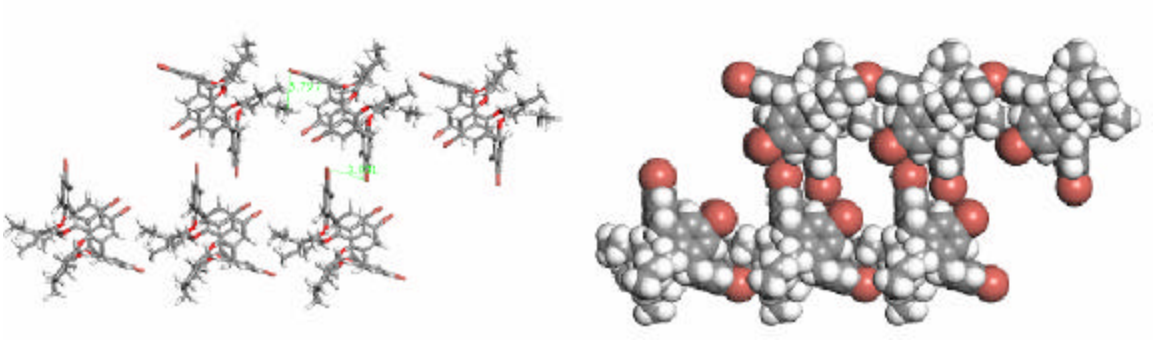

Figure 2.9. Detailed view of the interactions Br-Br between the columns of two adjacent layers observed in compound 1

When the lower rim is substituted by hexyl chains, the situation differs entirely. The calixarene molecules in compound **3** assemble in a helical motif. Each helix results from hexameric motifs of calixarenes that are sustained by strong, directional bromine-bromine interactions and aromatic edge-to-face stacking interactions. Figure 2.10. shows the resulting helical packing motif. In the crystal structure of **3**, bromine atoms of two adjacent calixarenes point towards the inside of the helix and interact with distances d(Br···Br) of 3.57 and 3.76 Å, shorter than the sum of van der Waals radii of bromine atoms,[29,196] with corresponding angles ?(C-Br_d···Br_a) = 88.12° and 88.85° and ?(C-Br_a···Br_d) = 138.00° and 158.14°, where Br_d is the donor and Br_a the acceptor bromine. Halogen interactions of this type have recently been used in the perspective of crystal engineering[195,197] but the formation of such helical architecture by self-organization of calixarene molecules has yet only been reported in the case of the presence of substituents selected for their hydrogen bonding capabilities[198] and related tubular assemblies obtained through metal-induced self-assemly of sulfonato-calixarenes.[75,82] It is should also be noted that few O-alkylated calixarenes[199,200] and resorcinarenes[201] derivatives have been reported to exhibit helical arrangements but in all cases the alkyl

chains pointed towards the axis of the helix.

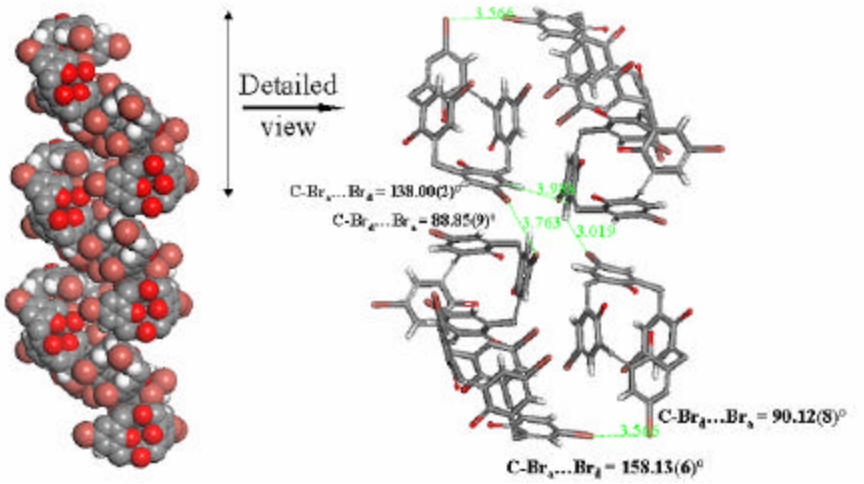

Figure 2.10. Representation of the helical motif sustained by compound 3 and detailed view of the hexamer of calixarenes forming the helix, alkyl chains are omitted for clarity

In the case of alkyl chains containing more than 6 carbon atoms functionalizing the lower rim, pseudo-amphiphilic calixarenes adopt a different type of crystalline arrangement. In particular, compounds **4** and **5** engage in a pseudo-bilayer motif, Figure 2.11. Their structures are sustained by head-to-head and edge-to-face p-p stacking interactions, with distances in a range of 3.40 to 3.70 Å, and tail-to-tail van der Waals interactions between the alkyl chains. The crystal packing of these compounds can be described as the superimposition of three non-equivalent layers parallel to [100], which pack on top of each other and spatially generate two distinct regions, aromatic and aliphatic, Figure 2.12. In two of the three layers, calixarene molecules adopt a similar herringbone pattern as that observed in compounds **1** and **2**. Every two herringbone-type layers possess opposite orientations. In the third layer, the pseudo-amphiphilic molecules exhibit an ordered bilayer motif where the alkyl chains are interdigitated within the

aliphatic region. Every three layer repeats to result in a pseudo-bilayer packing type, where the widths of the aromatic region are 7.63 and 8.00 Å and those of the aliphatic region are 8.86 and 9.43 Å for **4** and **5** respectively.

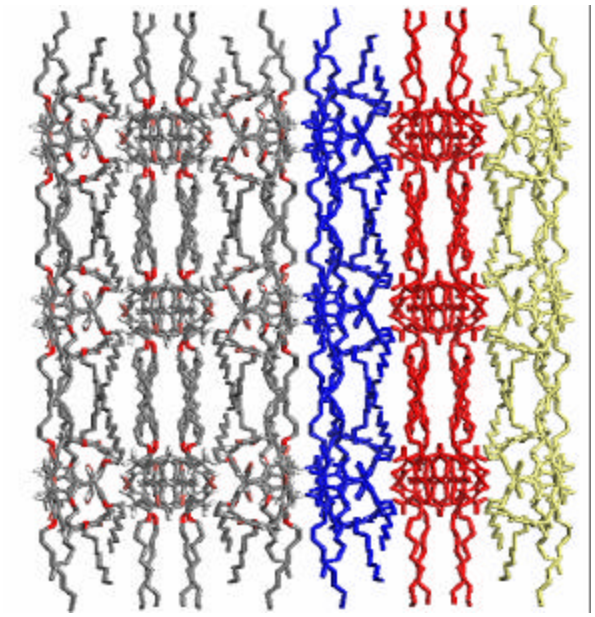

Figure 2.11. Representation of the crystal packing of compounds 4 and 5 down [001], hydrogen atoms of the alkyl chains are omitted for clarity

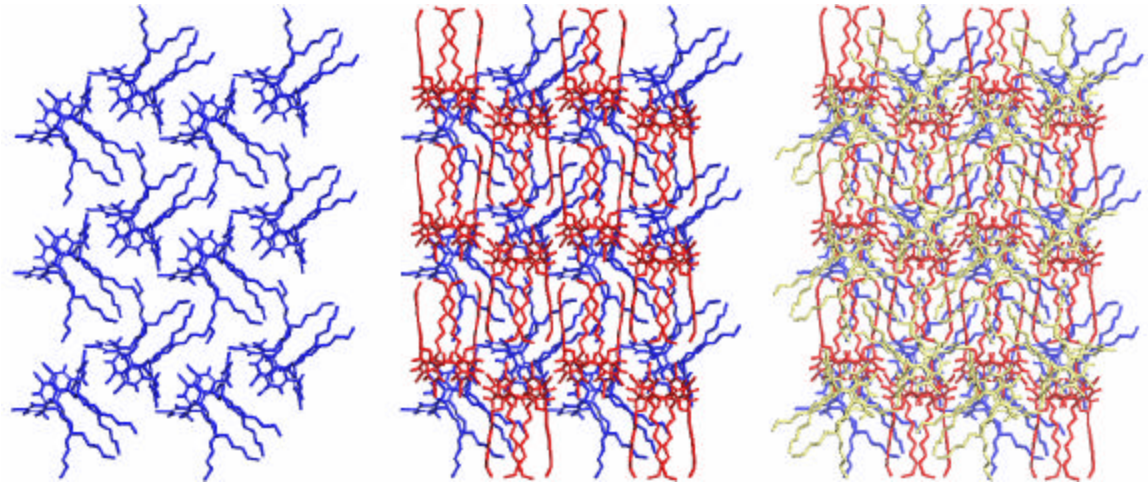

Figure 2.12. Representation of the non-equivalent layers in compounds 4 and 5 and their superimposition down [100]

In compounds **1-5**, most alkyl chains were observed to possess partial structural disorder. Such patterns are common for the presence of conformationally flexible moieties. The weak diffraction intensities observed for the crystals of calixarenes **6-8,** which possess longer alkyl substituents at the lower rim, are most likely due to the higher disorder affecting these structures.

Compound **9** crystallizes in $P2_1/c$ and presents no disorder. In the calixarene molecule of the asymmetric unit, the brominated rings present dissimilar inclinations with respect to the vertical C_2 axis of the calixarene, Table 2.4. The significant difference between the proclivities of the two unparallel rings is due to the orientation and conformation of alkyl chains. In effect, one of the four alkyl chain presents a gauche conformation of the first carbon atoms linked to the phenolic oxygen with a torsion angle of 62.3° for O-C_1-C_2-C_3 and results in the projection of the corresponding aliphatic chains toward the direction of the C_2 axis of the calixarene, this projection causes a decrease in the inclination (-4.3°) of the aryl unit bearing the alkyl chain, which presents the gauche conformation, while the adjacent aromatic ring exhibits a higher proclivity with respect to the axis of the calixarene. The alkyl chains are not parallel but present a slight curvature with respect to the C_2 axis of the macrocycle, Figure 2.13.

Figure 2.14 shows the spatial arrangement of **9**, which forms well ordered bilayers, in which the alkyl chains are tilted in one direction, down [010] of *ca.* 19.1° with regard to the axis perpendicular to the bilayer. This compares to the values of 45° found in the series of amphiphilic *para*-acyl-calixarenes[184] and the typical tilt angle of 28° for the aliphatic chains in phospholipids.[202]

In the crystal structure of **9**, the alkyl chains are deeply interdigitated, Figure 2.14, the width of the aromatic layer is *ca.* 4.00 Å when the length of the alkyl chain is *ca.* 14.5 Å (such values are those of the distances perpendicular to the bilayer axis). The positions of the alkyl chains are very well defined due to the tight van der Waals interactions between the chains with shortest distances between the hydrogen atoms of alkyl chains of two calixarenes in a range of 2.32-2.50 Å. The overall length of each alkyl chain in **9** is d(O···C) = 15.1 Å (between the phenolic oxygen and the corresponding carbon of the terminal methyl) while the overall bilayer thickness is 18.5 Å. The curvature of the chains leads to a flattened oblique structure down [010]. It should be noted that such a result is comparable to the crystal structure of the amphiphilic crown ether, N,N-didodecyldiaza-18crown-6, reported in the work of Gokel,[203] where the C_{12} chains presented similar interdigitation generating a very compact bilayer motif.

The bilayer structure of compound **9** is also sustained by head-to-head interactions between calixarene molecules. These interactions are stabilized by bromine-bromine interactions with d(Br_d···Br_a) = 3.90 Å and corresponding angles ?(C-Br_d···Br_a) = 91.6° and ?(C-Br_a···Br_d) = 139°. These Type II halogen-halogen contacts allow the interaction between calixarenes, which adopt a non-parallel orientation of the flattened cones, across the interlayer plane. Finally non-included molecules of acetone solvent, which do not participate in the overall crystal packing, were found within the voids of the aromatic layer.

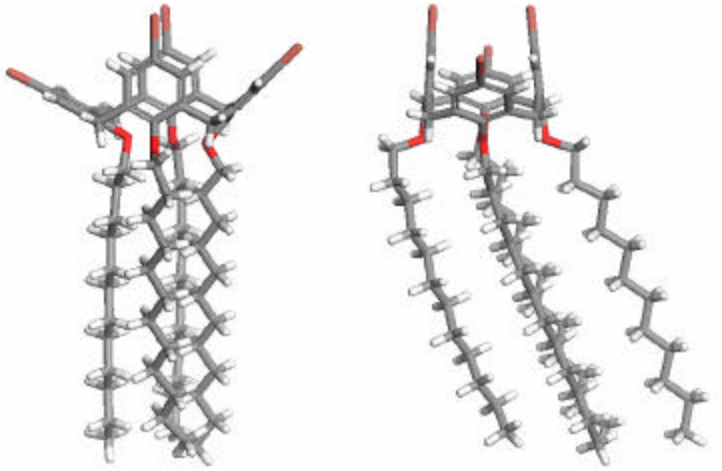

Figure 2.13. Representation of the molecular structure of *para*-Br-tetra-O-dodecyl-calix-4-arene in compound 9

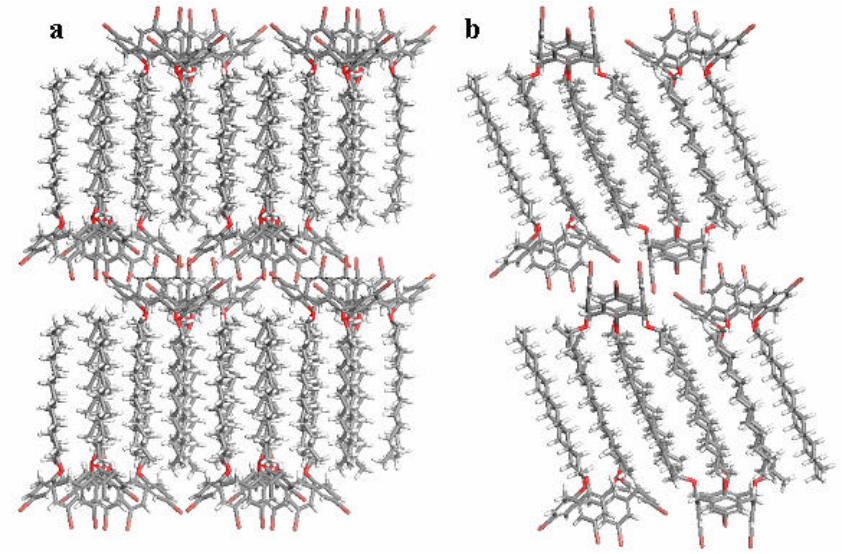

Figure 2.14. Representation of the crystal packing of compound 9 down [001] (a) and [010] (b)

In summary, general trends can be delineated from this study where increasing the length of the aliphatic part of a series of pseudo-amphiphilic calix-4-arenes has resulted in the evolution of their self-assembly from herringbone type layers for **1** and **2** to a highly ordered bilayer system in **9** with intermediates that corresponded to a hybrid between the two motifs, observed in the pseudo-bilayer systems sustained by the structures of compounds **4** and **5**. These results have demonstrated that rational

modification of the building units can afford the possibility of controlling the crystalline architecture and may be important towards the design of supramolecular materials based upon such pseudo-amphiphilic molecules. Of particular interest, the helical assembly based upon hexameric units of calixarenes that resembles a macrocycle, generated in the structure of **3**, constitutes a very novel and interesting structure, transition between the bilayer[83] and the tubular[82] types of structures previously described as relevant motifs adopted by typical amphiphilic calix-4-arene molecules.

2.4.2. Influence upon the crystal packing through variation at the upper rim

The second part of this study consists in examining the systematic variation of upper rim functionalities in the particular case of calix-4-arenes substituted by O-hexyl chains at the lower rim. The crystal structures resulting from selective functionalization at the *para*-positions with 2Br + 2H, 4H, 4*t*Bu have to be associated with the structure of compound **3** in the perspective of evaluating the effect of such directing agents upon the self-assembly of these molecules.

Treating the molecular level of these systems, Figure 2.15 and Table 2.5 show that the four calixarene derivatives adopt the expected flattened cone conformation due to the O-hexyl tetrasubstitution at the lower rim. However, the presence of large, polarizable, electronegative substituents at the upper rim additionally affects the usual C_2 symmetry as illustrated by compounds **3** and **10** possessing bromine substituents, which induce higher inclination of the two farthest opposite rims.

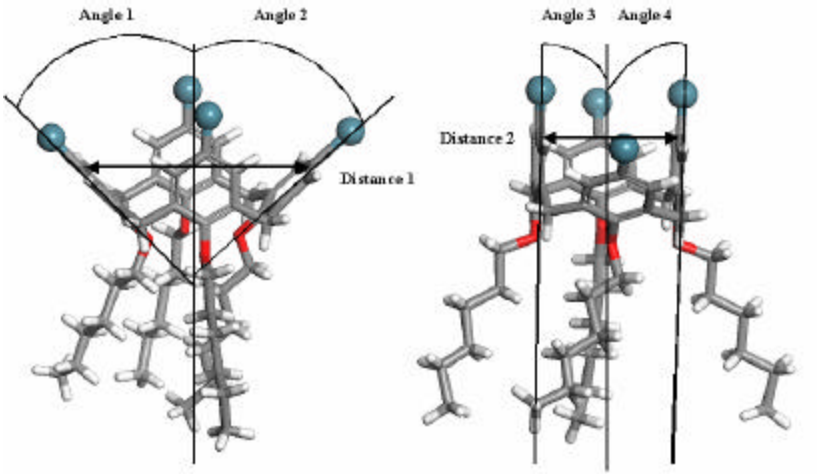

Figure 2.15. Representation of the flattened cone conformation observed in O-hexyl-calix-4-arenes derivatives and designation of the distances and angles used to describe their geometry

Table 2.5. Ring inclination angles and corresponding distances between opposite aryl groups in the crystal structures of compounds 3 and 10-12

Compound	Angle 1 (°)	Angle 2 (°)	Angle 3 (°)	Angle 4 (°)	Distance 1 (Å)	Distance 2 (Å)
3	61.6	52.7	-14.7	-5.47	10.1	4.32
10	54.6	53.7	-7.85	-2.85	9.90	4.82
11	48.5	41.6	2.01	0.62	9.44	5.35
12	48.7	43.3	-4.84	-0.53	9.53	5.24

In the case of introduction of two bromine substituents at the opposite upper rims in compound **10**, the presence of functionalities inducing electrostatic interactions results in a strongly organized bilayer arrangement of the calixarenes molecules governed by halogen-halogen interactions between dibrominated calixarenes in association with hydrophobic interactions between the alkyl chains, Figure 2.16.

Interestingly, two phases of the structure of the dibrominated derivative were observed at -73°C (LT), **10a**, and at 25°C (RT), **10b**. They exhibit similar crystal packing sustained by head-to-head aromatic and Br-Br interactions and tail-to-tail van der Waals

interactions with a slightly more ordered situation in the structure collected at room temperature.

The head-to-head interactions are stabilized by edge-to-face aromatic interactions with d(C···Ar) = 3.77 to 3.83 Å (LT) and 3.80 to 3.85 Å (RT) and by bromine-bromine interactions, d(Br···Br) = 3.89 (LT) to 4.11(RT) Å, ?(C-Br···Br) = 77.2° and 151° (LT) and 80.2° and 149° (RT), Figure 2.17. These values diverge from the Type II situation classified by Desiraju and Parthasarathy and the distance between the two bromine atoms is slightly higher than the sum of van der Waals radii. The bromine-bromine interactions between opposite rims in compound **10b** are equivalent since they are related by inversion. The non-parallel orientation of the calixarene molecules is essentially governed by edge-to-face p-p stacking between adjacent calixarene molecules positioned at the same side of the bilayer with distances ranging from 3.76 to 3.81 Å. In the bilayer structure of **10**, the alkyl chains are not interdigitated, the widths of the aromatic layers are 6.90 Å (LT) and 7.86 Å (RT), the lengths of the alkyl layers are 13.1 Å (LT) and 11.2 Å (RT), these values are those of the distances perpendicular to the bilayer axis. Along the *y*-axis, the dimensions between calixarenes expand by 0.36 Å from 25°C to -73°C. The expansions/contractions in the dimensions of the crystalline assembly are reversible through several heating/cooling cycles.

The two crystalline phases are not liquid crystals under the true definition of a liquid crystal since there is not enough disorder; however, they correspond to a non-standard type of matter that may be classified as a type of crystalline liquid crystal where the chains form a fluid domain and the calixarene rims the rigid part.

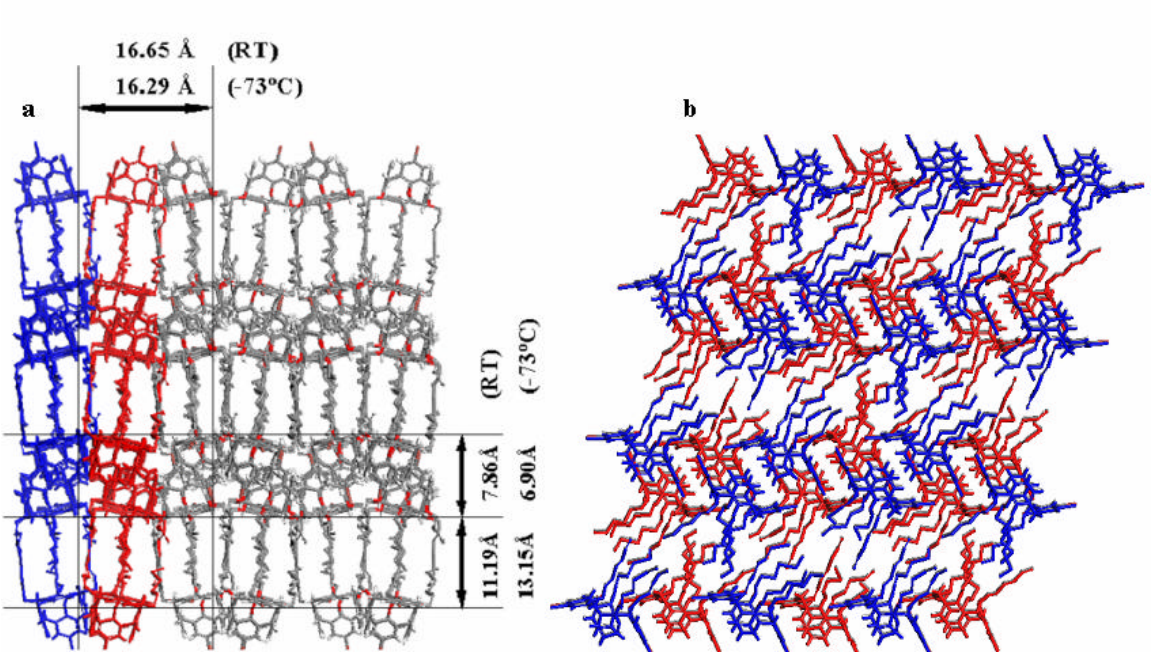

Figure 2.16. Representation of the crystal packing of compound 10 down [001] (a) and down [010] (b), hydrogen atoms of the alkyl chains are omitted for clarity

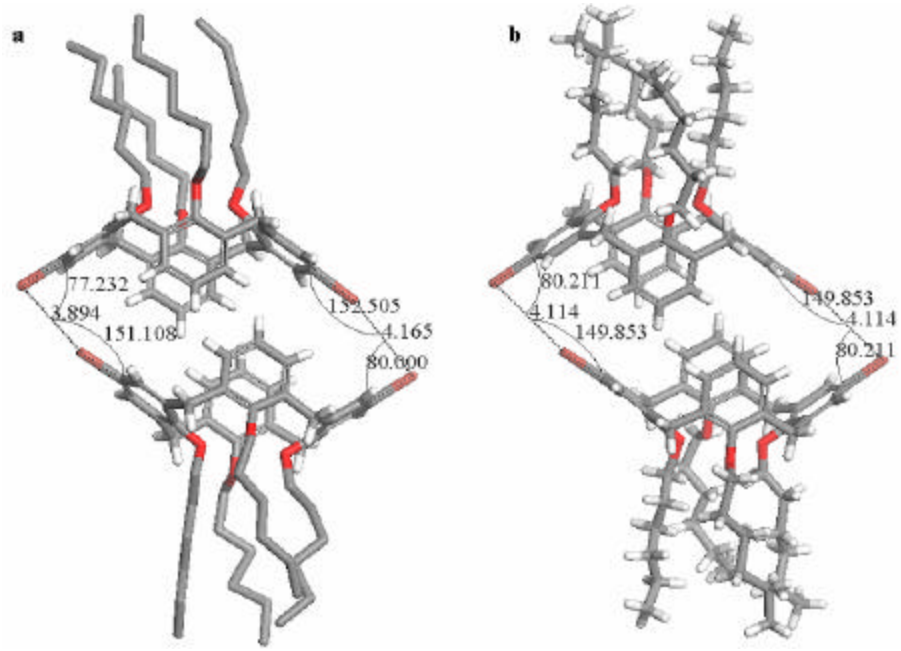

Figure 2.17. Detailed view of the Br-Br interactions in compound 10a (a) and 10b (b)

In the *para*-H system, **11**, Figure 2.18, the overall supramolecular arrangement is sustained by face-to-face, d(C···C) = 3.65 Å, and edge-to-face, d(C···C) = 3.93 to 3.99 Å, aromatic stacking interactions between the upper rims of two opposite calixarene cones that are twisted of *ca.* 90° with each other and between the rings of adjacent molecules that are slightly slipped in the *z*-direction of 4.64 Å. This molecular organization results in the formation of a rippled bilayer system that is additionally stabilized by weak van der Waals interactions within the layers of non-interdigitated alkyl chains with distances between the hydrogen atom centers in a range of 2.55 to 3.45 Å. In the rippled bilayer system of **11**, the widths of the undulated aromatic and aliphatic layers are *ca.* 9.98 Å and *ca.* 11.1 Å respectively.

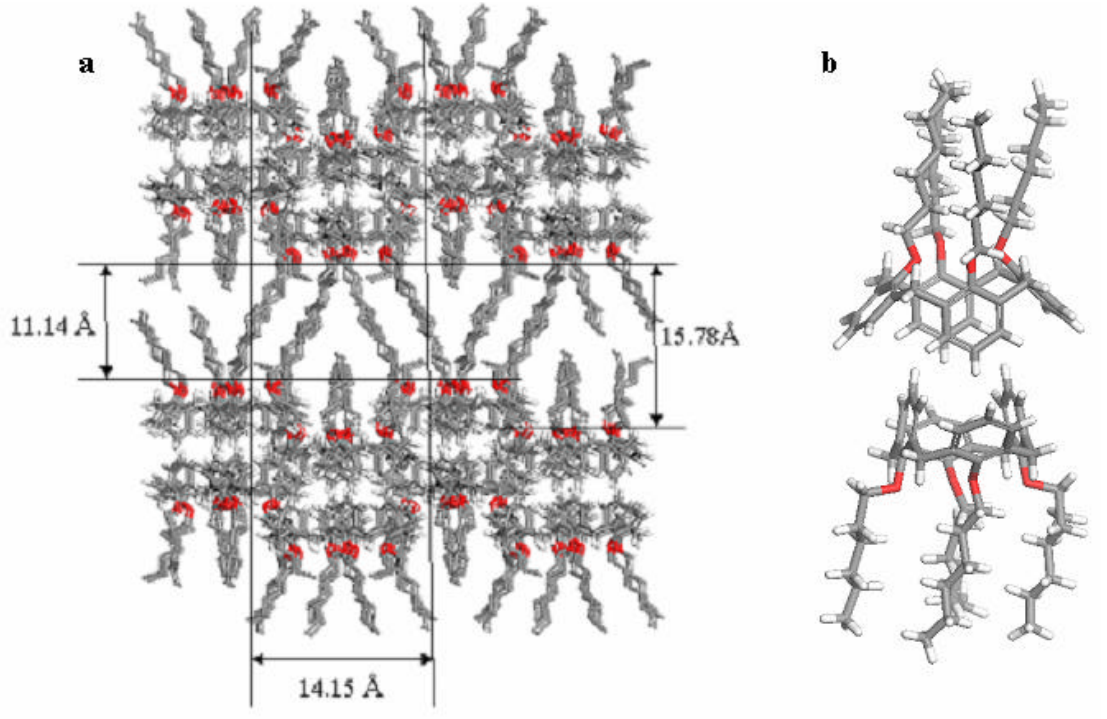

Figure 2.18. Representation of the crystal packing of compound 11 down [010] (a), hydrogen atoms of the alkyl chains are omitted for clarity, and detailed view of the head-to-head aromatic stacking interactions (b)

The presence of bulky groups such as *tert*-butyl in compound **12** disrupts the common head-to-head/tail-to-tail spatial arrangement sustained by the model compound *para*-H-O-hexyl-calix-4-arene, **11**. Figure 2.19 illustrates how the steric constraints induced by the additional bulky groups *t*Bu in association with the hydrophobic interactions between the different alkyl groups result in a disordered layered packing motif where the aromatic stacking interactions are now impossible and substituted by weak van der Waals interactions between the methyl of the bulky groups and the alkyl chains with interatomic distances H···H in a range of 2.28 to 2.71 Å.

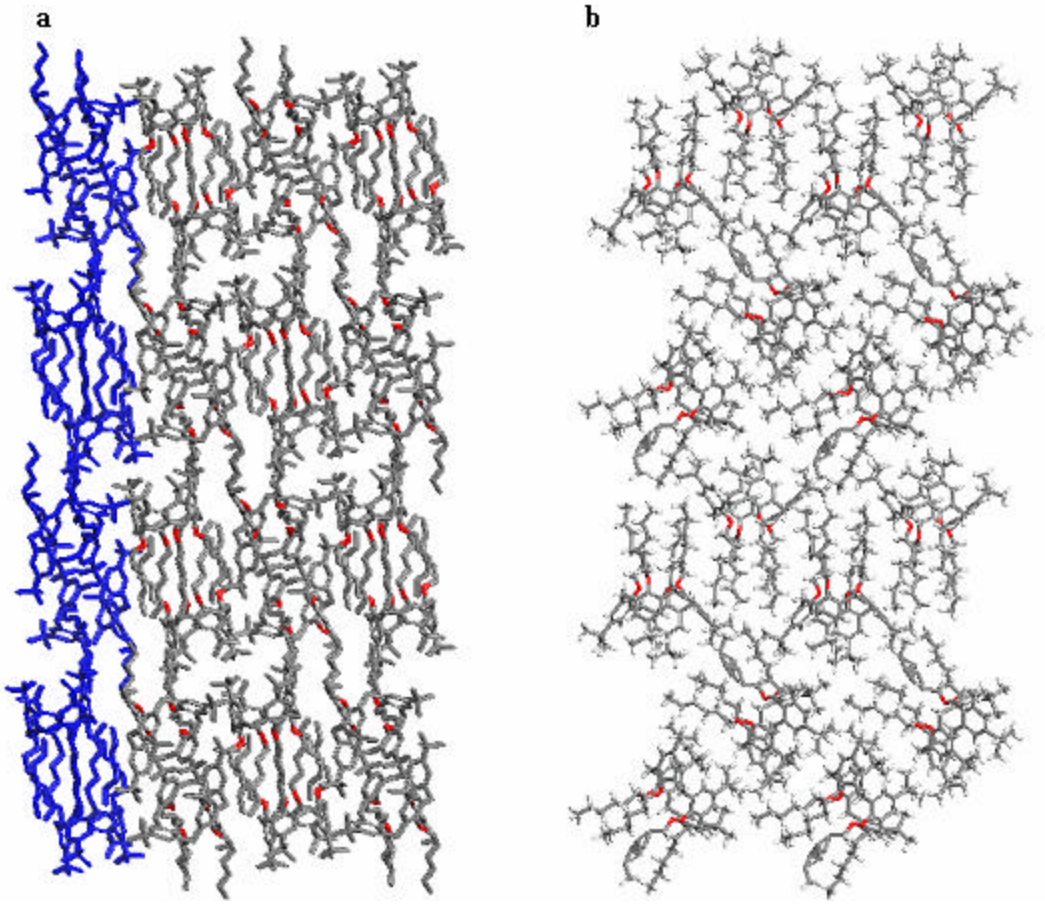

Figure 2.19. Representation of the crystal packing of compound 12 down [010] (a) and [100] (b)

The three-dimensional arrangement of **12** can be described as the superimposition of two non-equivalent layers that repeat along the *x*-direction. In each layer the calixarenes adopt alternate arrangements based upon the herringbone motif due to steric hindrance and van der Waals repulsion between the bulky substituents *tert*-butyl and a bilayer-type assembly caused by the partial pseudo-amphiphilic effect of the alkyl chains, Figure 2.19b. Such crystal packing constitutes a hybrid situation between the herringbone and bilayer types resulting from the presence of two opposing directing substituents at the upper and lower rims of the calixarenes.

The structures generated by the four pseudo-amphiphilic calixarene derivatives **3**, **10, 11** and **12** are controlled by the synergy between intermolecular forces at the upper rim, the varying strength of the van der Waals forces between the pendant alkyl chains and the steric constraints induced by these alkyl chains. When one of these factors dominates, simple packing motifs occur. For example with long chain substituents and only weak aromatic interactions at the upper rim (*e.g. p*-H tetra-substitution) a rippled bilayer system is favored. When there is a balance between the forces, more or less simple motifs predominate: steric effect of the *t*Bu groups and halogen-halogen interactions between dibrominated calixarenes in association with the hydrophobic interactions between the alkyl chains afford a disrupted bilayer and a strongly organized bilayer, respectively. However in situations where there is imbalance between the controlling forces (*i.e.* bromine-bromine interactions along with an increase of the molecular dipole moment) complex packing motifs are observed. In this particular case, the resulting helical packing motif of the corresponding tetrabromo-substituted molecules

is sustained by highly orientated Br-Br interactions between 6 calixarenes.

2.5. Conclusions

Structural study of the 12 compounds presented herein has demonstrated that it is possible to control the formation of specific structural motifs, for instance the bilayer-type crystal packing, through the use of appropriately modified pseudo-amphiphilic calix-4-arene with respect to the chain length at the lower rim and the functionality at the *para*-positions. Such an understanding of the principles controlling the self-assembly of calixarenes in the solid state might lead to the rational design of new classes of materials. Selective functionalization and exploitation of interactions in calixarene systems should develop and expand their applications in a variety of domains such as physics (optics, electronics), material science (sensors, surfaces), catalysis or biomimetics.

Of particular note, the auto-organizing properties of compounds **9** and **10**, resulting from the cooperative combination of oriented brominated head groups and the presence of alkyl chains of selective lengths capable of forming a tightly packed hydrophobic layer in **9** or a softer expandable aliphatic region in **10**, may lead to broader perspectives towards the rational design of tunable supramolecular amphiphilic or pseudo-amphiphilic systems possessing the ability to self-assemble at interfaces. Incorporation of a variety of functional groups selected for their intrinsic properties (polarity, magnetism, etc.) or variation of the size of the macrocycle (calix-6, calix-8-arenes) may allow this class of supramolecular materials to be widely applicable.

One can also find potential advantages resulting from the logical progression observed in the crystalline organizations that are adjustable through a limited set of

supramolecular parameters. Specifically, the transition between the helical motif of compound **3** and the pseudo-bilayer or bilayer organizations of **4** and **10** resulting from little molecular variation of the building units represents a significant outcome that is particularly relevant to supramolecular and crystal engineering strategies. Expansion of this study to a wider range of conditions during crystallization or to the use of closely related calixarene derivatives may enable switching between such structural motifs and afford supramolecular diversity in systems that could be comparable, to some extent, to the polymorphic phases of amphiphilic biomolecules.

Chapter 3

Metal-Organic Networks based upon organic ligands containing two types of functionality: Supramolecular isomerism and Functionalization

3.1. Introduction

3.1.1. Metal-Organic Networks based upon pyridinecarboxylate ligands

Supramolecular chemistry provides a successful approach to the self-assembly of simple molecular building units preselected for their complementary geometrical and binding capabilities.[23] In particular, the rational design of supramolecular architectures based upon metal coordination geometries and multifunctional organic ligands has led to a variety of coordination polymers with predictable network architectures.[60,66,204-207] An important outcome of this approach is represented by the structural diversity in metal-organic networks that can occur through the existence of phenomena such as interpenetration[122,123] or supramolecular isomerism[93,208] and it is thereby possible to generate a wide range of structures from even simple ligands and known chromophores. In such a context, *m*-pyridinecarboxylates represent readily available ligands that have already been shown to be capable of generating coordination polymer networks that exhibit properties such as polarity,[209-212] porosity[213-216] or magnetism.[217-221]

Typical *m*-pyridinecarboxylates are angular ligands resulting from deprotonation of pyridine-3-carboxylic acid (nicotinic acid) or pyridine-3,5-dicarboxylic acid (dinicotinic acid), Figure 3.1, and contain concomitantly anionic carboxylate and neutral N-donor functionalities. These ligands can be seen as hybrid molecules that possess the coordination capability of both functionalities. Specifically metal-organic networks can be strategically constructed using such unsymmetrical difunctional ligands *via* a thorough understanding of the topological features of the numerous structures resulting from the use of linkers containing one type of coordination site, *e.g.* 4,4'-bipyridine[66,89-92,99-101,222] or benzene dicarboxylate,[95,206,223-237] with respect to chemical composition and propensity of the chromophore coordination geometry. However, considering the intrinsic asymmetry present in *m*-pyridinecarboxylate ligands, there is a range of opportunities for the variation of the network connectivity pattern and therefore a higher degree of structural diversity is expected.

Another outcome of the use of such ligands is the expectation that the resulting infinite networks may provide novel materials possessing zeolitic or clay-like features related to the 3D[213-215,238,239] or 2D[209,211,240-242] host-guest compounds that can be generated from metal-organic self-assembly in presence of guest molecules in addition to the potential properties such as chirality[209,243] due to the use of unsymmetrical ligands.

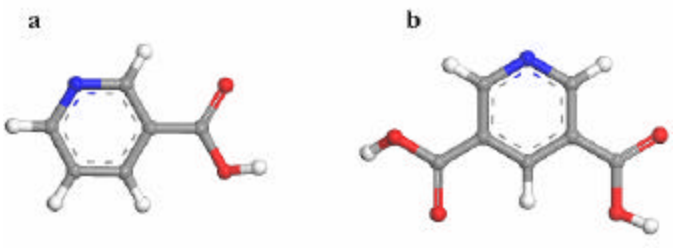

Figure 3.1. Representation of the ligands nicotinic acid (a) and dinicotinic acid (b)

3.1.2. Network topologies

Prior reports have already shown that the use of a ligand possessing two different functional groups as simple as nicotinate has allowed the construction of non-centrosymmetric structures with optical properties.[210-212,244] Most of these networks can easily be described as 2D clay-like type networks, square or rhombus grids, or 3D zeolite type networks, diamondoid or pillared sheets; however, certain results have shown that the introduction of a supplementary function generates more complex metal-organic networks.[214] In this regard, consideration of the network topology represents a convenient tool for the comparison of multi-dimensional structures where the metal centers constitute the nodes of the network and the organic ligands their connecting links. A metal-organic network can thus be defined by its circuit notation $n^p = n_1.n_2\ldots n_p$, where n_p represents the series of n-gons meeting at each node, all node being equivalent.[245] For example, a 2D square grid is a 4.4.4.4 = 4^4 network since one node defines 4 circuits going through 4 adjacent nodes to join itself in a circuit; in a similar manner, a 3D diamondoid structure can be described as a 6^6 network. For more complex 3D nets, there may be more than one type of circuit starting out from one node, the corresponding circuit notation used is $n^p m^q$ in which p n-gons and q m-gons meet at each node. For example, the topologies of well-known lattices of inorganic materials such as NbO,[88] $CdSO_4$[246] or PtS[245] can be simplified by the representation of the connectivity of their nodes corresponding to the center of each element or ionic species. These three networks are all based upon 4-connected nodes and their circuit notations are $6^4.8^2$, $6^5.8$ and $4^2.8^4$ respectively, Figure 3.2. It is interesting to note that the five network topologies presented

herein possess the same stoichiometry 1:2 of node with respect to the links that connect them.

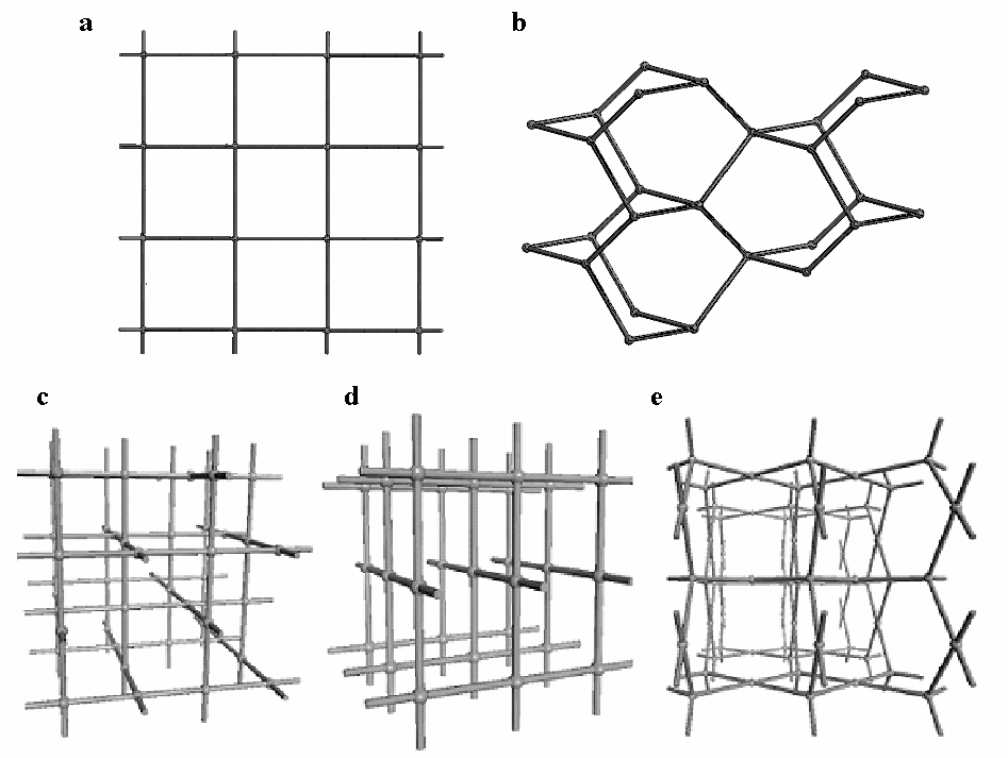

Figure 3.2. Network topologies of the 2D square grid, 4^4 (a), 3D diamondoid, 6^6 (b), NbO, $6^4.8^2$ (c), $CdSO_4$, $6^5.8$ (d) and PtS $4^2.8^4$ (e)

The knowledge of network topology of complex metal-organic networks is relevant not only in the perspective of describing and comparing coordination polymers but also towards the prediction of structures and supramolecular isomers that can be generated from molecular building units thus reduced to their geometrical counterparts. However, if the organic difunctional ligand is easily simplified, particular attention should be devoted to the coordination geometry that can be adopted by the node metal center, which constitutes the critical variable towards generation of specific topologies.

3.2. Zn and Cu Coordination Nodes: a Database Study

Zn(II) centers generally exhibit tetrahedral coordination[88] and, as revealed by Figure 3.3, can in appropriate circumstances serve as pseudo square planar nodes. Therefore, coordination of an angular bifunctional ligand, *e.g.* nicotinate, to a tetrahedral Zn(II) ion can result in a 4^4 (square grid) network, Figure 3.3c. Indeed, [Zn(nicotinate)$_2$], **A**, exhibits such toplogy,[209,211] Figure 3.4. However, as seen above, there are other possible topologies that are based solely upon square planar nodes: the 3D networks NbO ($6^4.8^2$)[88] and $CdSO_4$ ($6^5.8$).[246] It should also be noted that PtS exhibits ($4^2.8^4$)[245] topology but it is sustained by both square planar and tetrahedral nodes in a 1:1 ratio. In this regard, a hydrogen-bonded network[247] and a metal-organic network[248] solely based upon a square planar geometry of the nodes with $4^2.8^4$ topology have been recently reported.

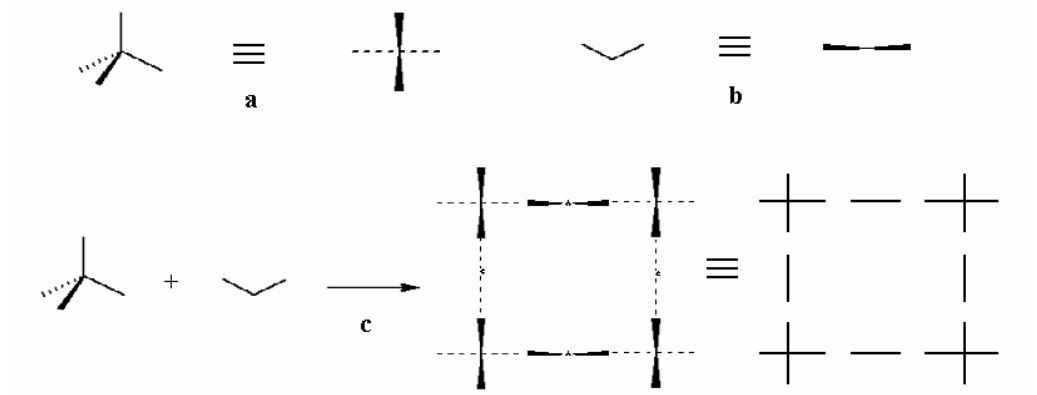

Figure 3.3. A tetrahedral node projected down the 2-fold axis affording a pseudo square planar geometry (a), a projection of an angular spacer (b), a projection of a four-connected circuit from tetrahedral nodes and angular spacers (c)

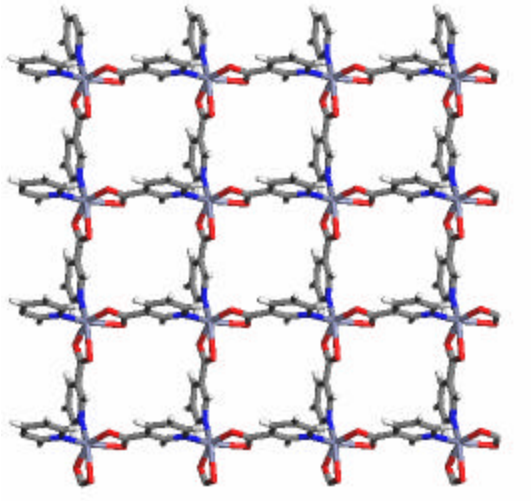

Figure 3.4. Crystal structure of the square grid $[Zn(nicotinate)_2]_n$, A

Clearly the specifics in terms of topological features and coordination propensity represent important elements towards the rationalization of the diversity of coordination network structures that can result from a given set of molecular components. Accordingly, a structural analysis of the geometrical preferences determined from a survey of the structures reported in the literature that contain the metal centers considered in this study may reveal of interest towards developing an understanding of the factors affecting supramolecular control.

The coordination of Zn(II) with two different functionalities N-donor and carboxylate has generated two types of 4-connected nodes, in which the carboxylate function can adopt monodentate or bidentate coordination to metal center, Figure 3.5. A survey of the CSD revealed that out of 45 non-equivalent nodes containing the mononuclear Zn center coordinated to two nitrogen donor and two oxygen carboxylate, 14 exhibit the bidentate coordination mode of the carboxylate moieties and 31 the monodentate mode. In all coordination compounds, the Zn-N distances range between

1.90 and 2.22 Å with an average of 2.06 Å (standard deviation s = 0.04). For the Zn-O distances, Figure 3.6 illustrates the two types of coordination modes. The distances corresponding to the bidentate carboxylate moities range between 2.01 and 2.43 Å with an average of 2.19 Å (s = 0.12); while the distances between Zn and bonded oxygen in the monodentate mode vary between 1.84 and 2.03 Å (average 1.96 Å, s = 0.03). For the non-bonded oxygen, in the monodentate coordination mode, values of d(Zn-O) above 3.5 Å have been proven to be outliers (with 90% confidence that those values can be rejected based on Q-testing) so the corresponding distances Zn-O effectively limit to the range 2.6-3.0 Å for 80% of confidence level, s = 0.125.

It should be noted that only 17 structures are polymeric, most of them afford the diamondoid topology based upon tetrahedral nodes.[249] However the infinite networks generated from the connectivity of pseudo square planar nodes of Zn(II) present the typical *cis*-coordination of the N-donor and carboxylate function around the metal center,[209] Figure 3.4.

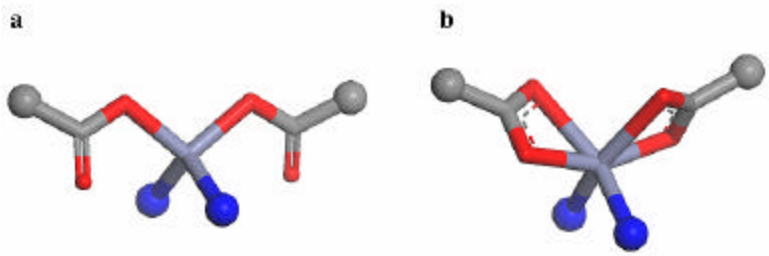

Figure 3.5. Representation of the two coordination geometries resulting from coordination of tetrahedral mononuclear Zn(II) with the two different functionalities N-donor and monodentate (a) or bidentate (b) carboxylate

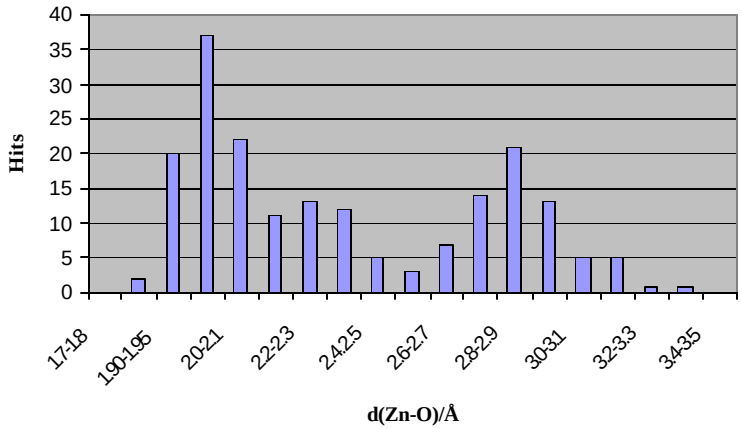

Figure 3.6. Histogram showing the distribution of Zn-O distances among the structures containing the mononuclear Zn in coordination with two functionalities N-donor and carboxylate

A similar study of Cu(II) chromophores shows that their coordination capabilities are more versatile since they can exhibit square planar, tetrahedral, square pyramidal or octahedral coordination,[88] Figure 3.7. The coordination of a mononuclear Cu(II) with two different functionalities N-donor and carboxylate has hitherto generated 277 non-equivalent chromophores: 99 chromophores contain a 4-coordinate metal center, 92 are 5-coordinate and 86 are 6-coordinate. In all coordination compounds, the Cu-N distances range between 1.92 and 2.40 Å with an average of 2.03 Å (standard deviation s = 0.07). The distribution of Cu-O distances is shown in Figure 3.8. The narrow region corresponding to distances inferior than 2.30 Å represents the coordination metal-oxygen, while the broad repartition of d(Cu-O) above 2.30 Å may be divided in two distinct regions corresponding to different geometries adopted by the carboxylate group around the metal center. The shortest distances corresponding to the bonded oxygen of the carboxylate moieties in a tetrahedral geometry and these positioned in the equatorial plane of the transition metal range between 1.88 and 2.24 Å with an average of 1.97 Å (s

= 0.05). For the secondary oxygen, the separate study of 4-, 5- and 6-coordinate reveals interesting trends. In effect, the non-coordinated oxygen atoms of 4-coordinate chromophore present a higher occurrence in the range 2.55 to 2.80 Å (average at 2.78 Å), these of 5-coordinate Cu were in higher proportion between 3.00 and 3.30 Å (average at 3.06 Å). The 6-coordinate tetrahedral or octahedral chromophores present both maxima. Careful analysis of the other parameters of the different structural types reveals that the difference does not only correspond to the difference in binding of the two oxygen of each carboxylate group, there is more monodentate character in the carboxylate of 5- and 6-coordinate chromophores and more bidentate character in the carboxylate of 4-coordinate and tetrahedral chromophores; the Cu-O distances are also representative, to some extent, of the position of the oxygen with respect to the octahedral or square pyramidal coordination sphere of the metal center so the statistic data illustrates as well the common axial elongation along the fourfold axis of the octahedron observed in Cu(II) "4+2" coordinated chromophores.[88]

It should be noted that the relative orientation of the two types of ligands around the metal node is relatively homogeneous between *cis*- and *trans*-configurations (*ca.* 35% and 65% respectively). However, examination of the 49 infinite network structures provides significant insight concerning these tendencies. The coordination of polyfunctional ligands generally favorizes the *trans* configuration of square planar nodes as exemplified by the 2D square grid of $[Cu(isonicotinate)_2]_n$ represented in Figure 3.9 unless one type of coordinating group acts as chelating agent resulting in the alternative *cis*-configuration.

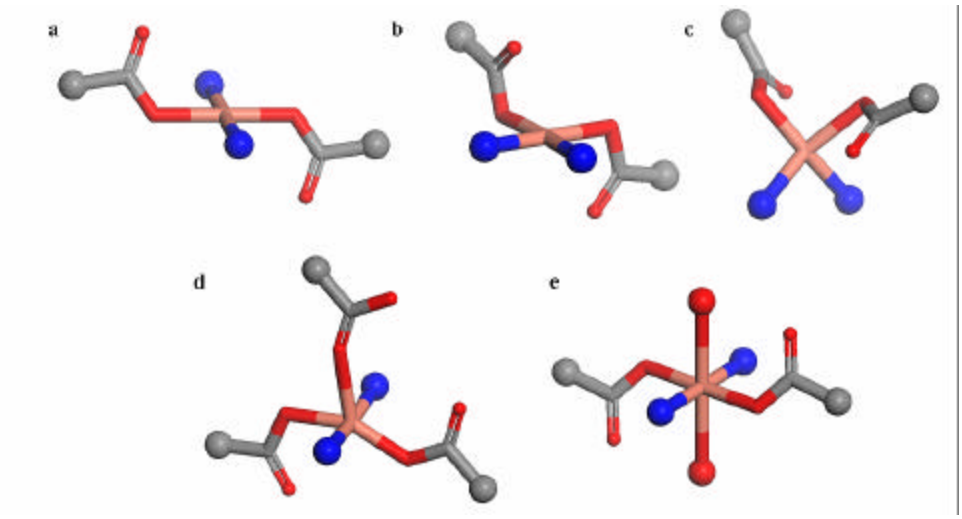

Figure 3.7. Representation of the chromophores of mononuclear Cu(II) containing the two functionalities N-donor and carboxylate: 4-coordinate *trans* square planar (a), *cis* square planar (b), tetrahedral (c), 5-coordinate square pyramidal (d) and 6-coordinate octahedral (e)

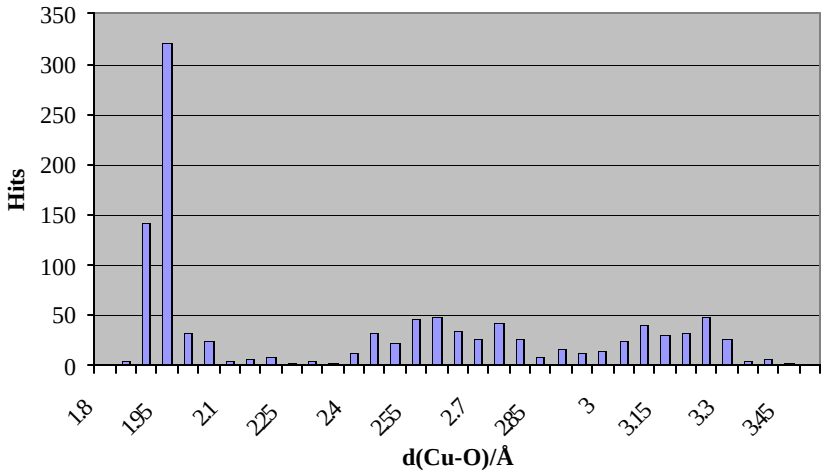

Figure 3.8. Histogram showing the distribution of Cu-O distances among the structures containing the chromophore mononuclear Cu in coordination with two functionalities N-donor and carboxylate

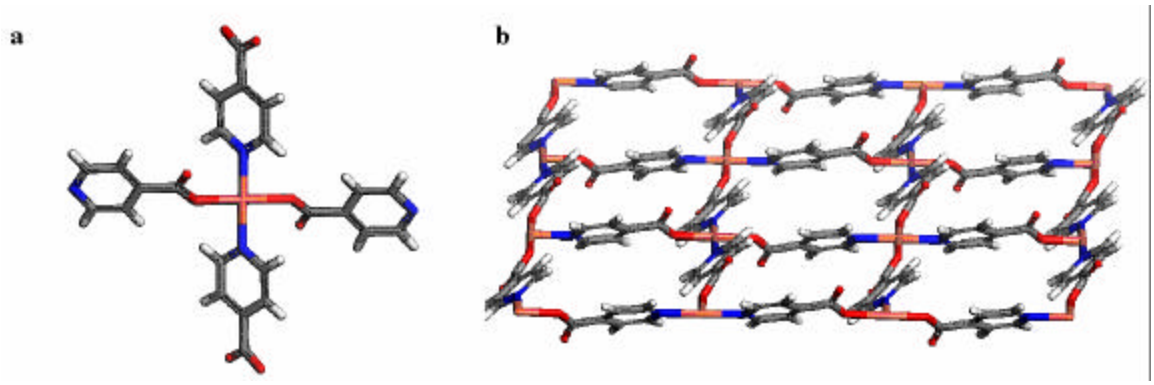

Figure 3.9. Representation of the *trans*-configuration adopted by the Cu(II) chromophore (a) in the structure of $[Cu(isonicotinate)_2]_n$ (b) (unpublished results)

3.3. Experimental

3.3.1. Materials and Methods

Each synthesis was conducted using materials as received from chemical sources (Sigma-Aldrich or Fischer Scientific); solvent methanol was purified and dried according to standard methods.[250] IR spectra were recorded on a Nicolet Avatar 320 FT-IR spectrometer. Thermogravimetric analysis was performed under nitrogen at a scan speed of 4ºC/min on a TA Instrument TGA 2950 Hi-Res. XRPD data were recorded on a Rigaku RU15 diffractometer at 30kV, 15mA for $Cu_{K\alpha}$ (? = 1.5418 Å), with a scan speed of 2°/min and a step size of 0.02° in 2? at room temperature. The crystals of all compounds were shown to be representative of the bulk by comparison of the XRPD patterns of the fresh samples with the corresponding patterns calculated from the crystal structures. The simulated XRPD patterns were produced using Materials Studio program package (Accelrys, Inc., © 2002) and Powder Cell for Windows Version 2.3 (programmed by W. Kraus and G. Nolze, BAM Berlin, © 1999). FT-IR spectra, TGA

traces and XRPD patterns of all compounds are presented in appendices C1-C5.

3.3.2. Syntheses

Synthesis of {[Zn(nicotinate)$_2$]·CH$_3$OH·2H$_2$O}$_n$, ***13***[251]

A methanolic solution of Zn(NO$_3$)·6H$_2$O (0.149 g, 0.500 mmol) was carefully layered onto a methanolic solution of nicotinic acid (0.123 g, 1.00 mmol), pyridine (0.079 g, 1.00 mmol) and toluene (3.00 ml, 28.0 mmol) under ambiant conditions. The solution was left undisturbed for 48h and colorless crystals of **13** (0.112 g, 0.303 mmol, 60.5 %) formed at the interlayer boundary in addition to a white precipitate (0.060 g, 0.193 mmol, 38.7 %) that was characterized by x-ray powder diffraction to be the square grid {[Zn(nicotinate)$_2$]}$_n$ synthesized by W.B. Lin in 1998.[209]

Synthesis of {[Zn(nicotinate)$_2$]·C$_{10}$H$_8$}$_n$, ***14***[251]

Compound **14** was prepared in a similar manner as **13** with naphthalene, (640 mg, 5.00 mmol) instead of toluene dissolved in the solution of nicotinic acid and pyridine. After 1 month colorless crystals of **14** (0.015 g, 0.034 mmol, 6.9 %) were collected from the mother liquor by physical separation.

Synthesis of {[Zn(nicotinate)$_2$]·2C$_6$H$_5$NO$_2$}$_n$, ***15***[251]

Compound **15** was prepared in a similar manner as **13** with nitrobenzene, (3.00 ml, 29.0 mmol), instead of toluene dissolved in the solution of nicotinic acid and pyridine. After 9 months, colorless crystals of **15** (0.119 g, 0.214 mmol, 42.8 %) were collected from the mother liquor by physical separation.

*Synthesis of {[Cu(nicotinate)$_2$(CH$_3$OH)$_2$}$_n$, **16***

A solution of nicotinic acid (0.123 g, 1.00 mmol) dissolved in 10 ml methanol was layered onto a solution of $Cu(NO_3)_2 \cdot 2.5H_2O$ (0.116 g, 0.50 mmol) dissolved in 10 ml methanol. Dark blue crystals of **16** (0.128 g, 0.344 mmol, 68.8%) formed at the interlayer boundary after 1 day.

*Synthesis of {[Cu(dinicotinate)$_2$·1CH$_3$OH·1H$_2$O}$_n$, **17***

A methanolic solution of 3,5-pyridinedicarboxylic acid (dinicotinic acid) (0.167 mg, 1 mmol) was layered onto a solution of $Cu(NO_3)_2 \cdot 2.5H_2O$ (0.116 mg, 0.5 mmol) in 10 ml methanol. Light blue crystals of **17** (0.160 g, 0.364 mmol, 72.8%) formed at the interlayer boundary after 1 day.

3.3.3. Guest sorption studies

Crystals of **13-17** were observed to lose their single-crystallinity in days to weeks when removed from the mother liquor. High-resolution thermogravimetric analysis on a fresh sample of **13** revealed a weight loss of *ca.* 16.5% between 100ºC and 250ºC, which is consistent with the removal of solvent molecules (calculated loss of 18% for 2 molecules of H_2O and 1 molecule of MeOH). Compounds **14** and **15** were observed to desorb or partially desorb their guest molecules in similar range of temperatures. FT-IR and TGA analysis showed that the solvent molecules in the two compounds **16** and **17** were readily desorbed upon exposure to atmosphere. Thermogravimetric analysis of **16** revealed a weight loss of 8.6% between 60 and 120ºC, which is consistent with the removal of one coordinated methanol molecules (calculated loss of 8.6% for one solvent

molecule). A TGA measurement effected on a sample of **16** let under ambient atmosphere for *ca.* one hour showed no weight loss in this range of temperature. The infra-red spectra of **17** shows the absence of bands characteristic of solvent molecules.

3.3.4. X-ray Crystallography

In crystal structures of **13-17**, all non-hydrogen atoms were refined with anisotropic displacement parameters except for the atoms of solvent in **13** and **17**. The H atoms of the C-H groups were fixed in calculated positions except for the carbon atom of methanol solvent in **13** and **17**. The two molecules of solvent in the asymmetric unit of **13** were disordered, the water molecule was refined with fixed site occupation factors (s.o.f). values of 0.5 for each oxygen atom, the methanol molecule was 2-fold disordered and refined over two equally occupied positions of the O atoms. In the asymmetric unit of **16**, one methanol molecule was found to be coordinated to Cu ion, its OH hydrogen atom was located via difference Fourier map inspection and refined with riding coordinates and isotropic thermal parameters based upon the corresponding O atoms [U(H) = 1.2Ueq (O)]. In **17**, the carbon and oxygen atoms of the solvent methanol were disordered over several general positions and refined with fixed s.o.f. for occupancies of 0.5 for each carbon and 0.25 for each oxygen; the water molecules in the asymmetric unit of **17** were disordered and refined with fixed s.o.f. values of 0.5 for each oxygen atom. Full crystallographic data can be found in the electronic supplementary data. Crystal data and structure refinement parameters of compounds **13-17** are presented in Table 3.1.

Table 3.1. Crystallographic data for compounds 13-17

Compound	**13**	**14**	**15**	**16**	**17**
Chemical formula	$C_{13}H_{16}N_2O_7Zn$	$C_{22}H_{16}N_2O_4Zn$	$C_{24}H_{18}N_4O_8Zn$	$C_{14}H_{16}CuN_2O_6$	$C_{15}H_8CuN_2O_{10}$
Formula weight	370.09	437.74	555.79	371.83	439.77
Temperature, K	200(2)	200(2)	200(2)	200(2)	100(2)
Crystal system	Tetragonal	Monoclinic	Monoclinic	Monoclinic	Monoclinic
Space group	I-42d	C2/c	C2/c	P2(1)/c	P2(1)/c
a, Å	21.351(3)	10.899(2)	11.922(3)	7.075(3)	12.3438(12)
b, Å	21.351(3)	11.292(2)	9.990(2)	7.705(3)	10.5840(10)
c, Å	6.9183(15)	15.358(3)	20.107(5)	14.248(6)	14.9068(14)
a, deg	90	90	90	90	90
ß, deg	90	100.47(3)	93.708(4)	99.714(8)	94.856(2)
γ, deg	90	90	90	90	90
V, $Å^3$	3153.9(10)	1858.6(7)	2389.9(9)	765.5(6)	1940.5(3)
Z	8	4	4	2	4
ρ_{calcd}, $g.cm^{-3}$	1.559	1.564	1.545	1.613	1.505
μ, mm^{-1}	1.593	1.354	1.086	1.459	1.179
F(000)	1492	896	1136	382	884
Crystal size, mm	0.2x0.2x0.15	0.2x0.15x0.1	0.2x0.2x0.15	0.50x0.20x0.05	0.10x0.05x0.05
θ range for data collection, deg	1.91 to 28.25	2.62 to 28.26	2.03 to 25.00	2.90 to 27.11	1.66 to 27.50
Limiting indices	-8<=h<=27 -25<=k<=12 -8<=l<=8	-13<=h<=5 -15<=k<=14 -9<=l<=20	-14<=h<=11 -11<=k<=8 -23<=l<=23	-9<=h<=8 -8<=k<=9 -16<=l<=18	-15<=h<=16 -13<=k<=13 -16<=l<=19
Reflections collected	4472	2739	5878	4399	13095
Unique reflections	1767	1692	2099	1679	4377
R(int)	0.0442	0.0294	0.0552	0.0550	0.0800
Completeness to θ	91.9	73.2	99.9	99.4	98.3
Absorption correction	SADABS	SADABS	SADABS	SADABS	SADABS
Max. and min. transmission	1.000 and 0.777	1.000 and 0.777	1.000 and 0.808	1.000 and 0.805	1.000 and 0.867
Data / restraints / parameters	1767 / 0 / 125	1692 / 0 / 132	2099 / 0 / 168	1679 / 0 / 107	4377 / 0 / 259
Goodness-of-fit on F^2	1.152	0.883	1.035	1.019	1.022
Final R indices [I>2sigma(I)]	R1 = 0.0449, wR2 = 0.1112	R1 = 0.0427, wR2 = 0.0838	R1 = 0.0463, wR2 = 0.0896	R1 = 0.0461, wR2 = 0.0998	R1 = 0.0589, wR2 = 0.1566
R indices (all data)	R1 = 0.0541, wR2 = 0.1134	R1 = 0.0574, wR2 = 0.0872	R1 = 0.0696, wR2 = 0.0977	R1 = 0.0700, wR2 = 0.1099	R1 = 0.0883, wR2 = 0.1799
Absolute structure parameter	0.10(3)	N/A	N/A	N/A	N/A
Largest diff. peak and hole, $e.Å^{-3}$	0.538 and -0.329	0.551 and -0.349	0.371 and -0.280	0.414 and -0.335	0.945 and -0.978

3.4. Results and Discussion

3.4.1. Supramolecular isomers of $[Zn(nicotinate)_2]_n$

Self-assembly of $Zn(NO_3)_2$ with nicotinate under mild conditions has afforded several products including a novel 3D network that has a connectivity based solely upon square planar nodes defined by the circuit symbol $4^2.8^4$, $\{[Zn(nicotinate)_2]\cdot MeOH\cdot 2H_2O\}_n$, **13**, and two new forms of the 2D network $[Zn(nicotinate)_2]_n$,[209] **A**, presented above, $\{[Zn(nicotinate)_2]\cdot naphthalene\}_n$, **14**, and $\{[Zn(nicotinate)_2]\cdot 2\ nitrobenzene\}_n$, **15,** both of which exhibit the same 4^4 topology as **A**.

The crystal structure of **13** is illustrated in Figure 3.10a. The metal coordination is the same as that in the square grid $[Zn(nicotinate)_2]_n$ **A** represented in Figure 3.4. However, when one examines the connectivity of the Zn centers, adjacent square planar nodes are twisted at an angle of *ca.* 25º, resulting in a 3D network, Figure 3.10b, instead of a 2D square grid. The circuit symbol of this network is $4^2.8^4$. PtS[245] is defined by the same circuit symbol; however, the two nets are fundamentally different and the projections down [100] are non-superimposable, Figure 3.11. The nodes are eclipsed along the *z*-axis with a vertical distance between two Zn atoms of 6.92 Å and there are edge-to-face interactions between the pyridyl rings of nicotinate ligands with a shortest distance d(C-C) = 3.8 Å. **13** possesses cavities of effective dimensions 4.35 X 4.35 Å that form infinite channels parallel to the *z*-axis, Figure 3.10, left. These channels contain columns of disordered solvent molecules. The density of **13** is 1.56 $g.cm^{-3}$ (1.30 $g.cm^{-3}$ without solvent).

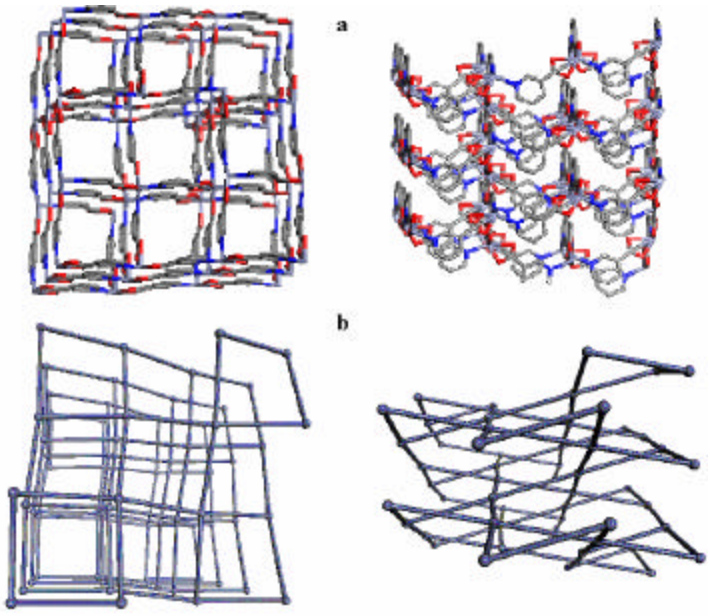

Figure 3.10. Crystal structure of the 3D network $[Zn(nicotinate)_2]_n$, guest molecules are omitted for clarity (a). Schematic representations of the connectivity of the Zn centers for the network of 13 (b).

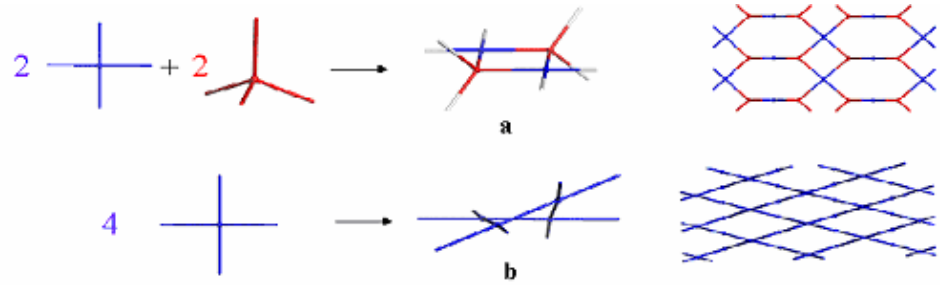

Figure 3.11. Connectivity of 2 tetrahedral and 2 square planar nodes to form the $4^2.8^4$ network of PtS (a) and connectivity of 4 square planar nodes to form 13 (b) and projections of the two networks down [100].

In order to systematically determine the effect of templates on the formation of **A** or **13**, the same reaction was conducted in the presence of several aromatic guests: benzene, nitrobenzene, naphthalene, chlorobenzene, *o*- and *p*-xylenes, *p*-nitroaniline and anisole, as well as in the absence of template. Analysis of simulated and freshly collected XRPD patterns, presented in Figures 3.12-3.13, indicated that most reactions resulted in the formation of **A** whereas nitrobenzene affords **13** or **15** and naphthalene affords **14**.

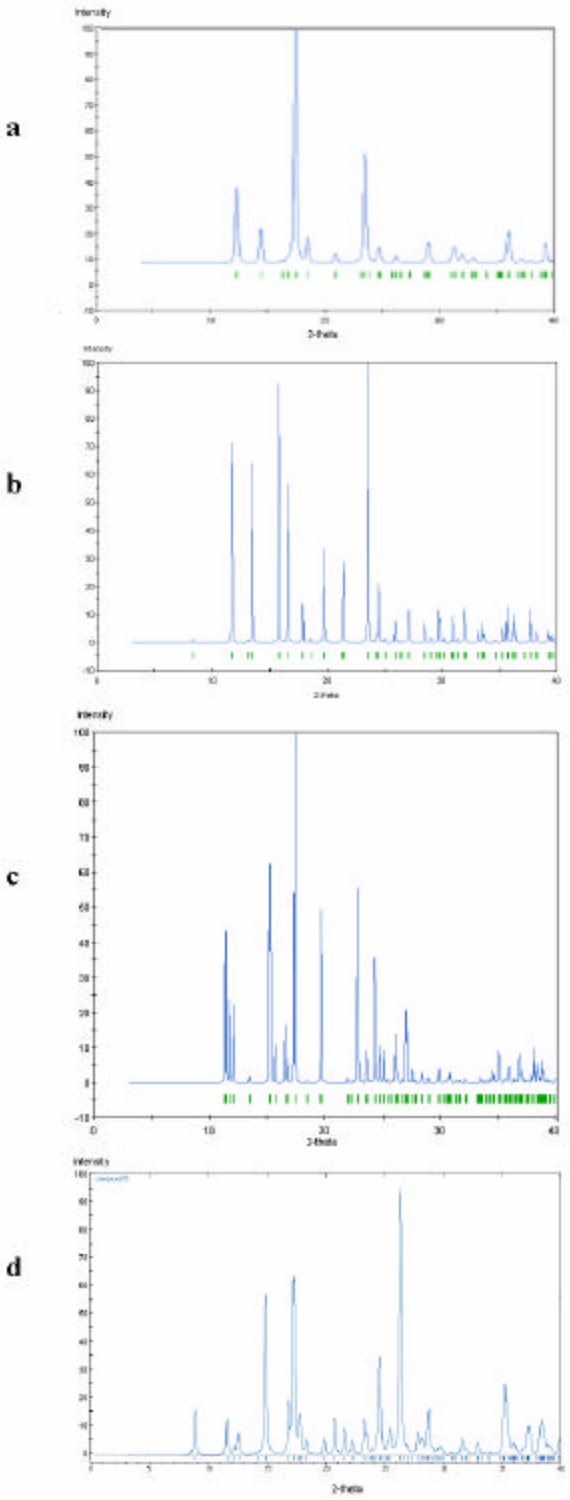

Figure 3.12. X-ray powder diffraction pattern calculated from the single crystal structures of A (a), 13 (b), 14 (c) and 15 (d)

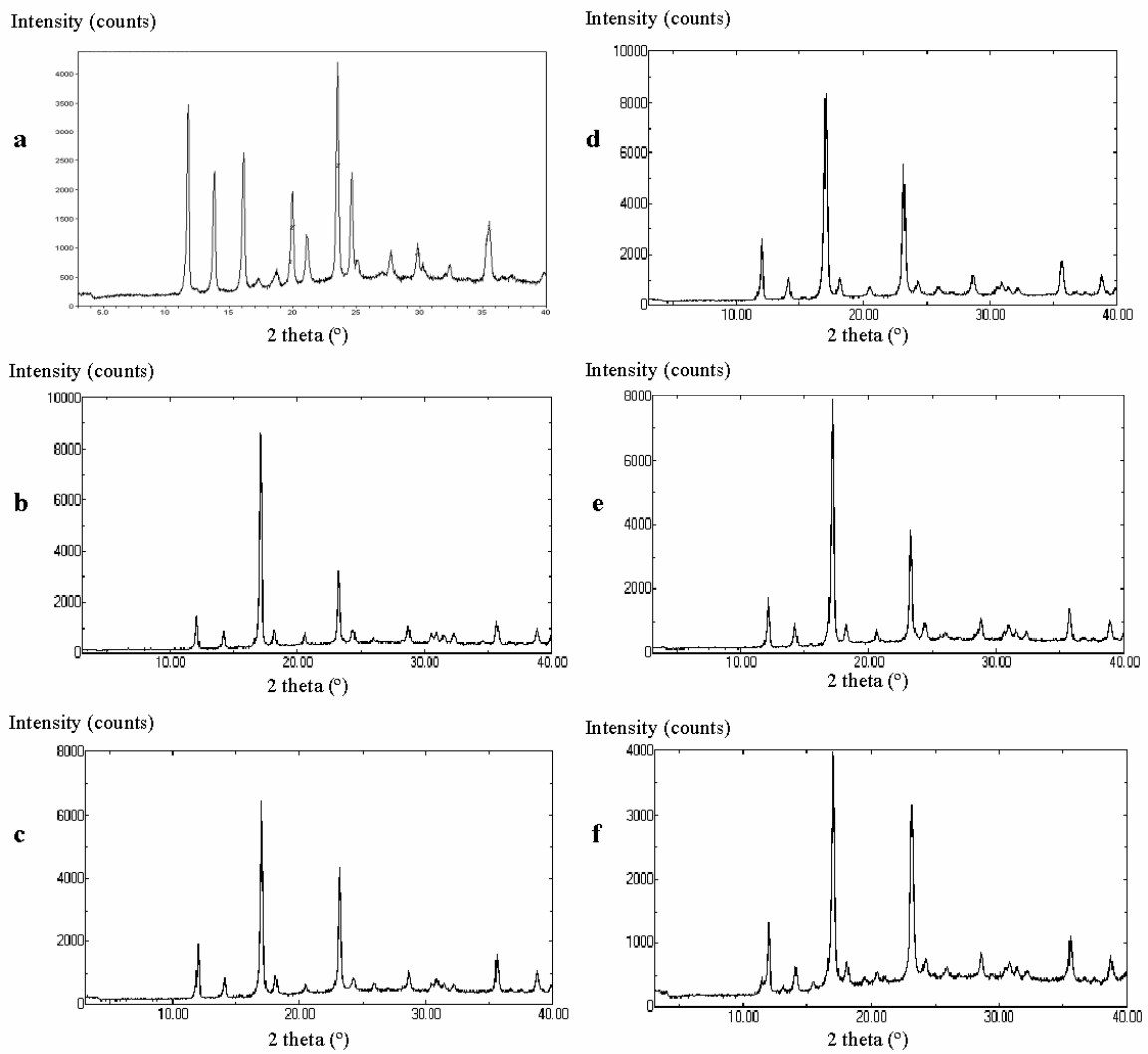

Figure 3.13. X-ray powder diffraction patterns of the products of the reaction $Zn(NO_3)_2$ + Nicotinate in different conditions: (a) first product of the reaction in $PhNO_2$, (b) MeOH only, (c) PhH, (c) PhCl, (d) *o*- and *p*-$Ph(CH_3)_2$, (e) *p*-H_2NPhNO_2 and (f) $PhOCH_3$.

14 and **15** contain 2D square grid networks (4^4), Figure 3.14a. **14** crystallizes in the centrosymmetric space group *C*2/*c*, the parallel infinite layers of square grids are eclipsed and the d(Zn-Zn) separations are 7.68 Å, resulting in the formation of parallel channels perpendicular to the planes of the square grids. Each cavity has effective dimensions of 4.45 X 4.45 Å, and is filled by one molecule of naphthalene that interacts

with the aromatic rings of the surrounding nicotinate ligands by face-to-face p-p stacking with distances between the centroids in a range of 3.4 to 3.7 Å. The density of **14** is 1.56 $g.cm^{-3}$ (1.10 $g.cm^{-3}$ without guest). **15** contains a larger amount of guest (density without guest = 0.86 $g.cm^{-1}$) and exhibits much larger interlayer separations than either **A** or **14** (d(Zn-Zn) = 10.05 Å), Figure 3.14. It should be noted in **A** adjacent grids are staggered whereas in **14** and **15** they are almost eclipsed.

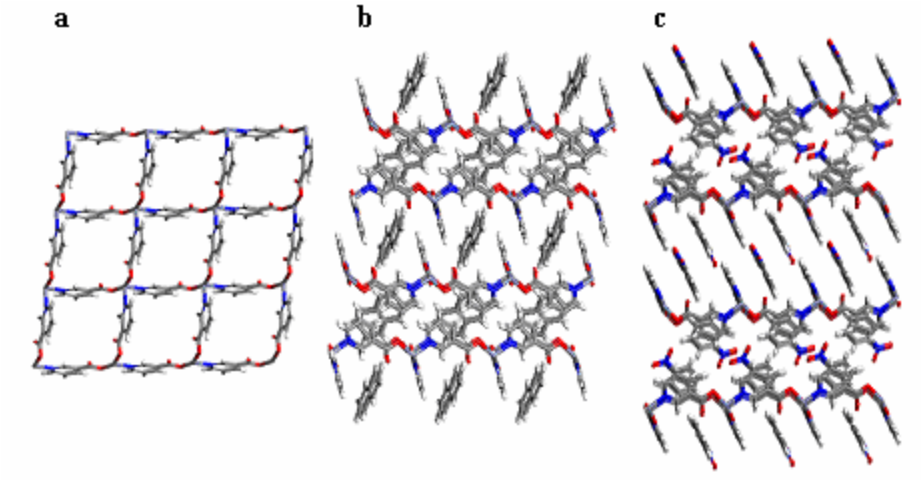

Figure 3.14. Crystal structure of the 2D square grid in 14 and 15 (a) and the vertical stacking between parallel infinite layers showing the intercalation of naphthalene (b) and nitrobenzene (c) molecules.

Crystals **13**, **14** and **15** are sustained by the same node. Only a subtle difference of the conditions during crystallization influences which phase is generated. A summary of the relationships between the structural supramolecular isomers is shown in Figure 3.15. The characterization of components, achieved by powder diffraction and thermogravimetric analysis, reveals that heating above 220°C results in conversion of **13**, **14** and **15** to **A**. Figures 3.16-3.18 represent the comparison between simulated and freshly collected powder patterns of the three compounds presented herein, the expected

structures that would result from their guest desorption without structural change and the corresponding samples obtained after thermal treatment, the later presenting identical patterns as that of the 2D $[Zn(nicotinate)_2]_n$ shown in Figure 3.12a. **A** was formed *via* hydrothermal conditions and it should therefore be unsurprising that it appears to be the thermodynamically favored product.

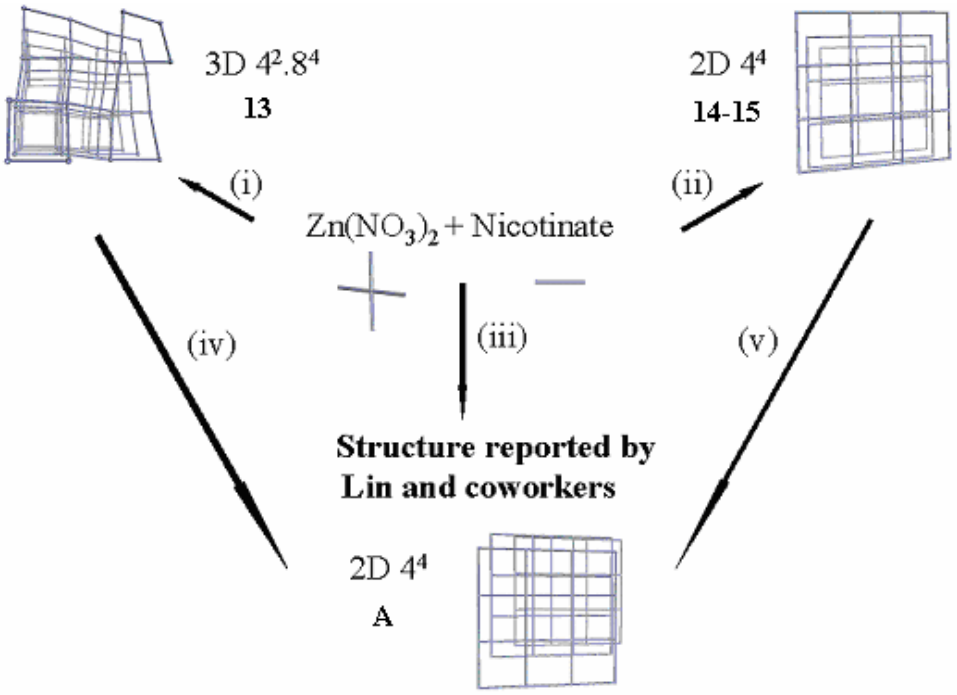

Figure 3.15. The relationship between 13-15 and A. *Reagents and conditions*: (i) $PhCH_3$ or $PhNO_2$ in MeOH, diffusion; (ii) $C_{10}H_8$ or $PhNO_2$ in MeOH, slow diffusion; (iii) MeOH or PhH or PhCl or *o*-, *p*-$Ph(CH_3)_2$ or *p*-H_2NPhNO_2 or $PhOCH_3$ in MeOH, precipitation; (iv) and (v) 220-250°C, 1 hour.

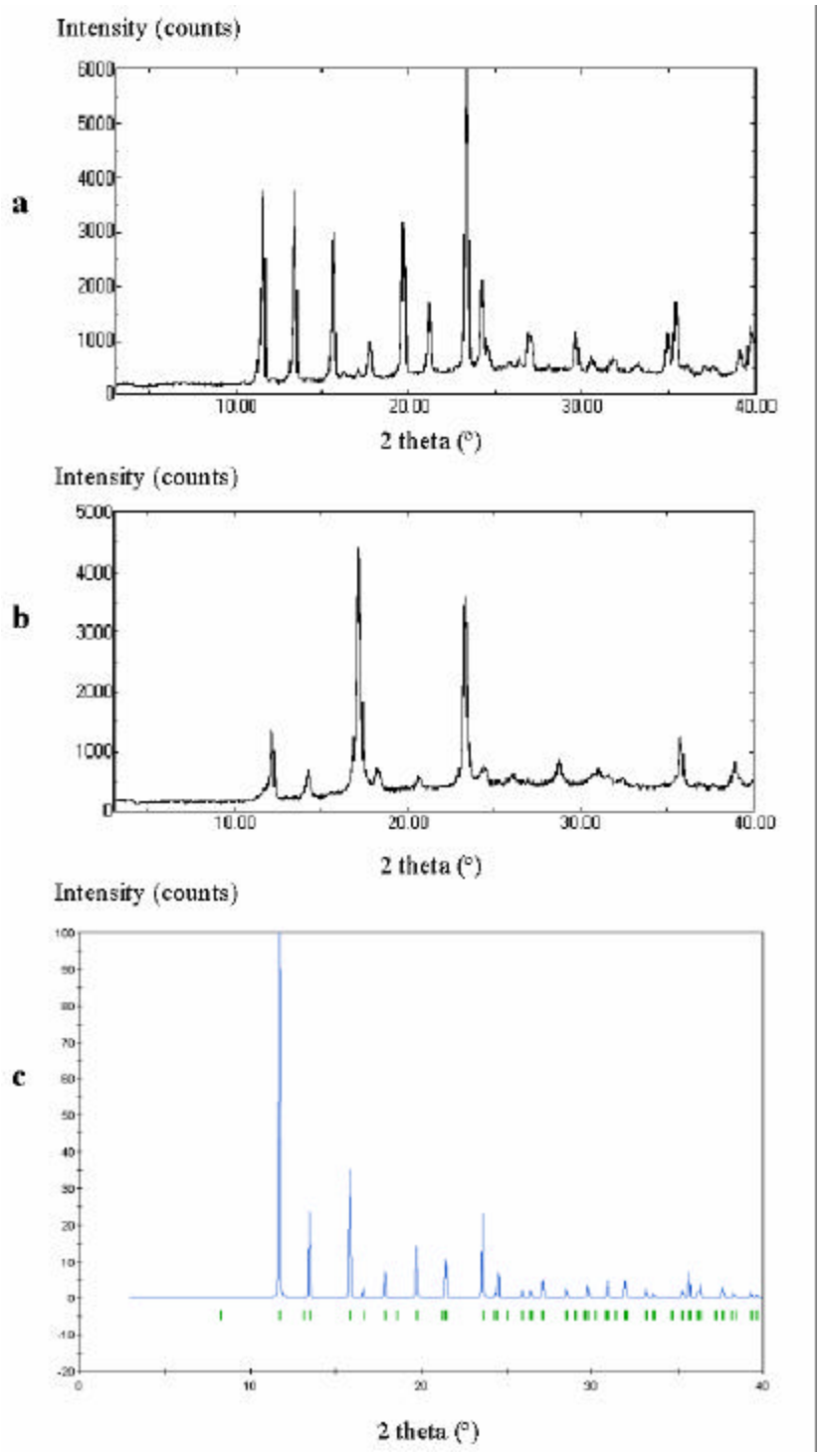

Figure 3.16. X-ray powder diffraction patterns of 13 (a) fresh sample, (b) sample heated to 250°C and (c) calculated from the single crystal structure without guest.

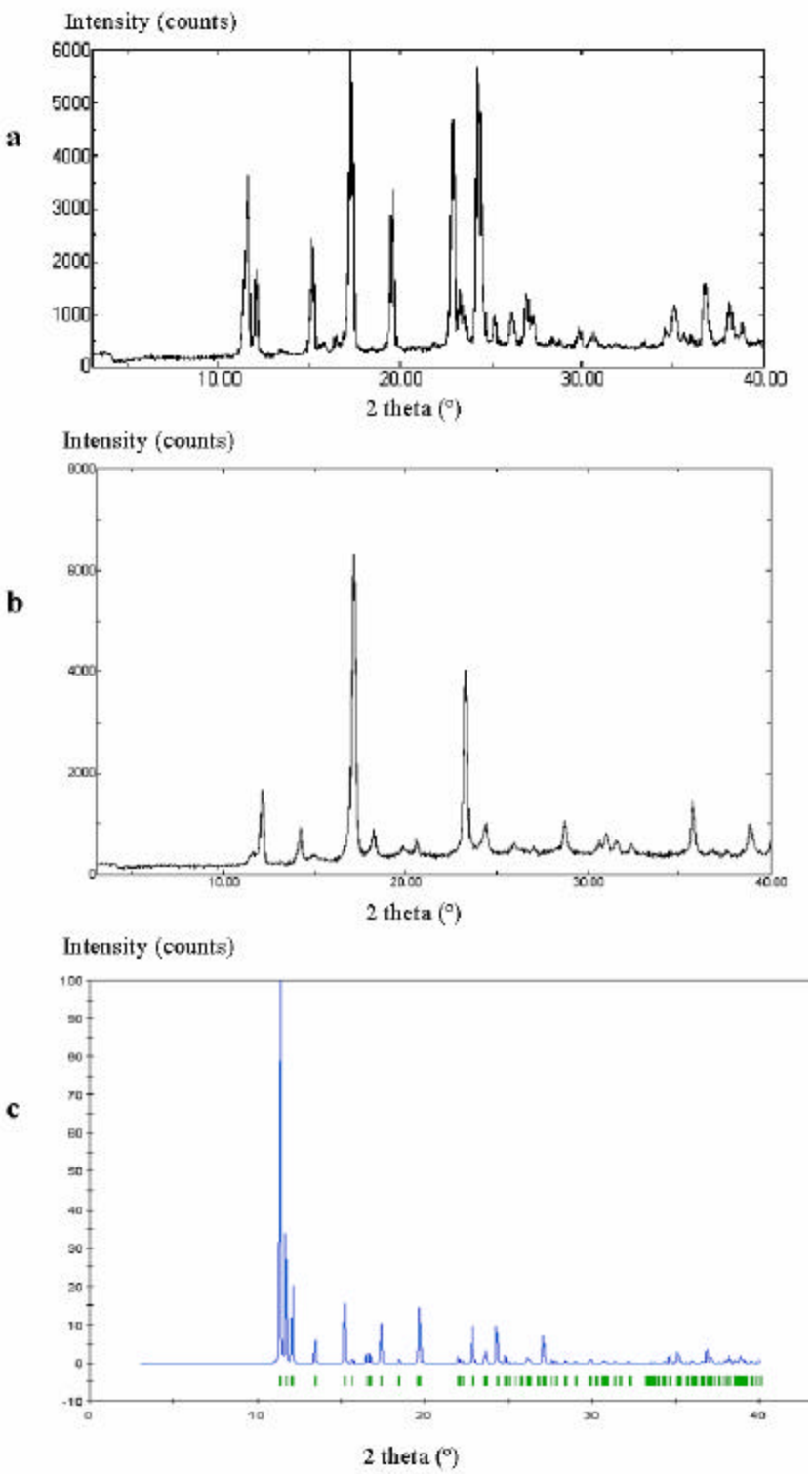

Figure 3.17. X-ray powder diffraction patterns of 14 (a) fresh sample, (b) sample heated to 220ºC and (c) calculated from the single crystal structure without guest

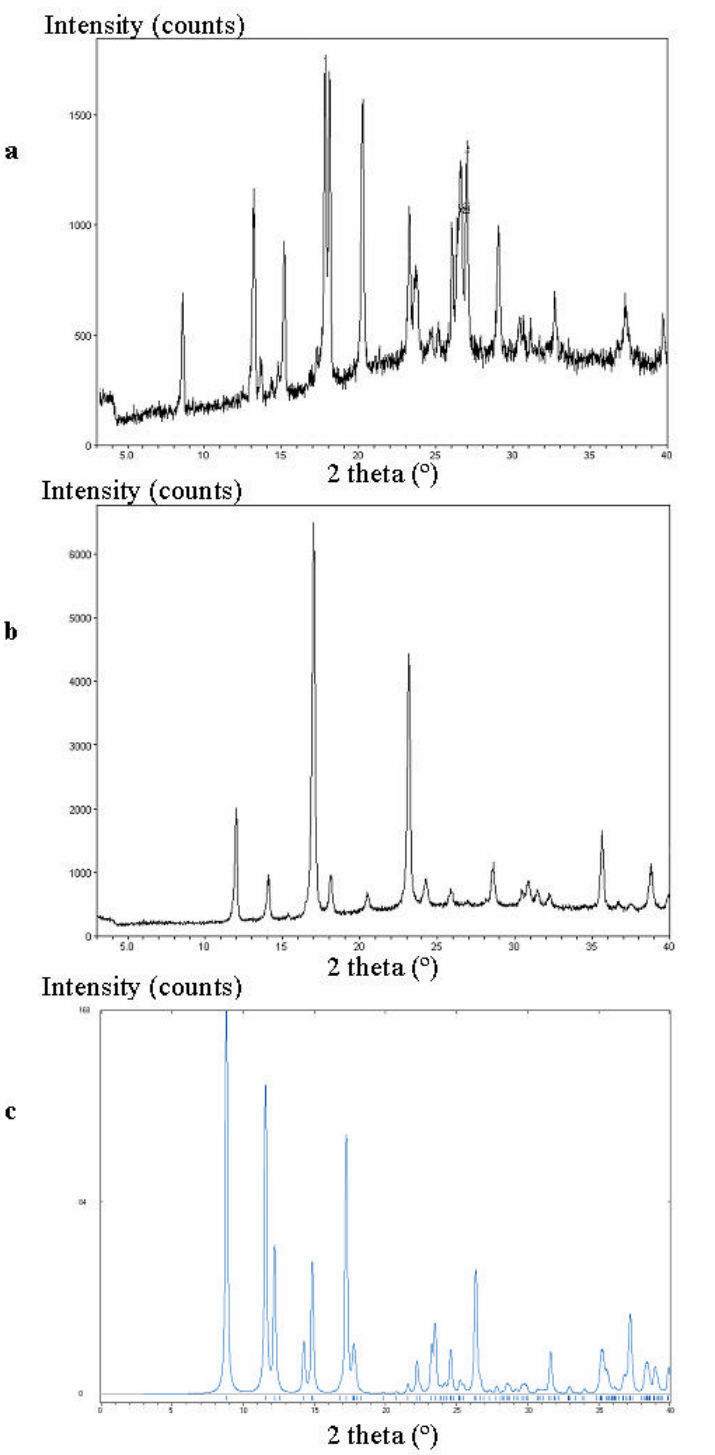

Figure 3.18. X-ray powder diffraction patterns of 15 (a) fresh sample, (b) sample heated to 250ºC and (c) calculated from the single crystal structure without guest.

3.4.2. Additional Functionality: Structures of $[Cu(nicotinate)_2]_n$ and $[Cu(dinicotinate)_2]_n$

The reaction of $Cu(NO_3)_2 \cdot 2.5H_2O$ and nicotinate in methanol has afforded the novel 2D rhombus grid network 4^4 $[Cu(nicotinate)_2(MeOH)_2]_n$, **16**. The use of the organic ligand dinicotinate that contain an additional functional group carboxylic acid has led to the formation of a related 3D network, **17**, extended version of the 2D 4^4 network by pillaring *via* coordination of the neutral oxygen donor of the additional functionality.

The crystal structure of compound **16** consists of a 2D rhombus grid network. Each Cu center is coordinated to two pyridyl groups and two monodentate carboxylate moieties of four nicotinate ligands in a *trans* configuration. The Cu center is further coordinated to the oxygen atoms of two methanol molecules in the axial positions of the octahedral coordination geometry, Figure 3.19a. The axial Cu-O(methanol) distances of 2.65 Å are significantly longer than the distances Cu-O(nicotinate) and Cu-N(nicotinate) of 1.97 and 2.00 Å respectively due to the axial elongation along the fourfold axis of the octahedral environment of Cu(II) chromophore. The non-bonded oxygen atoms of the carboxylate groups are at a distance $d(Cu\text{-}O_{non\text{-}bonded}) = 3.15$ Å. These values are consistent with the corresponding standards presented above for this chromophore. The rhombus-shaped cavities deviate from regular square geometry by angles of 56.8° and 123°. Along the *x*-axis, the parallel rhombus grids are eclipsed and the d(Cu-Cu) separations are 7.07 Å, generating parallel channels perpendicular to the planes of the grids, Figure 3.19.

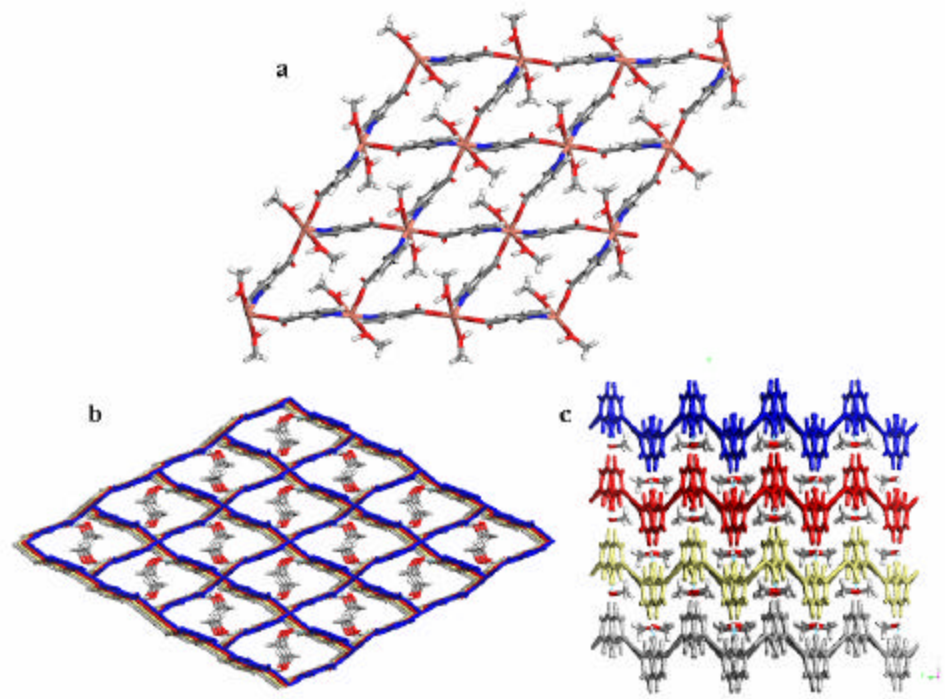

Figure 3.19. Crystal structure of the 2D square grid in 16 (a) and vertical stacking between parallel infinite layers down [100] (b) and [001] (c)

Each cavity has effective dimensions of 4.70 X 4.70 Å, and is filled by two molecules of coordinated solvent methanol. The hydroxyl group of each coordinated methanol interacts via hydrogen bonding with the non-bonded oxygen atoms of the monodentate carboxylate of the nicotinate ligands (d(O-H···O = 2.67 Å). The density of **16** is 1.61 $g.cm^{-3}$ (1.33 $g.cm^{-3}$ without coordinated solvent).

Compound **17** crystallizes in the monoclinic space group $P2_1/c$. The asymmetric unit of **17** contains one Cu center and two dinicotinate ligands. Figure 3.20 shows the Cu(II) chromophore in **17**. The metal adopts a square pyramidal coordination geometry with two pyridyl groups (d(Cu-N) = 2.00 Å) and two monodentate carboxylate moieties ($d(Cu\text{-}O_{bonded})$ = 1.95 Å, $d(Cu\text{-}O_{non\text{-}bonded})$ = 2.97 and 3.22 Å) in a *trans* configuration in the equatorial positions and one of the oxygen of the additional carboxylic group of the

dinicotinate ligand is coordinated onto the axial position (d(Cu-O) = 2.35 Å). The non-deprotonated carboxylic group concomitantly interacts *via* hydrogen bonding between the hydroxyl proton and the carboxyl group of an adjacent square grid with d(O-H···O) = 2.53 Å. Figure 3.20 illustrates the environment of the Cu(II) center in compound **17**. The overall network of **17** can be described as 2D distorted square grids, represented in Figure 3.21, that are pillared by the additional carboxylic functions hence resulting in a 3D network that possesses a topology related to the a-polonium net, Figure 3.22. **17** possesses cavities of effective dimensions 3.67 X 3.67 Å that form infinite channels perpendicular to [101]. These channels contain columns of disordered solvent molecules. The density of **17** is 1.50 g.cm^{-3} (1.35 g.cm^{-3} without solvent).

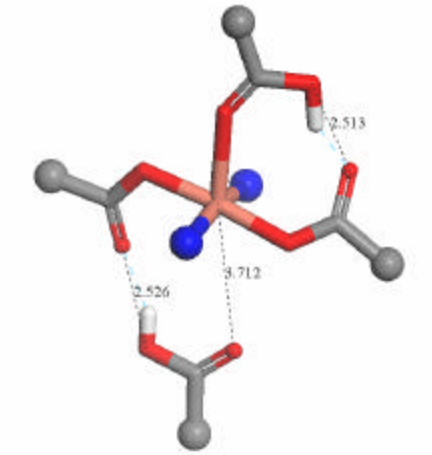

Figure 3.20. Representation of the chromophore mononuclear 5-connected in compound 17

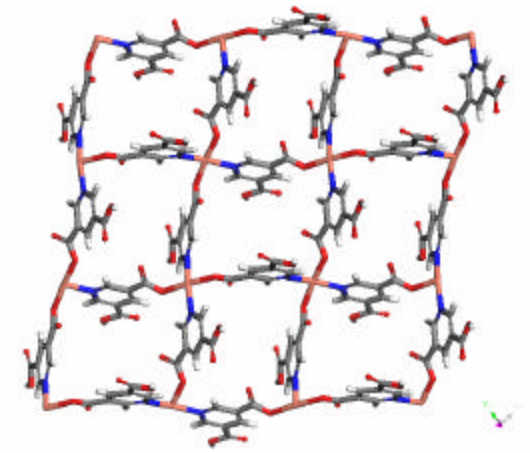

Figure 3.21. View of the 2D square grid network within the crystal structure of 17, guest molecules are omitted for clarity

Compounds **16** and **17** contain 2D 4^4 networks. The presence of an additional functionality carboxylic acid in the ligand used to generate **17**, does not disrupt the topology of the 2D net but only slightly affects the conformation of the grids from a rombus grid to a distorted square grid. The fact that the additional carboxylic is not deprotonated is not surprising considering the necessity of conservation of charge, effectively the Cu(II) chromophore considered in this study can only be coordinated to two carboxylate groups. As a sideline, it is interesting to mention that a possible supramolecular isomer of compound **17** based upon 2D nets purely hydrogen bonded *via* the complementary carboxylic functions is possible although the synthesis conditions have ruled it out since the strength of coordination bond and the efficiency of the overall crystal packing predictably favorize the formation of the 3D net **17**. Finally these results exemplify the modular nature of supramolecular metal-organic networks, which can be rationally functionalized through variation of the building units without critical change upon the primitive network topology.

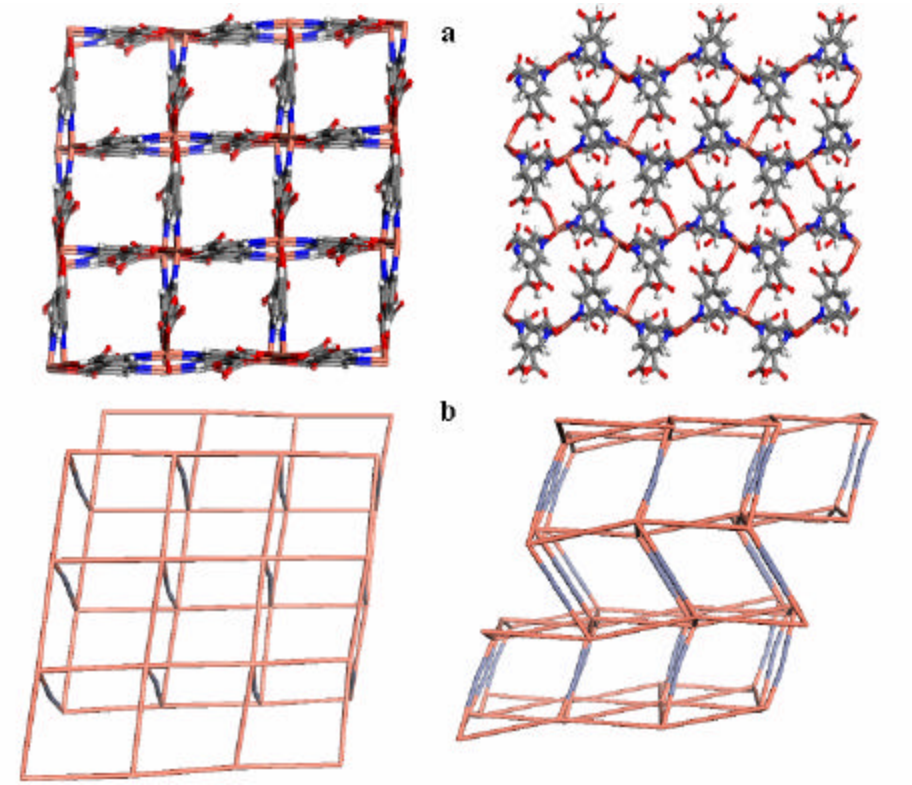

Figure 3.22. Crystal structure of the 3D network [Cu(dinicotinate)$_2$], guest molecules are omitted for clarity (a). Schematic representations of the connectivity of the Cu centers for the network of 17 (b).

3.5. Conclusions

In summary, the five compounds presented herein illustrate structural diversity and modularity of supramolecular metal-organic networks. There are three salient features of **13-17** that deserve note.

First, a novel $4^2.8^4$ network based upon a single 4-coordinated node has been generated and it can be rationalized on the basis of the connectivity and the geometry of the molecular building blocks. The ability of guests to intercalate in the square grid form of [Zn(nicotinate)$_2$] is perhaps unsurprising[64,97] but to our knowledge such a wide range of separations has not yet been seen in laminated coordination polymers. This study

further confirms how supramolecular isomerism can afford superstructural diversity from even the most simple chemical building blocks.

Second, the presence of an additional functionality that can hydrogen bond and even coordinate to the node metal center does not appear to prevent or even strongly influence the topology of the primitive 2D coordination network.

Finally, these five new examples of rationalization of networks topology based upon geometry and connectivity of organic and inorganic building blocks suggest that topological approaches to the design of hybrid solids could represent an opportunity of broad relevance towards the construction of novel functional supramolecular materials.

Chapter 4

Metal-Organic Networks based upon conformationally labile organic ligands: Porosity and Flexibility

4.1. Introduction

4.1.1. Metal-Organic Networks based upon dimetal cluster nodes

Crystal engineering of metal-organic networks *via* self-assembly of metal ions and multifunctional ligands has attracted considerable attention because of the structural diversity present in such compounds which in turn facilitates systematic evaluation of structure property relationships.[93,94,144,145] In this context, bimetallic building units constitute an ubiquitous class of nodes in coordination chemistry,[95,206] in particular dimetal tetracarboxylate chromophores possess a well-known geometry and coordination capabilities that make them ideal building blocks for the design *via* self-assembly of metal-organic coordination polymers. Figure 4.1 shows a representation of the chromophore resulting from the complexation of Cu(II) with carboxylate ligands and how it can serve, in appropriate circumstances, as square planar or octahedral node. Therefore, coordination of a bifunctional dicarboxylate ligand to Cu(II) can afford infinite metal-organic networks with predictable topology. For example, self-assembly of a square planar node with a linear linker has afforded the square grid Cu_2(benzene-1,4-

dicarboxylate)$_2$,[252] such a 2D network can also be pillared *via* the use of N,N'-donor ligands generating an octahedral network.[253,254] Figure 4.1 shows a schematic representation of metal-organic square grids and octahedral networks generated from square planar and octahedral metal nodes, they represent prototypical infinite networks and they inherently possess cavities that are suitable for interpenetration or enclathration of a range of organic guest molecules.[66,90-92,97-103,105,110-116,119,122,236,255] In a sense, they have structural features that compare to both clays and zeolites since they can be lamellar or porous. In this perspective, the use of building blocks specifically chosen for their functionality has been shown to generate metal-organic networks that exhibit properties such as luminescence,[256] porosity[114,119,236] or magnetism.[125]

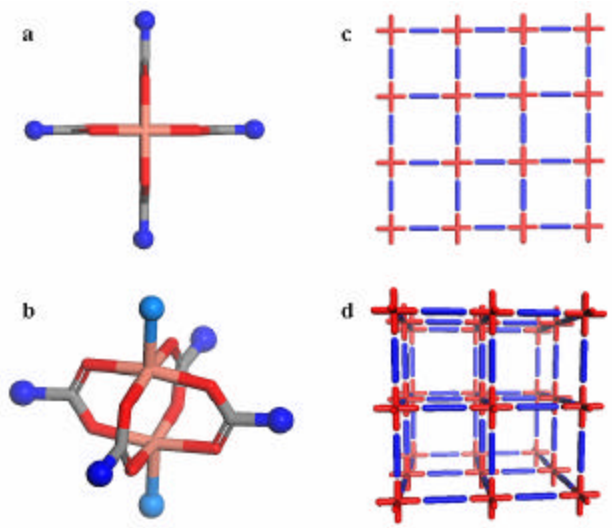

Figure 4.1. Top (a) and side (b) views of the dimetal tetracarboxylate chromophore and schematic representation of the 2D square grid (c) and 3D octahedral (d) networks that can be generated through use of appropriate linear linkers.

4.1.2. Conformational lability of the organic linker

The rational design of supramolecular metal-organic networks based upon preselected rigid building blocks has afforded an increasing number of novel compounds

since the early 1990's.[60,66] In this respect, the use of flexible linkers or spacers has yet to be fully developed. In effect, according to a comparative CSD survey, the number of structures reported that contain transition metals in coordination with N- or O-donor ligands that possess only rigid aromatic groups represents *ca.* 10 times the number of corresponding metal-organic compounds that contain at least two flexible methylene groups (16661 hits for the former search *vs.* 1756 hits for the latter). Rigid ligands have been shown to be capable of generating multiple supramolecular isomers for a given set of molecular components and a range of reaction conditions.[251] However, use of flexible ligands should in principle offer a greater degree of structural diversity and there has been interest in such ligands for magnetic[257-259] or porous[260-262] materials.

While most interest in the literature of coordination polymers containing saturated fragments has focused on introduction of flexibility *via* alkyl substituents within otherwise rigid ligands,[208,235,260,263-269] the use of long bifunctional alkyl chains has generated several coordination networks that present either interpenetration[270] or amphiphilic-like behavior[271,272] due to the expected all *anti* conformation of the aliphatic parts. However there has been very little work designed to show how systematic variation of the elemental constituents or the crystallization conditions can direct such flexible ligands to adopt specific conformations.[208,266,269,273] In this regard, the generation of flexible architectures with variable shapes and sizes should represent great potential for useful developments in supramolecular chemistry, since the resulting structures may expand the concept of supramolecular isomerism to its conformational counterpart and provide a route to the generation of a novel class of nanostructures possessing atypical

properties towards practical applications.

The research presented herein intends to demonstrate how the utilization of bifunctional ligands possessing small aliphatic chains that are related to well-known rigid linkers can provide the basis for a farther in-depth understanding of the factors that control conformational flexibility/isomerism towards the generation of novel functional metal-organic networks. The acquired knowledge will allow the strategic extension of this research to the development of highly tunable hybrid materials.

The glutarate anion is a readily available bifunctional ligand which is effectively a flexible variant of benzene-1,3-dicarboxylate, a ligand which can sustain discrete[225,274] and infinite[230,275] structures with nanoscale features. In a similar vein, the ligand adipate can be seen as a flexible variant of benzene-1,4-dicarboxylate, Figure 4.2.

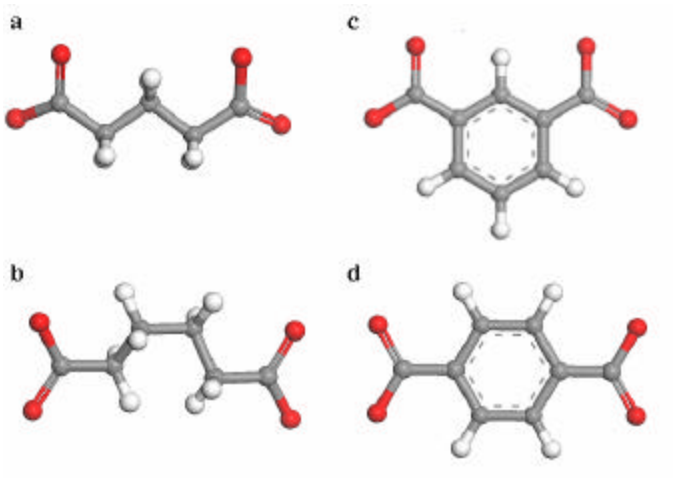

Figure 4.2. Representation of the glutarate (a), adipate (b), benzene-1,3-dicarboxylate (c) and benzene-1,4-dicarboxylate anions (d).

As revealed by Figure 4.3, glutarate anions possess a three carbon aliphatic backbone and there exist three likely conformations: *anti-anti*, *anti-gauche* and *gauche-gauche*.

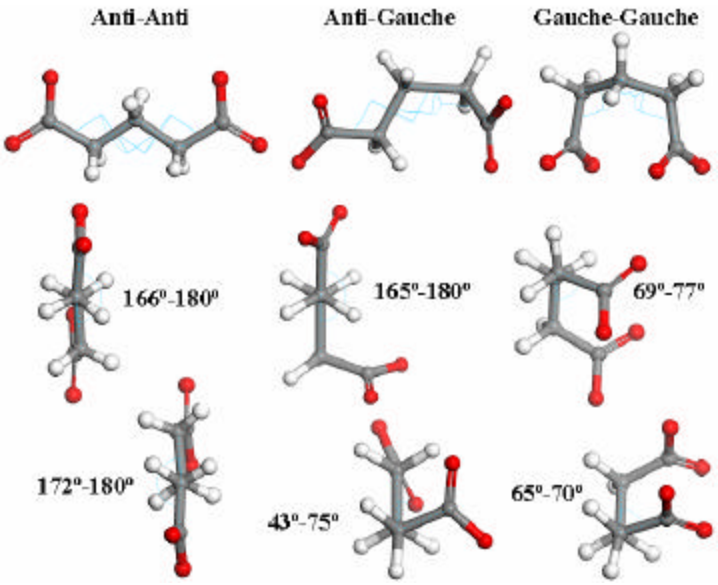

Figure 4.3. The three possible conformations of glutarate alkyl chains and the corresponding projections down the Csp^3-Csp^3 bonds with the range of torsion angles observed in the structures deposited in the CSD.

A survey of the Cambridge Structural Database revealed that the *anti-anti* and *anti-gauche* conformations tend to be favoured in coordination compounds. A conformational analysis of crystal structures containing the glutarate fragment and metals was conducted using the CSD and revealed that out of 31 non-equivalent glutarate ligands, 13 exhibit the *anti-anti* mode, 13 the *anti-gauche* mode and 5 the *gauche-gauche* conformation, Table 4.1. It should be noted that the orientation of the carboxylate moieties with respect to the backbone is fairly variable although the observed trends are in favor of the staggered conformation for the *anti-gauche* mode *versus* the eclipsed conformation for the *anti-anti* mode.

Table 4.1. Conformational analysis of crystal structures containing the glutarate fragment and metals conducted using the CSD.

CSD Refcode	Torsion Angles (°)				Conformation
	C1-C4	C2-C5	O1-C3	O5-C3	
MIYMOW	65	75	17.5	43.5	**Gauche-Gauche**
ZADJUJ	69	70	32	82.5	
MEZSALa	69	69	4.5	4.5	
XATNIPa	69.5	69.5	4	4	
TODNAB	70	77	20	7	
QANKOF	43	180	95	35	**Gauche-Anti**
VIRYUQ	46	172	66.5	85.4	
GLUECU	59	170	77.6	31.5	
QIVHAE	62	165	6	77	
MASXINa	62	180	23	70.5	
ACBRUA	65	178	26.5	87.5	
GLTECU	68	177	19.5	27	
SIFWEJ	68	177	43.5	54	
SUJXEA	68	178	21.5	48	
HOTGOM	71	170	0.8	75	
QIWKEM	71	179	8	49	
TODNEF	74	172	6.5	49.5	
QANKIZ disordered	60-66	150-163	3-9	30-77	
OCENUF	166	179	51	34.5	**Anti-Anti**
MASXINb	169	174	17	21	
XEDCUE	169	176	88	88	
QIVGUX	172	172	7	7	
TEGMIB	172	173	10	15.5	
VIRZAX	173	173	34.5	95	
CDGLTR	173	175	4.8	0.35	
XODFUR	174	174	34	85	
MIYMUC	175	176	0.5	32	
FUMCUL	177	180	3.2	0.3	
HOTHAZ	179	179	11	8	
XATNIPb	179	179	10	10	
MEZSALb	180	180	10	10	
BOMXOQ	structure unavailable				

Figure 4.4 shows the five conformations *anti-anti-anti, anti-anti-gauche, anti-gauche-anti, anti-gauche-gauche* and *gauche-anti-gauche* observed for the four methylene of the ligand adipate.

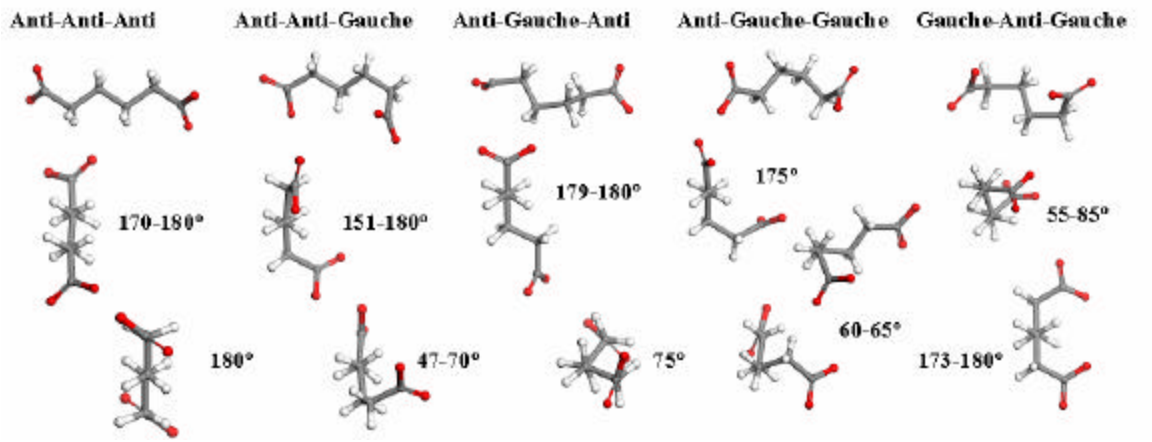

Figure 4.4. The five observed conformations of adipate alkyl chains and the corresponding projections down the Csp^3-Csp^3 bonds with the range of torsion angles observed in the structures deposited in the CSD.

The corresponding survey of the CSD revealed that the *anti-anti-anti* and *gauche-anti-gauche* conformations are favoured in coordination compounds: out of 35 non-equivalent adipate ligands, 12 exhibit the *anti-anti-anti* mode and 12 the *gauche-anti-gauche* conformation, Table 4.2.

Such a study has also revealed the extreme scarcity of extended structures based upon dimetal tetracarboxylate chromophores,[276] which are of considerable interest to strategically prepare metal-organic compounds by self-assembly.[95,206,223-232]

Our strategy towards the rational design of specific structures based upon the coordination between bimetallic building units and flexible spacers was inspired by the analogy between the flexible bifunctional ligands glutarate and adipate and the rigid benzene-1,3 and 1,4-dicarboxylate anions. In this respect, it is possible to delineate important trends regarding the influence of the conformation adopted by the aliphatic chain of the dianion associated with the geometry of the node upon the topology of the resulting networks.

Table 4.2. Conformational analysis of crystal structures containing the adipate fragment and metals conducted using the CSD.

CSD RefCode	Torsion Angles (°)					Conformation
	C1-C4	C2-C5	C3-C6	O1-C3	O6-C4	
NIPHAV	60	65	175	58	12	**Gauche-Gauche-Anti**
ECIVUH	60	180	60	55	57.5	**Gauche-Anti-Gauche**
WIPQER	63	180	63	41	41	
TODNIJ	69	180	69	45	45	
ZEMZUM	80	180	80	10	10	
MITHUSa	68	179	69	38	50	
MIYNAJa	56	180	56	60	61	
MIYNAJb	59	173	59	84	82	
MIYNENa	59	180	59	57	59	
MIYNENb	55	175	55	79	79	
MIYNIRa	57	180	57	58	61	
MIYNIRb	55	176	55	75	75	
IBODOS	85	180	75	66	39	
OCENOZ	47	151	169	38	5	**Gauche-Anti-Anti**
ADIECU	60	170	170	55	3.5	
FOQLOM	60	180	180	64	7	
NOVHAH	60	180	180	90	20	
JOSNAGa	62	175	180	55	47	
POSBAA	65	180	170	62	3	
MITHUSb	68	176	170	32	25	
IGIDOR	69	176	178	50	14	
WOSDAJ	70	180	180	25	5	
MITHUSc	179	75	180	86	80	**Anti-Gauche-Anti**
LOTDON	170	180	180	8.5	80	**Anti-Anti-Anti**
QOPLAI	175	180	175	20	20	
HUTYOK	177	180	177	17	17	
ADIQNI	180	180	180	55	55	
JOSNAGb	180	180	180	67.5	67.5	
QOPLEM	180	180	180	20	20	
QOPLIQ	180	180	180	1.5	4	
TUDHOP	180	180	180	1.5	5.5	
WAVCAX	180	180	180	7.5	90	
WEGJUN	180	180	180	5	5	
WIPQAN	180	180	180	55	55	
WOSDEN	180	180	180	60	60	

Considering the case of a dimetal tetracarboxylate chromophore as 4-connected node, complexation with the flexible link glutarate, in a given conformation *anti-anti,* is

expected to generate similar topologies as those obtained with benzene-1,3-dicarboxylate.[225,230-232] When the glutarate anion adopts the *anti-gauche* mode, it can be schematically seen as a curved spacer and, afford 4 possible geometries around the bimetallic unit, Figure 4.5:

- all glutarate ligands in *"trans"* with each other, adopting a C_2 symmetry with respect to the metal-metal axis, are expected to generate a 1D, double chain, topology;

- all glutarate ligands in *"syn"* with each other, adopting a C_4 symmetry with respect to the metal-metal axis, are expected to generate a 2D, distorted square grid, topology;

- an alternate coordination modes around the dimetal cluster in "*syn-syn-trans-trans*" or "*syn-trans-syn-trans*" should lead to geometrical constraints and force the dicopper tetraglutarate to extend its topology to a more complex 3D network.

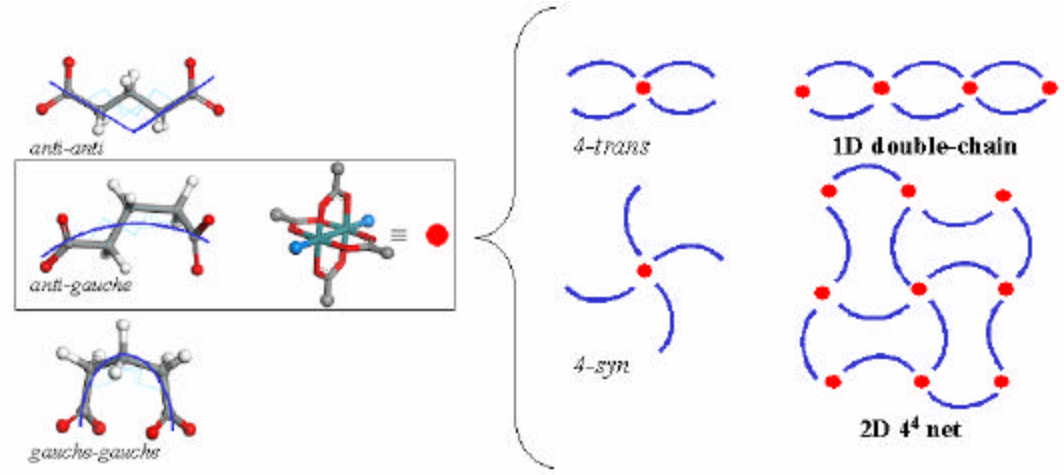

Figure 4.5. The three possible conformations of glutarate alkyl chains and the possible geometries of the glutarate *anti-gauche* anions around a bimetallic building unit leading to distinct 1D and 2D topologies.

In the case of glutarate anion adopting the *gauche-gauche* mode, coordination with a transition metal node may undergo high geometrical constraints and result in

unpredictable structures based upon atypical coordination as exemplified by the 2D polynuclear structure of silver(I)glutarate.[277] On the other hand the conformational constraints of the carbon backbone may be overcome by the variation of the torsion angle of the carboxylate groups with respect to the corresponding methylene groups and generate a curved linker that would afford similar topologies as those expected from the *anti-gauche* mode.

The adipate anion possesses a supplementary degree of freedom in addition to a wide range of possible conformations of the carboxylate functions with respect with the carbon backbone. The resulting metal-organic networks may reveal difficult to specifically predict; however, Figure 4.4 has shown that adipate may simply be seen either as a linear or as a curved ligand, and would therefore generate the corresponding topologies (2D square grid or distorted grid and 1D double chain) in appropriate circumstances.

In this context the coordination of glutarate and adipate anions with bimetallic building units has been systematically evaluated by variation of the neutral axial ligand and the reaction conditions. We have thus prepared a series of coordination polymers based upon these flexible ligands and have observed that the generation of dicopper tetraglutarate and tetraadipate chromophores has lead to the preferential conformations *anti-gauche* and *anti-gauche-gauche*, with the topologies of the products obtained being influenced by the coordination geometry. Since this work has been instigated with an eye towards the generation of supramolecular porous materials, it is important to address some of the significant developments concerning this area.

4.2. Porous metal-organic networks

4.2.1. Context

Since the discovery by Hofmann in 1897 of the first cyanide inclusion compound $Ni(CN)_2 \cdot NH_3 \cdot C_6H_6$,[36] which was only structurally characterized about fifty years later[38,39]; a large number of supramolecular metal-organic networks suitable for enclathration of a range of organic guest molecules has been subsequently generated and investigated in terms of network topology and host-guest interactions.

In this context, metal-organic networks structures exemplify predictability since their network structures can be controlled by the preselection of an appropriate node (metal coordination geometry) and spacer (organic ligand).[88,122,278,279] However their intrinsic properties such as thermal stability or porosity have been, to some extent, overlooked.[143] Recent intensive research in the field of metal-organic networks has resulted in an increasing number of novel porous compounds that possess characteristics unattainable in zeolite chemistry.[95,96,114,125,144,145,236,237,275,280-284]

In order to delineate a strategy towards predicting the self-organization of molecular building units into 1D, 2D or 3D networks that would possess a sufficient degree of robustness to sustain guest-free cavity, an in-depth study of the relationship between the specifics of such structures, strength and dimensionality of the network connections or potential for interpenetration, and their thermal and dynamic properties is of profound importance. Generally, most stable networks upon guest removal are 3D coordination networks, but 2D, 1D and even 0D topologies have also been reported to enable non-covalent interactions via hydrogen bonds, aromatic stacking or van der Waals

forces and generate relatively thermally stable porous networks.[64,285-288] The investigation of the stability of porous materials upon guest removal requires the use of experimental techniques that will provide structural information in addition to visual examination, gravimetric and thermal data of the apohost formed after desorption of the guest molecules. In this context, X-ray powder and single crystal diffraction represent the most appropriate tools for such studies. In effect, the diffraction pattern is representative of the crystalline structure of a given metal-organic network and can serve to identify the substance and hence to determine the structural integrity of the network after desorption and/or readsorption of its guest molecules. In this regard, the broadening of diffraction pattern constitutes a common feature observed upon guest removal due to the degradation of the long-range order that usually corresponds to the presence of crystalline imperfections within the apohost structure. In such cases, the network may be retained and, when reimmersed in a solution or in contact with a gas containing guest molecules, the initial pattern is restored, although the qualification of the material as porous may be inadequate since the possibility of recrystallization remains. The guest molecules can, in some instances, be directly exchanged without prior removal of the original guest species, but without information concerning the retention of structural features that indicate the conservation of the apohost topology; the corresponding supramolecular networks cannot yet be designated as porous materials. Finally, there have been recent examples of *flexible* structures based upon hydrogen bonds or containing conformationally labile components that undergo reversible structural change upon their transition from host-guest to apohost.[260,289] Their single- or micro-crystallinity was maintained demonstrating

their propriety of adjustability in response to external change. This so-called "sponge-like" behavior within the solid state may be a valuable feature for a new class of flexible porous materials. Figure 4.6 shows a significant example of such porous 2D metal-organic bilayer.

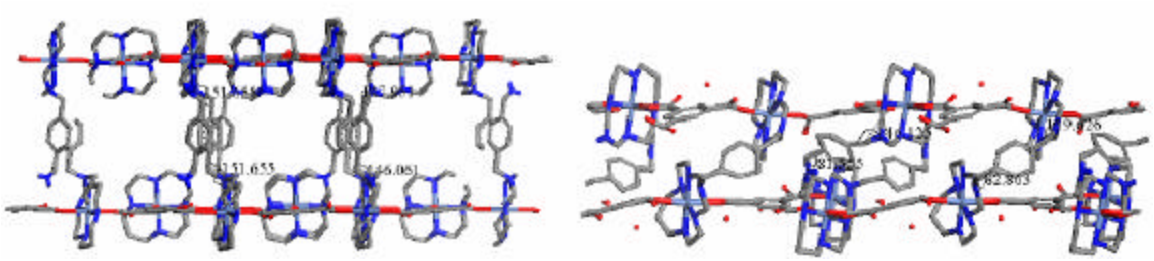

Figure 4.6. Sponge-like behavior of the metal-organic bilayer structure $Ni_2L_3(BTC)_4$[260] upon desolvatation and variation of the corresponding torsion angles of the flexible parts.

4.2.2. Classification of porous supramolecular metal-organic networks

Considering the numerous examples of porous supramolecular metal-organic networks that have been reported to date and the diversity in terms concerning the description of their sorption properties, their classification according to the stability and dynamic of these materials with respect to their response to guest desorption resulting in different types of micro- or nano-porosity properties is valuable.[284] In effect, it is important to distinguish non-porous structures that collapse upon guest removal from porous ones, which sustain empty cavities. However, it became evident from significant recent examples that such an organization can also be refined in order to take into account the fundamental changes that are associated with the host-guest/apohost transition. Along with the latest technological advances that render possible the determination of larger and more complex structures, it is now possible to obtain a precise knowledge of the structural evolution of porous networks. For example, the

structural elucidation of apohost networks via single-crystal or powder diffraction has evidenced the variation of structural parameters resulting from guest desorption. In this context, a classification of porous supramolecular metal-organic networks that retain single-crystallinity upon guest removal can reveal distinct features that are associated with the structures according to the preservation of chemical or structural integrity during the desorption process, Table 4.3. In a broader perspective, it should be noted that usual techniques utilized to characterize the porosity of metal-organic networks reported in the literature are sufficient. Nevertheless, in specific cases such as these presented in Table 4.3, when the structures present some degree of flexibility that generates more or less critical changes in the apohost network, an extensive study of these structural or chemical modifications may be of interest for potential applications (e.g. size/shape/function selectivity of the empty cavities for adsorbents or sensing devices, presence of active sites on uncoordinated metal centers for catalysis…). As a sideline, the retention of single-crystallinity after physical or chemical alteration of such porous compounds may be important for certain type of device applications.

Table 4.3. Classification of porous supramolecular metal-organic networks according to their behavior upon guest desorption/readsorption

	Dim	Network	Formula	Guest	Description of changes associated with host-guest/apohost transition	Ref.
No Structral Change	1D	Ladder	$Ni_2(4,4'\text{- bipy})_3(NO_3)_4$	MeOH	Lattice parameter *b* reduced by 0.53(9)% upon desorption (120ºC) Reversibility - Function selective readsorption	290
	2D	Bilayer	$Ni_2(4,4'\text{-bipy})_3(NO_3)_4$	EtOH	Less than 2.3% changes in cell dimensions upon desorption (100ºC) - Reversibility	291
	3D	Spiral net	$Cu(\text{Isonicotinate})_2$	H_2O	Less than 0.2% changes in cell dimensions upon desorption (140ºC) - Reversibility - Expension (up to 8% vol) upon readsorption of propanol - Size selective readsorption	238
	3D	Distorted diamondoid net	$Co_2(H_2O)(\text{Nicotinate})_4$	EtOH+ H_2O	Less than 0.2% changes in cell dimensions upon desorption (vacuum) – Reversibility No selectivity observed for readsorption capability	215
	3D	Cubic net	$Zn_4O(1,4\text{-BDC})_3$	DMF+ PhCl	Less than 0.9% changes in cell dimensions upon desorption (300ºC) Reversibility	292
	3D	Octahedral net	$Cu(4,4'\text{-bipy})_2(SiF_6)$	H_2O	Identical cell parameters of partially desolvated crystals - Reversibility	113,119
	2D	Square grid	$NiL^1{}_2(NO_3)_2{}^*$	*o*-xylene	Less than 0.5% changes in cell dimensions upon desorption (150ºC under vacuum) - No study on reversibility	103
	3D	Pillared rhombus grids	$Cu(\text{Isonicotinate})_2$	EtOH	Partial desorption at room temperature (sof 0.53 for EtOH molecules) No study on reversibility	218
	3D	Helical array	$Cd_2L^2{}_2(NO_3)_4{}^*$	Free L^2	Less than 3.0% changes in cell dimensions upon desorption (reflux in toluene solubilizing free L^2) - No study on reversibility	293
Sructural Change	0D	Packing forming hexagonal channels	$[CuL^3{}_2]*2/3(CH_2Cl_2)^*$	H_2O	Space group changes from $Cmc2_1$ to *R*-3 upon desorption (vacuum) Reversibility	294
	0D	Packing via H-bonds forming channels	$[Co(H_2O)_6]H_2(\text{TC-TTF})$	H_2O	Space group changes from *P*-1 to *P*112/*m* upon desorption Reversibility – Size/Function selective readsorption	289
	1D	3D assembly of chains *via* H bonds	$Cu_2L^4{}_2Ni(CN)_4(ClO4)_2{}^*$	H_2O	Space group changes from $P2_1/m$ to $P2_1/c$ upon desorption (100ºC) Reversibility – Size/Function selective readsorption	295
	2D	Bilayer	$Ni_2L^5{}_3(BTC)_4{}^*$	Pyr+ H_2O	Space group changes from *P*-1 to *P*1 upon desorption (75ºC) Reversibility	260
	2D	Rhombus grid 2-fold interpenetration	$Fe_2(4,4'\text{-azpy})_4(NCS)_4$	EtOH	Space group changes from *C*2/*c* to *Ibam* upon desorption (102ºC) Reversibility – Spin crossover switched upon transition	125
	3D	(10,3)-b net 2-fold interpenetration	$(ZnI_2)_3L^6{}_2{}^*$	$PhNO_2$	Space group changes from *C*2/*c* to *P*-1 upon desorption (170ºC) Reversibility	296
	0D	Assembly of complexes in chains	(*tBu*Salcam)MnCl	CH_2Cl_2	Lattice parameter *b* reduced from 49 to 15 Å upon desorption (with drastic conformational changes) - No study on reversibility	297
Chemical Change	3D	PtS net (decorated)	$Cu_2(ATC)$	H_2O	Space group changes from *C*2/*c* to $P4_2/mmc$ upon removal of coord. and uncoord. water Reversibility – Increased antiferromagnetic coupling upon desorption	298

* L^1 = 4,4'-bis(4-pyridyl)biphenyl, L^2 = 2,4'-(1,4-phenylene)bispyridine, L^3 = 1,1,1-trifluoro-5,5-dimethyl-5-methoxyacetylacetone, L^4 = bis(3-aminopropyl)methylamine, L^5 = $C_{26}H_{52}N_{10}$ bismacrocycle, L^6 = 2,4,6-tris(4-pyridil)triazine,

4.2.3. Properties and applications

Although porous metal-organic networks do not compare to zeolite materials in terms of robustness or thermal stability, their inherent modularity allows specific functionalization to provide desirable properties. In effect, the presence of metal centers affords the potential for a variety of redox, acid-base or magnetic properties; the use of asymmetric organic ligands can generate chirality or non-linear optical properties within the resulting supramolecular networks. The overall topology may be fine-tuned in terms of size and shape of the cavities and create specific host-guest interactions. As a result, these materials present various potential applications as adsorbents,[299] sensors,[300] catalysts[66] or in separation[301] and ion exchange.[113]

Among the porous coordination compounds mentioned above, few examples are known of structures that contain a flexible component, comparatively to their rigid counter-parts, because such a lack of rigidity leads to a higher degree of difficulty in terms of designing such materials. However, the rational utilization of non-rigid building units based upon the strategic principles presented above can provide a range of supramolecular metal-organic networks and extend their potential applications to the development of highly tunable hybrid materials that will possess properties related to the characteristics of their molecular components such as the possible ability of adaptation of such materials to their surrounding chemical environment.

4.3. Experimental

4.3.1. Materials and Methods

General methods, instruments and software suites have been described in Chapter 3, Section 3.3.1. FT-IR spectra of all compounds are presented in appendices C6-C11. The crystals of all compounds were shown to be representative of the bulk by comparison of the x-ray powder diffraction pattern of fresh samples with the corresponding pattern calculated from the crystal structures. All XRPD patterns can be found in appendices C6-C11. Thermogravimetric analysis was performed in air for readsorption monitoring on TA Instruments TGA 2950 Hi-Res. For guest readsorption experiments, the solvents used were HPLC grade (H_2O = 0.009%) and the concentration changes were measured on a Shimadzu GC-17A gas chromatograph with flame ionization detector (GC-FID) using toluene as the internal standard. The data were fitted to the equation previously published by K. S. Min and M. P. Suh.[301]

4.3.2. Syntheses

Synthesis of {[Cu_2(glutarate)$_2$(dimethylformamide)$_2$]}$_n$, ***18***

A solution of $Cu(NO_3)_2 \cdot 2.5H_2O$ (0.233 g, 1.00 mmol), glutaric acid (0.264 g, 2.00 mmol) and dimethylformamide (4.72 g, 64.6 mmol) dissolved in 15 ml methanol was stirred briefly before heating to *ca.* 80°C for 2 hours. The clear blue solution was left undisturbed at room temperature. Green-blue crystals of **18 (**0.230 g, 0.431 mmol, 86.2%), suitable for X-ray studies, appeared after 2 weeks.

Synthesis of {[Cu_2(adipate)$_2$(pyridine)$_2$]}$_n$, ***19***

According to an analogous method as the synthesis of 18, the reaction of $Cu(NO_3)_2 \cdot 2.5H_2O$ (0.233 g, 1.00 mmol), adipic acid (0.292 g, 2.00 mmol), pyridine (0.316 g, 3.99 mmol) in 20 ml methanol gave green crystals of **19** (0.138 g, 0.241 mmol, 48.2%) after 48h.

Synthesis of {[Cu_2(glutarate)$_2$(pyridine)$_2$]}$_n$, ***20***

In a solution of $Cu(NO_3)_2 \cdot 2.5H_2O$ (0.233 g, 1.00 mmol), glutaric acid (0.264 g, 2.00 mmol) and pyridine (0.158 g, 2.00 mmol) dissolved in 30 ml methanol, green crystals of **20 (**0.268 g, 0.491 mmol, 98.2%), suitable for X-ray studies, appeared after 24h.

Synthesis of {[Cu_2(glutarate)$_2$(4,4'-bipyridine)]$\cdot 3H_2O$]}$_n$, ***21***[302]

Compound **21** forms *via* reaction of $Cu(NO_3)_2 \cdot 2.5H_2O$ (1.165 g, 5.009 mmol), glutaric acid (1.982 g, 15.00 mmol) and 4,4'-bipyridine, bipy, (0.390 g, 2.50 mmol) in water. The initial product formed, as characterized by x-ray powder diffraction of the light blue powder obtained during the synthesis of **21**, was found to be isostructural with $ML_{1.5}$ ladder[269] compound. The initial product was converted to green crystals of **21** by heating the reaction mixtures at *ca.* 80ºC for several hours. Yield of 1.392g (2.353 mmol, 93.95%) was obtained; excess glutaric acid was recycled by filtration of the supernatant solution and recrystallization.

Synthesis of {[Cu_2(glutarate)$_2$(1,2-bis(4-pyridyl)ethane)]$\cdot 5H_2O$]}$_n$, ***22***[302]

Green crystals of **22**, were obtained in a similar manner as those of compound **21**

with 1,2-bis(4-pyridyl)ethane, bipyethane, (0.460 g, 2.52 mmol) instead of bipy with a yield of 1.615g (2.479 mmol, 98.98%). The initial product formed, as characterized by single crystal unit cell determination of the dark blue crystals obtained during the synthesis of **22** (Monoclinic, *C2/c*, *a* = 25.21, *b* = 9.19, *c* = 19.75 Å, ß = 94.98 deg, volume = 4548 $Å^3$) and x-ray powder diffraction, was found to be isostructural with $ML_{1.5}$ bilayer[208] compound.

Synthesis of $\{[Cu_2(adipate)_2(1,2\text{-bis}(4\text{-pyridyl})ethane)]\cdot 1H_2O\cdot 1CH_3OH]\}_n$, ***23***

A solution of adipic acid (0.146 g, 1.00 mmol), NaOH (0.0800 g, 2.00 mmol), bipyethane (0.0921 g, 0.500 mmol) in 25 ml methanol was carefully layered onto a solution of $Cu(NO_3)_2\cdot 2.5H_2O$ (0.233 g, 1.00 mmol) in 10 ml water. An initial product formed, as a blue powder, was characterized by x-ray powder diffraction to be isostructural with $ML_{1.5}$ bilayer[208] compound and was converted to green crystals of **23** after one week. Yield of 0.180 g (0.260 mmol, 51.9%) was obtained.

4.3.3. Guest sorption studies

Crystals of **18**-**23** were observed to retain their single crystallinity when removed from the mother liquor. Thermogravimetric analysis of **21a** revealed that it is stable up to 300ºC with loss of *ca.* 8.5% mass between 60 and 120ºC, consistent with desorption of water molecules (calculated 9%). Interestingly, when heated at 150ºC for 3 days, crystals of **21a** were observed to remain crystalline and the crystal structure of the apohost, **21b**, confirmed that removal of guest molecules does not influence the 3D network. IR, thermal analysis and GC experiments were used to confirm that **21b** can readsorb water

molecules under various conditions to generate **21c**. The 3 compounds **21a**, **21b** and **21c** have been characterized by X-ray single crystallography. **22a** was observed to desorb its guest water molecules following exposure to the atmosphere for *ca.* 1 hour. The resulting apohost **22b** retained single crystallinity and was observed to adsorb water molecules *via* immersion in water. The resulting crystals, **22c,** were confirmed to be isostructural to **22a**.

4.3.4. X-ray Crystallography

In the crystal structures of **18-23**, all non-hydrogen atoms were refined with anisotropic displacement parameters except for the oxygen atoms of solvent in **22c**. The H atoms of the C-H groups were fixed in calculated positions except for the carbon atom of methanol solvent in **23**. The 2 molecules of solvents water and methanol in **23** were observed to exhibit high thermal motion. The two molecules of water in the asymmetric unit of **21a** lie at general and special positions, thereby affording the reported 1:3 stoichiometry. The water molecules of **21c** were disordered over several positions and were refined with fixed site occupation factors (s.o.f.). In **22**, the oxygen atoms of the solvent were disordered over several general positions (8 for **22a**, 5 for **22b** and 9 for **22c**) and refined with fixed s.o.f. for total of occupancies of 2.5, 1 and 2.5 respectively. These correspond to 1:5, 1:2 and 1:5 stoichiometries since the tetracarboxylate moities lie around special positions. Full crystallographic data can be found in the electronic supplementary data. Crystal data and structure refinement parameters of compound **18-23** are presented in Table 4.4.

Table 4.4. Crystallographic data for compounds 18-23

Compound	**18**	**19**	**20**	**21a**	**21b**	**21c**
Chemical formula	$C_{16}H_{26}Cu_2N_2O_{10}$	$C_{22}H_{26}Cu_2N_2O_8$	$C_{20}H_{22}Cu_2N_2O_8$	$C_{20}H_{26}Cu_2N_2O_{11}$	$C_{20}H_{20}Cu_2N_2O_8$	$C_{20}H_{20}Cu_2N_2O_{11}$
Formula weight	533.47	573.53	545.48	597.51	543.46	591.46
Temperature, K	293(2)	293(2)	100(2)	100(2)	100(2)	100(2)
Crystal system	Monoclinic	Triclinic	Orthorhombic	Monoclinic	Monoclinic	Monoclinic
Space group	P2(1)/c	P-1	Pbca	C2/c	C2/c	C2/c
a, Å	9.0201(12)	8.1820(19)	13.1322(12)	21.191(2)	21.011(2)	21.351(2)
b, Å	7.8902(10)	8.6312(19)	8.4963(8)	13.1900(13)	13.0520(14)	13.1381(13)
c, Å	14.9020(19)	9.245(2)	18.8964(18)	8.5212(9)	8.5284(9)	8.5699(9)
a, deg	90	107.860(4)	90	90	90	90
ß, deg	106.012(2)	106.494(4)	90	100.314(2)	100.679(2)	101.007(2)
γ, deg	90	100.433(4)	90	90	90	90
V, $Å^3$	1019.4(2)	569.5(2)	2108.4(3)	2343.3(4)	2298.3(4)	2359.8(4)
Z	2	1	4	4	4	4
ρ_{calcd}, $g.cm^{-3}$	1.738	1.672	1.718	1.694	1.571	1.665
μ, mm^{-1}	2.143	1.919	2.069	1.878	1.897	1.864
F(000)	548	294	1112	1224	1104	1200
Crystal size, mm	0.08x 0.07x0.02	0.02x0.02x0.02	0.07x0.05x0.02	0.08x0.08x0.08	0.08x0.08x0.08	0.08x0.08x0.08
θ range for data collection, deg	2.35 to 25.02	2.48 to 25.03	2.16 to 28.32	1.83 to 27.48	1.85 to 27.14	1.83 to 27.12
Limiting indices	-10<=h<=10 -9<=k<=8 -17<=l<=14	-9<=h<=5 -10<=k<=10 -10<=l<=10	-15<=h<=17 -11<=k<=11 -24<=l<=19	-19<=h<=27 -17<=k<=14 -11<=l<=10	-26<=h<=21 -15<=k<=16 -10<=l<=10	-27<=h<=27 -9<=k<=16 -10<=l<=10
Reflections collected	5225	3027	12708	7149	7048	6920
Unique reflections	1798	1987	2549	2670	2532	2582
R(int)	0.0492	0.0649	0.0623	0.0322	0.0387	0.0304
Completeness to θ, %	99.9	98.4	97.0	99.4	99.6	99.3
Absorption correction	SADABS	SADABS	SADABS	SADABS	SADABS	SADABS
Max. and min. transmission	1.000 and 0.820	1.000 and 0.777	1.000 and 0.848	1.000 and 0.843	1.000 and 0.861	1.000 and 0.806
Data / restraints / parameters	1798 / 0 / 138	1987 / 0 / 154	2549 / 0 / 145	2670 / 4 / 159	2532 / 0 / 147	2582 / 0 / 182
Goodness-of-fit on F^2	1.055	1.023	1.063	1.046	1.038	1.094
Final R indices [I>2sigma(I)]	R1 = 0.0349, wR2 = 0.0866	R1 = 0.0642, wR2 = 0.1220	R1 = 0.0452, wR2 = 0.0885	R1 = 0.0376, wR2 = 0.0921	R1 = 0.0342, wR2 = 0.0859	R1 = 0.0380, wR2 = 0.1071
R indices (all data)	R1 = 0.0397, wR2 = 0.0892	R1 = 0.0941, wR2 = 0.1357	R1 = 0.0632, wR2 = 0.0956	R1 = 0.0452, wR2 = 0.0963	R1 = 0.0431, wR2 = 0.0904	R1 = 0.0465, wR2 = 0.1112
Largest diff. peak and hole, $e.Å^{-3}$	0.420 and -0.345	0.826 and -0.631	0.471 and -0.510	0.946 and -0.575	0.533 and -0.416	0.628 and -0.328

Table 4.4. (continued)

Compound	**22a**	**22b**	**22c**	**23**
Chemical formula	$C_{22}H_{24}Cu_2N_2O_{13}$	$C_{22}H_{24}Cu_2N_2O_{10}$	$C_{22}H_{24}Cu_2N_2O_{13}$	$C_{26}H_{28}Cu_2N_2O_{12}$
Formula weight	651.51	603.51	651.51	687.58
Temperature, K	100(2)	100(2)	100(2)	100(2)
Crystal system	Monoclinic	Monoclinic	Monoclinic	Monoclinic
Space group	C2/c	C2/c	C2/c	C2/c
a, Å	24.238(2)	24.047(8)	23.911(3)	24.808(6)
b, Å	13.0527(13)	11.784(4)	11.8685(15)	12.827(3)
c, Å	8.6313(8)	9.059(3)	9.2063(12)	9.031(2)
a, deg	90	90	90	90
ß, deg	91.473(2)	91.044(6)	90.350(2)	93.368(5)
γ, deg	90	90	90	90
V, $Å^3$	2729.8(5)	2566.4(14)	2612.5(6)	2868.7(12)
Z	4	4	4	4
ρ_{calcd}, $g.cm^{-3}$	1.585	1.562	1.656	1.592
μ, mm^{-1}	1.625	1.713	1.698	1.549
F(000)	1328	1232	1328	1408
Crystal size, mm	0.15x0.07x0.05	0.10x0.02x0.02	0.07x0.05x0.02	0.07x0.05x0.05
θ range for data collection, deg	1.68 to 27.48	1.69 to 25.07	1.70 to 24.99	1.64 to 25.00
Limiting indices	-30<=h<=30 -16<=k<=11 -10<=l<=11	-28<=h<=28 -13<=k<=13 -10<=l<=9	-28<=h<=28 -14<=k<=13 -10<=l<=9	-28<=h<=29 -4<=k<=15 -9<=l<=8
Reflections collected	8295	6194	6627	3378
Unique reflections	3082	2257	2292	2145
R(int)	0.0286	0.0949	0.0479	0.0413
Completeness to θ, %	98.4	98.8	99.4	84.5
Absorption correction	SADABS	SADABS	SADABS	SADABS
Max. and min. transmission	1.000 and 0.858	1.000 and 0.473	1.000 and 0.815	1.000 and 0.751
Data / restraints / parameters	3082 / 0 / 222	2257 / 0 / 186	2292 / 0 / 187	2145 / 0 / 190
Goodness-of-fit on F^2	1.049	1.083	1.022	1.037
Final R indices [I>2sigma(I)]	R1 = 0.0410, wR2 = 0.0941	R1 = 0.0741, wR2 = 0.1487	R1 = 0.0402, wR2 = 0.0885	R1 = 0.0630, wR2 = 0.1553
R indices (all data)	R1 = 0.0484, wR2 = 0.0972	R1 = 0.1139, wR2 = 0.1618	R1 = 0.0558, wR2 = 0.0948	R1 = 0.0920, wR2 = 0.1740
Largest diff. peak and hole, $e.Å^{-3}$	0.594 and -0.417	0.873 and -0.725	0.525 and -0.476	0.899 and -0.524

4.4. Results and Discussion

4.4.1. 1D structures

The structure of compound **18** is based on dimetal tetracarboxylates building units bridged by two pairs of glutarate ligands, where the four flexible linkers adopt a *syn* configuration with each other around the bimetallic node, forming an arrangement in double chains of $[Cu_2(glutarate)_2]_n$ along the *y*-axis, Figure 4.7. The center of each dicopper tetracarboxylate chromophore lies on an inversion center, which generates two crystallographically equivalent Cu^{2+} ions separated by 2.61 Å that are additionally coordinated at their axial positions to the oxygen atoms of two DMF solvent molecules. The individual double chains align in layers parallel to [001] sustained by weak hydrogen bonds between the methyl groups of the DMF ligands of one 1D array and the coordinated oxygen atoms of the glutarate ligands of the adjacent double chains (d(C···O) = 3.67 Å), Figure 4.8a. The layers are aligned antiparallel with respect to the orientation of the axial ligand DMF and each layer is slipped with respect to the layer beneath along the *y*-direction by *b*/2 = 3.95 Å, Figure 4.8b. In the *z*-direction the 3D packing is facilitated by weak interactions between the methylene groups of the glutarate ligands and the oxygen of the coordinated carboxylate moieties of adjacent double-chains *via* hydrogen bonds with (d(C···O) = 3.65 to 3.67 Å). The glutarate ligands adopt the *anti-gauche* mode with torsion angles of 175º and 57º and the orientation of the carboxylate moieties with respect to the backbone generates dihedral angles of *ca.* 43º and 37º.

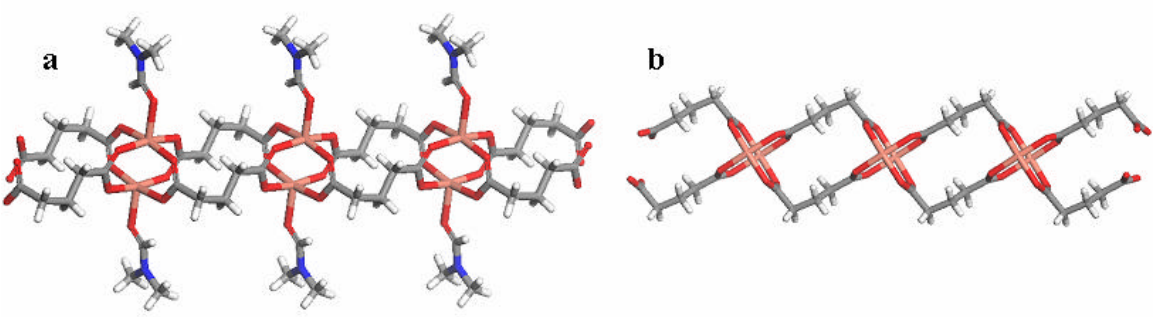

Figure 4.7. Detailed view of the 1D double chain of $[Cu_2(glutarate)_2(DMF)_2]_n$ formed by compound 18 down [001], (a) and [100] (b)

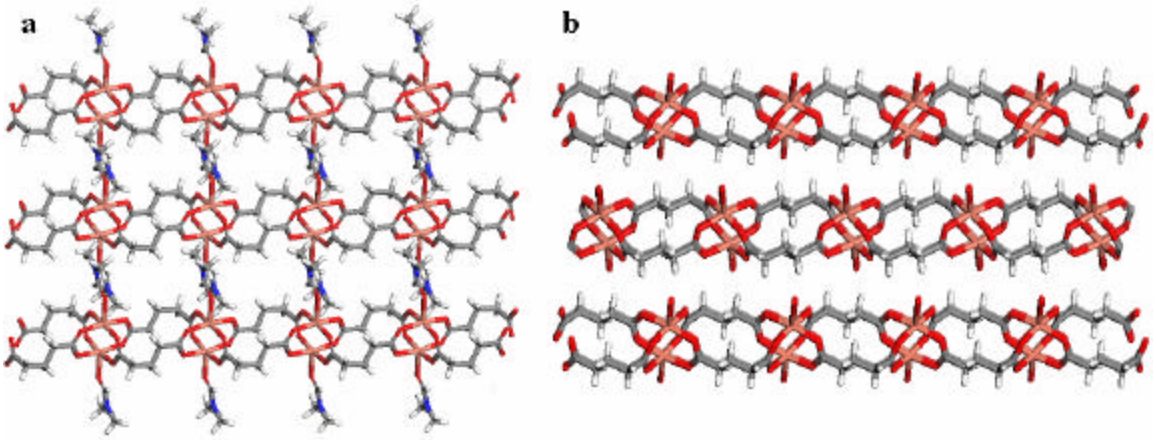

Figure 4.8. Crystal packing of the 1D nets of compound 18 down [001] (a) and [100] (b)

Compound **19** crystallizes in the space group P-1 and forms a similar 1D topology as described in compound **18** with pyridine molecules instead of DMF as the axial ligands of the dicopper tetraadipate chromophore, Figure 4.9. The 2D systems of adjacent double chains parallel to [001] allow p-p face-to-face interactions between the pyridine ligands of adjacent layers (d(C···C) = 3.31 to 3.53 Å), all layers are parallel and present the same orientation relative to the pyridine ligands. Figure 4.10 shows a representation of the crystal packing of the structure of **19** parallel to [001] and [110]. In **19** the conformation of the adipate ligands corresponds to the *anti-gauche-gauche* mode with

torsion angles of 170º, 67º and 65º and the orientation of the carboxylate moieties with respect to the backbone generates dihedral angles of *ca.* 36º and 31º, Figure 4.9. Interestingly, a related 1D network based upon dicopper tetraadipate, where cyclohexanol molecules act as the axial ligands has been reported in a structure that contains analogous double chains stacking between 2D sheets based upon the same metal-organic building blocks, Figure 4.11. In the double chain of $[Cu(adipate)(C_6H_{11}OH)]_n$, the dihedral angles adopted by the adipate ligand in the *anti-anti-gauche* mode are 176º, 170º and 68º (Table 4.2, CSD code MITHUS).[276]

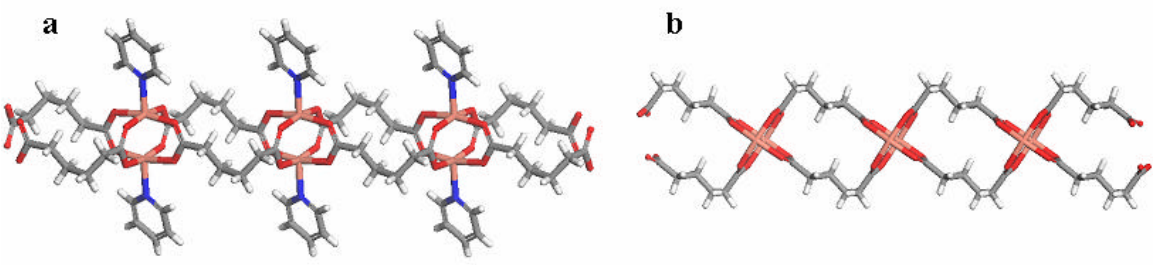

Figure 4.9. Detailed view of the 1D double chain of $Cu_2(adipate)_2(pyridine)_2$ formed by compound 19 down [100] (a) and [001] (b)

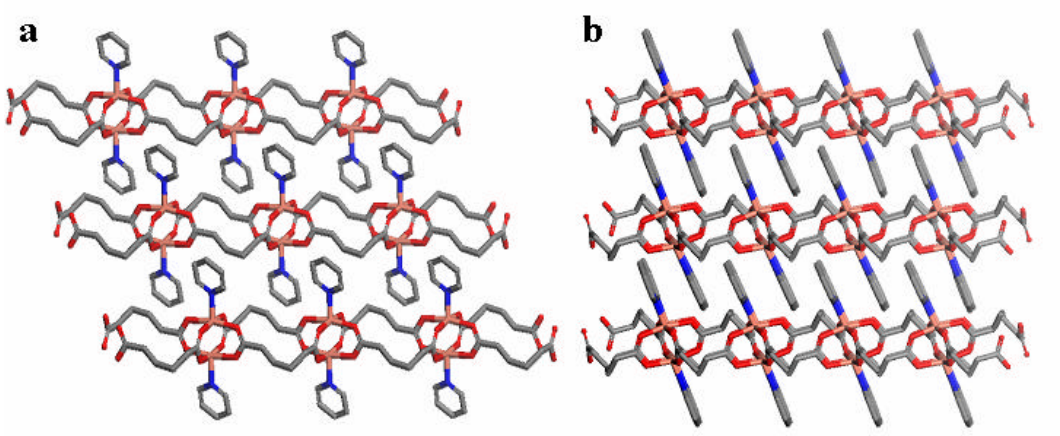

Figure 4.10. Crystal packing of the 1D nets of 19 down [100] (a) and [110] (b), hydrogen atoms are omitted for clarity

The two novel compounds **18** and **19** based upon a 4-connected node and flexible

links glutarate and adipate, in constrained conformations *anti-gauche*, *anti-anti-gauche* and *anti-gauche-gauche*, have afforded the 1D, double chain, topology resulting from the $C_{2?}$ symmetry of the angled ligands with respect to the dimetal axis.

In the alternative case of all flexible linkers adopting a $C_{4?}$ symmetry around the bimetallic node, the 2D topology is expected, Figure 4.5.

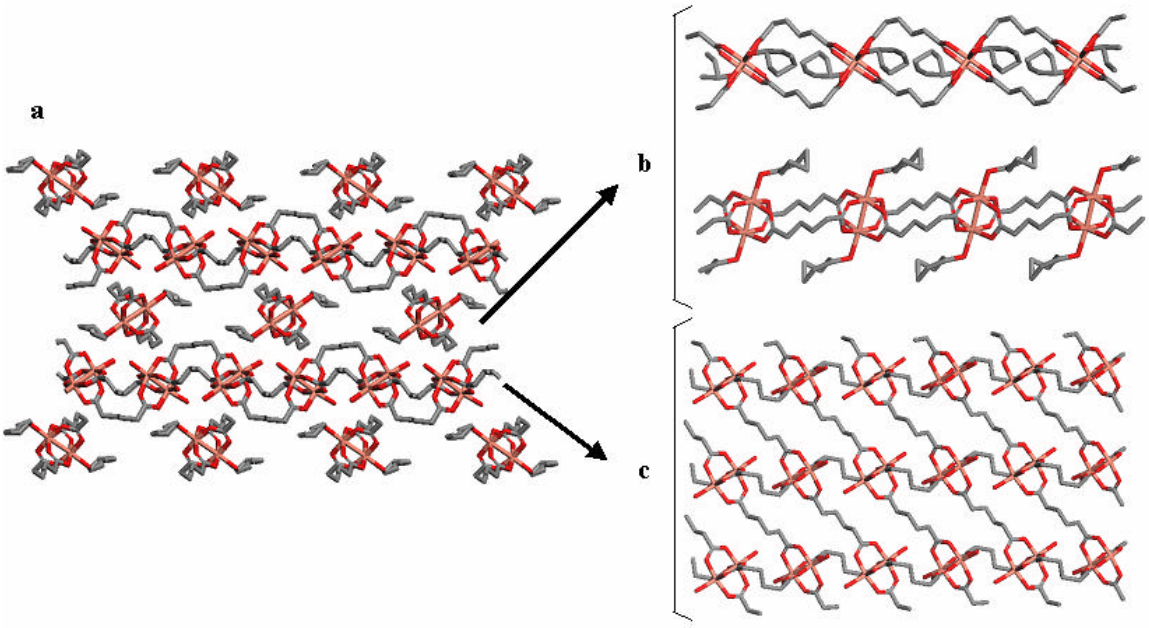

Figure 4.11. Crystal structure of $[Cu_3(adipate)_3(H_2O)_2(C_6H_{11}OH)]_n$[276] (a) showing the 1D double chain of $[Cu(adipate)(C_6H_{11}OH)]_n$ (b) and the 2D sheets of $[Cu_2(adipate)_2(H_2O)_2]_n$ (c), hydrogen atoms are omitted for clarity

4.4.2. 2D structures

Compound **20** consists of corrugated sheets of metal-glutarate moieties parallel to [001], Figure 4.12a. The glutarate backbone possesses an *anti-gauche* conformational mode with torsion angles of 174º and 56º and a relative orientation of the carboxylate moieties with respect to the backbone of *ca.* 42º and 35º, Figure 4.12a. The axial pyridine ligands of a same 2D sheet interact *via* p-p face-to-face stacking (d(C···C) = 3.53 to 3.58 Å) while there is no evidence of strong interaction between two adjacent 2D networks.

The 3D arrangement results from the piling of antiparallel sheets where pyridine molecules are filling of the voids generated by adjacent corrugated sheets, Figure 4.12b-c. The topology of the 2D network in the structure of **20** can be described as a distorted rhombus grid, or 4^4 network, comparable to the 2D metal-organic network $[Cu_2(adipate)_2(H_2O)_2]_n$ represented in Figure 4.11c. Attempts to incorporate various guest molecules during crystallization of **20** were unsuccessful (benzene, toluene, nitrobenzene and anisole) and resulted in the formation of **20**. Attempts to adsorb these guests by direct contact with **20** were also unsuccessful. X-ray single crystal unit cell determination, FT-IR spectra and X-ray powder diffraction patterns of the product obtained were identical to these of compound **20**.

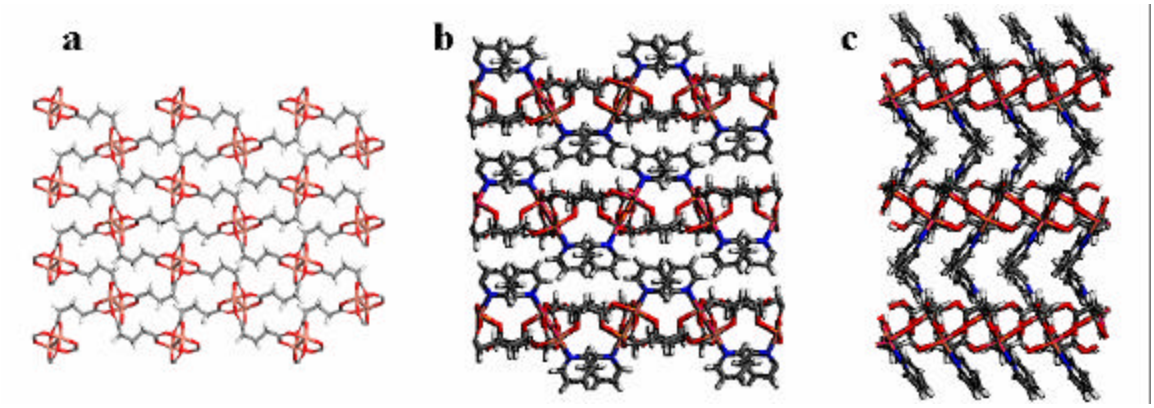

Figure 4.12. Detailed view of the $[Cu_2(glutarate)_2]_n$ sheets down [001] (a), crystal structure of the 2D net of 20 down [010] (b) and [100] (c)

The structure directing agents to the formation of a 1D double chain *versus* a 2D network based upon the same chromophore dicopper tetraadipate have been interpreted as resulting from the biphasic solvothermal synthesis leading to the generation of the double chain in the organic phase of cyclohexanol whereas the 2D sheets are present in the aqueous phase.[276] We have herein obtained analogous 1D and 2D structures from

glutarate ligand in organic conditions. The formation of the double chain over the 2D network appears to be mainly dependant upon the temperature at which the reaction takes place. These results illustrate how subtle differences of the conditions (temperature, solvent, pH…) during crystallization influence which topology is generated.

4.4.3. 3D structures

As mentioned above, the use of glutarate and adipate anions in coordination to bimetallic building units is capable, in appropriate circumstances, of sustaining 2D sheets. We report herein how such 2D networks can be rationally extended by pillaring *via* the use of bifunctional N,N'-donor ligands to generate the modular 3D nets $\{[Cu_2(L^1)_2L^2]\cdot G\}_n$, L^1 = glutarate, L^2 = 4,4'-bipyridine (bipy), **21** (G = $3H_2O$, **21a**, G = 0, **21b**, G = $3H_2O$, **21c**), L^1 = glutarate, L^2 = 1,2-bis(4-pyridyl)ethane (bipyethane), **22** (G = $5H_2O$, **22a**, G = $2H_2O$, **22b**, G = $5H_2O$, **22c**) and L^1 = adipate, L^2 = 1,2-bis(4-pyridyl)ethane (bipyethane), G = $1H_2O\cdot 1CH_3OH$, **23**.

21a consists of corrugated sheets of metal-glutarate moieties parallel to [100], Figure 4.13a, that are pillared via axial coordination of canted bipy ligands, Figure 4.13b. The resulting 3D network contains channels with effective dimensions of *ca.* 2.9 Å X 4.0 Å occupied by two crystallographically independent water molecules that form hydrogen bonded chains (d(O···O) = 2.81 and 2.97 Å) which interact with the methylene groups of the glutarate ligands (d(C···O) = 3.66-3.88 Å), Figure 4.13c. A similar 1D polymer of ordered water molecules was observed in a 3D hydrogen bonded ionic network that contains channels with the requisite size and environment. However, this structure does not survive desorption of the guest water molecules.[303] The glutarate ligands adopt the

anti-gauche mode with torsion angles of 175º and 57º and the orientation of the carboxylate moiety with respect to the backbone generates dihedral angles of *ca.* 43º and 37º, Figure 4.13a. The bridging bipy ligands connect the sheets in a criss-cross pattern that facilitates p-p face-to-face interactions (d(C···C) = 3.38 to 3.58 Å). Such a criss-crossed network possesses a topology related to the a-polonium net, a topology that has also been generated *via* $M(CN)_2$ sheets linked by pyrazine ligands.[304]

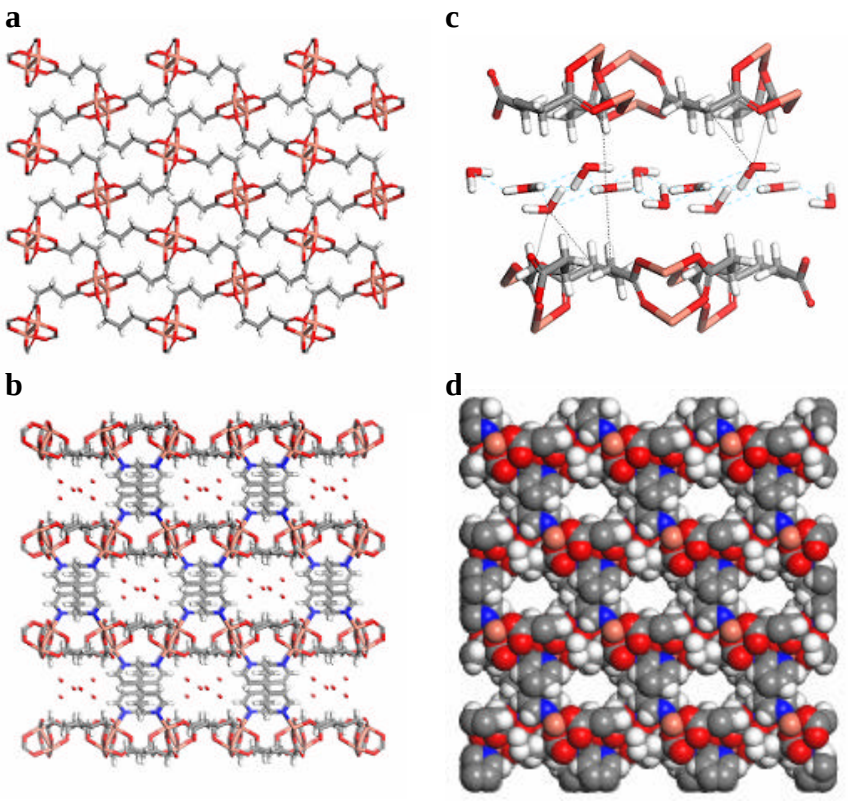

Figure 4.13. Detailed view of the $[Cu_2(glutarate)_2]_n$ sheets down [100] in 21 (a), crystal structure of the 3D net of 21a down [001] (b) and corresponding space filling representation (d) and view of a channel of water molecules in 21a (c)

Thermogravimetric analysis of **21a** revealed that it is stable up to 300ºC with loss of *ca.* 8.5% mass between 60 and 120ºC, consistent with desorption of water molecules (calculated 9%). Interestingly, when heated at 150ºC for 3 days, crystals of **21a** were

observed to remain crystalline and the crystal structure of the apohost, **21b**, confirmed that removal of guest molecules does not influence the 3D network. IR and thermal analysis were used to confirm that **21b** can adsorb water molecules under various conditions, Figures 4.14 and 4.15. For example, under an atmosphere of *ca.* 60% water vapour, a powdered sample of **21b** adsorbs water and reaches saturation after *ca.* 1 hour whereas single crystals of **21b** take *ca.* 15 hours to reach saturation. The X-ray crystal structure of such a sample, **21c**, revealed it to be crystallographically identical to **21a**. Attempts to incorporate other guest molecules during crystallization of **21** were unsuccessful (methanol, hexanes, mixtures of water: methanol (1:1, 1:5 and 1:10), benzene, nitrobenzene or anisole) and resulted in the formation of **21a**. Attempts to adsorb other guests by direct contact with **21b** were also unsuccessful (gas chromatographic experiments and infrared spectra indicated that methanol, ethanol, acetonitrile or n-hexane are not adsorbed under anhydrous conditions).

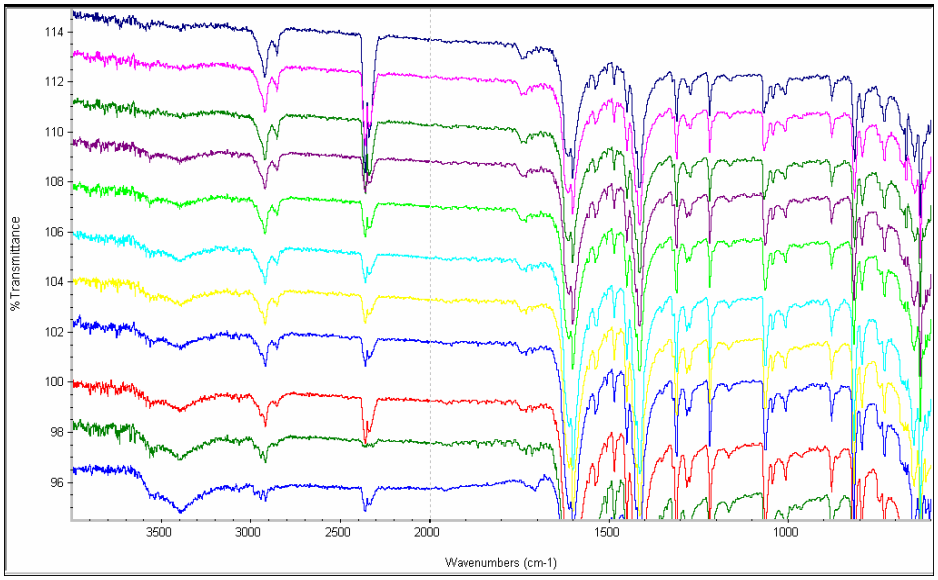

Figure 4.14. FT-IR spectra of compound 21b let in atmosphere for 55min (from t = 0, top, to t = 55min, bottom)

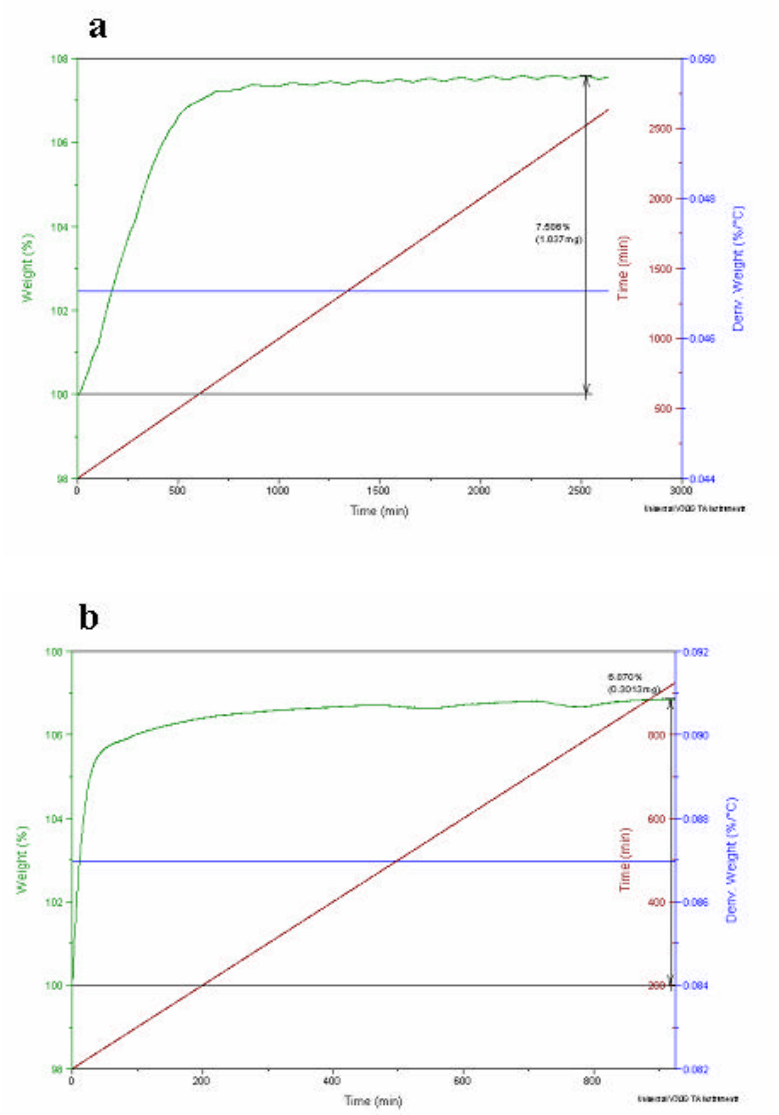

Figure 4.15. TGA traces of the rehydration of 21b crystals (a) and 21b powder (b) under ambient atmosphere

The crystal structure of **22** is similar to that of **21** with differences due to the presence of the additional ethylene moieties, Figure 4.16. **22a** contains channels with effective dimensions of *ca.* 3.5 Å X 4.4 Å occupied by 2.5 independent water molecules. The glutarate backbone possesses an *anti-gauche* conformation with torsion angles of 173º and 60º and a relative orientation of the carboxylate moieties with respect to the

backbone of *ca.* 39º and 33º. The bipyethane ligands are canted and criss-cross between the dicopper tetraglutarate sheets. They engage in edge-to-face aromatic stacking interactions (d(C···C) = 3.54 to 4.11 Å) reinforced by CH_2···CH_2 interactions (d(C···C) = 3.76 Å) and CH···p interactions (d(C···C) = 3.85 to 3.89 Å). **22a** was observed to desorb its guest water molecules following exposure to the atmosphere for less than 1 hour. Figure 4.17 shows the FT-IR spectra of the same sample of **22a** let in atmosphere for 45 min and the regular decrease in intensity of the broad band centered at 3500 cm^{-1} corresponding to the vibration of O-H bonds from the water guest molecules. The resulting apohost **22b** retained single crystallinity and was observed to adsorb water molecules *via* immersion in water. The resulting crystals, **22c,** were confirmed to be isostructural to **22a**. The slightly larger channels in **22a** would therefore appear to result in lower affinity for water molecules when compared to **21a**, which readily adsorbs from gas as well as liquid contact.

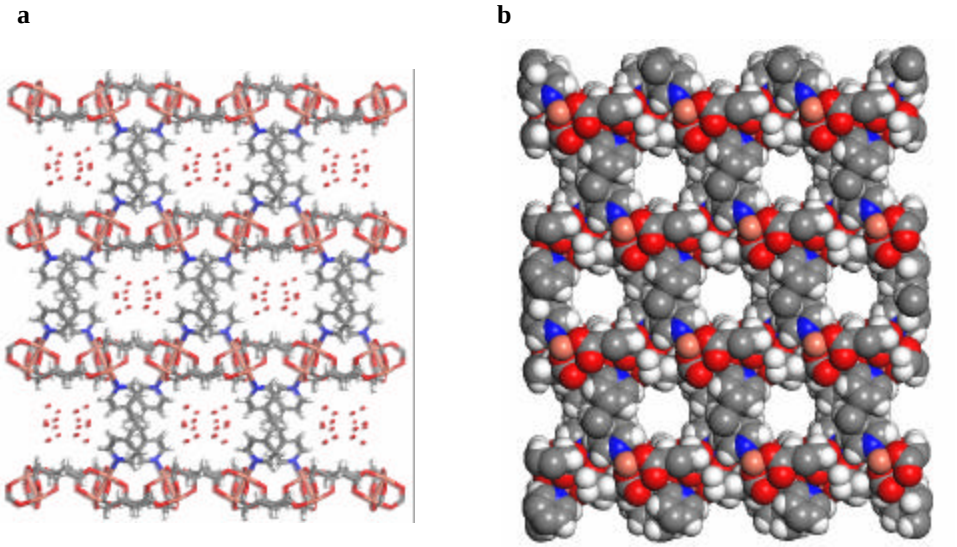

Figure 4.16. Crystal structure of the 3D net of 22a down [001] (a) and corresponding space filling representation where the guest water molecules are omitted (b)

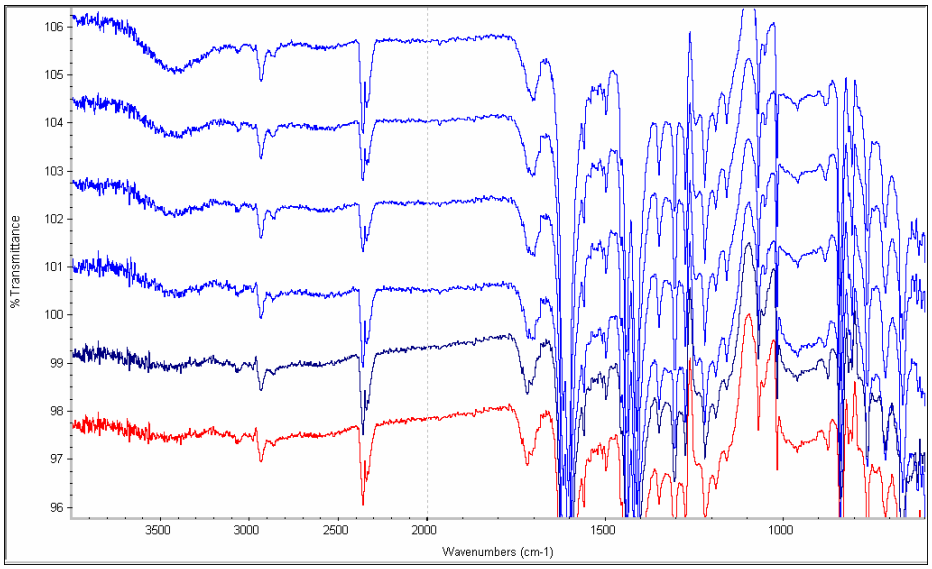

Figure 4.17. FT-IR spectra of compound 22a let in atmosphere for 45min (from t = 0, top, to t = 45min, bottom)

The crystal structure of **23** is similar to that of **22** with differences due to the presence of the additional methylene moiety in the adipate ligand, Figure 4.18. **23** contains channels with effective dimensions of *ca.* 3.1 Å X 4.3 Å occupied by disordered guest water and methanol molecules. The adipate backbone possesses an *anti-gauche-gauche* conformation with torsion angles of 170º, 57º and 53º and a relative orientation of the carboxylate moieties with respect to the backbone of *ca.* 69º and 16º. The bipyethane ligands are canted and criss-cross between the dicopper tetraadipate sheets. They engage in edge-to-face aromatic stacking interactions (d(C···C) = 3.84 to 4.29 Å) reinforced by $CH_2 \cdots CH_2$ interactions (d(C···C) = 3.91 Å) and CH···p interactions (d(C···C) = 3.98 to 4.02 Å). **23** was observed to readily desorb its guest molecules following exposure to the atmosphere for *ca.* 10 min. The apohost was observed to retain crystallinity but the quality of the resulting crystals was not sufficient to obtain an acceptable structure solution. The slight decrease in the dimensions of the channels in **23**, as compared with

those of **22**, is due to the presence of additional methylene groups of conformationally constrained adipate ligands, which, in return, render the cavities less hydrophilic than **21** and **22**. As a sideline, it should be mentioned that our attempt to prepare crystals of the corresponding network of $[Cu_2(adipate)_2]_n$ pillared by 4,4'-bipyridine ligands was unsuccessful. This is predictable since the shortening of aromatic linkers would generate destabilizing interactions between the adipate fragments contained in the channels and the 4,4'-bipyridine that criss-cross the dicopper tetraadipate sheets.

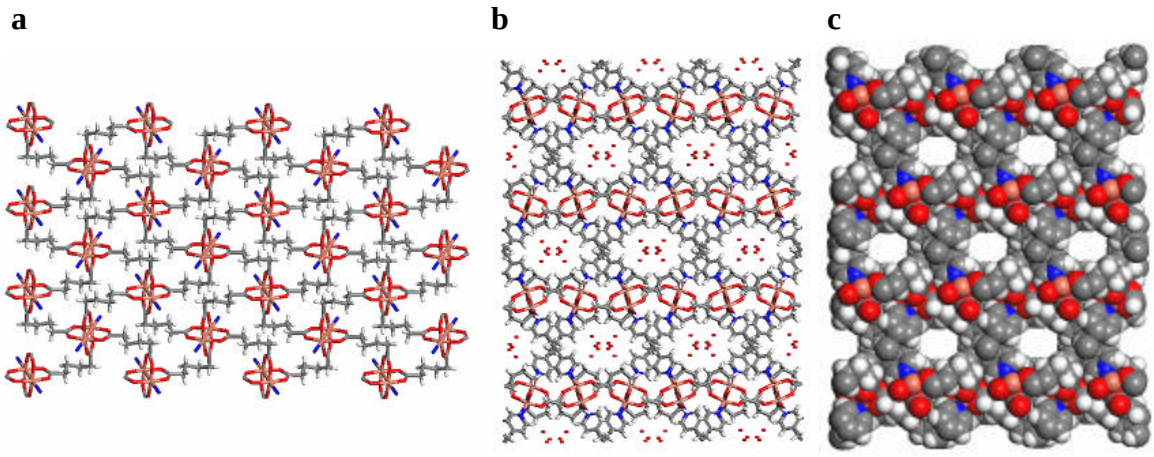

Figure 4.18. Detailed view of the $[Cu_2(adipate)_2]_n$ sheets down [100] in 23 (a), crystal structure of the 3D net of 23 down [001] (b) and corresponding space filling representation where the guest water molecules are omitted (c)

The five compounds studied herein are representative of a relatively new class of metal-organic networks based upon the two conformationally flexible ligands glutarate and adipate. They have formed the two types of networks 1D double chains and 2D grids that can be rationalized on the basis of the conformation adopted by the organic linkers and the connectivity and geometry of the molecular building units. The 1D, double chain, topology resulted from axial coordination of neutral O-donor DMF ligand in **18** or N-donor pyridine ligand in **19**. The formation of corrugated sheets $[Cu_2(glutarate)_2]_n$ in the

2D 4^4 network of **20** when pyridine molecules act as the two axial ligands has successfully generated extended modular 3D α-Po nets upon the utilization of the neutral difunctional axial N-coordinated ligand, the pillars being 4,4'-bipyridine, **21**, and 1,2-bis(4-pyridyl)ethane, **22** and **23**.

4.5. Conclusions

In conclusion, it should be emphasized that compound **21** represents a novel porous network that was generated in water and acts as a highly selective adsorbent for water molecules. That **21** retains single crystallinity might be attributed to the stability of the 2D sheets and the ability of the cross-linking ligands to engage in stacking interactions. Compounds **21** and **22** are new members of a relatively small group of molecular materials that reversibly desorb guest molecules with retention of single crystallinity.[113,125,215,236,238,260,289-291,294-296] In the context of porosity, it has been suggested that the generation of porous materials that retain crystallinity during reversible desorption and exhibit high selectivity towards guest molecules might be relevant as adsorbents for separations and sensing devices.[305]

These results further confirm how the rational use of flexible linkers has allowed the generation of predicted crystal structures. Such investigations have provided design strategies that apply to systems containing an inherently high degree of flexibility and an understanding of the essential mechanisms that control the geometrical adaptability typical of this class of compounds. Applications of these principles may lead to the construction of metal-organic networks possessing important novel properties directly connected to the conformational flexibility of the building units.

In this regard, it is interesting to speculate that a further use of flexible linkers may be rationally used to construct materials that possess sufficient flexibility to allow for geometrical and/or functional recognition. An especially intriguing and exciting aspect of such protocol would consist in the possibility to combine flexibility and porosity within supramolecular metal-organic networks, which may potentially lead to cooperative substrate binding. In other words, the networks may function as “living” or “smart” hosts in a manner reminiscent of biological systems.

Chapter 5

Conclusion and Future Directions

5.1. Summary

The generation and systematic study in terms of structures and properties of the metal-organic and organic systems presented in this dissertation have led to the development of strategies for understanding and controlling intermolecular interactions within the solid state. In particular, this research has contributed to the rationalization of self-assembly of a selection of calixarenes and metal-organic networks on the basis of supramolecular approaches towards the organization of individual molecular building units into desirable crystalline architectures. From the structural investigation of the novel supramolecular systems described throughout this thesis, three salient features deserve to be emphasized:

- Structural control over the crystal packing of pseudo-amphiphilic calixarenes is possible, given the use of appropriate functionalization of the building units owing to the knowledge of the relative effects resulting from the combination of two or more sets of supramolecular interactions. In effect, it has been established that well-organized bilayer structures can be generated from subtle exploitation of the balance between halogen and van der Waals interactions

introduced at the opposite faces of calixarene building units.

- New insights concerning structural diversity in supramolecular systems have resulted from the generation of three novel metal-organic networks based upon coordination between simple components that can afford different topologies according to their connectivity and geometry. Self-assembly of Zn(II), 4-connected node, and nicotinate, ligand possessing N-donor and carboxylate functions, has afforded a 3D $4^2 \cdot 8^4$ and two 2D 4^4 networks, structural supramolecular isomers interconnected through subtle variation of crystallization conditions. Such results especially emphasize that the composition of a material is not the only parameter to be considered prior to the generation of infinite networks since rational topological approaches are critical towards their construction.

- The use of organic ligands that contain conformationally labile fragments, glutarate and adipate, in metal-organic networks based upon the ubiquitous chromophore dicoppertetracarboxylate, has been investigated towards the generation of porous materials. In this context, the novel porous network $[Cu_2(glutarate)_2(4,4'\text{-bipyridine})]_n$ has been shown to retain single-crystallinity upon reversible guest desorption and to act as a highly selective adsorbent for water molecules.

In summary, this work has contributed to the rational design of metal-organic and organic systems that are applicable to the construction of a broader range of supramolecular materials.

5.2. Supramolecular Materials

Metal-organic networks and organic assemblies presented herein represent prototypical examples pertaining to two areas of supramolecular chemistry that are differentiable by the type of intermolecular interactions involved. General approaches have been delineated from the structural investigation of individual building units and their modulation to afford functional sites or geometries that are suitable for specific organization between molecules within the solid state. In this regard, preselection of complementary nodes-linkers, metal centers and organic ligands, that can self-assemble into predictable topologies has successfully afforded novel supramolecular materials possessing interesting properties. On the other hand, judicious functionalization of a single type of component possessing typical morphology, as exemplified by the cone-shaped calixarene molecules, has generated organic building units that possess adequate geometries and functions to self-assemble into predictable structures.

In both cases, preselection of molecular building units, consisting of one or more components that possess molecular recognition potential, represents the key factor to control the resulting supramolecular architectures. In the current intense research in the field of nanosciences towards the controlled manipulation of molecules in order to build nanostructured materials, the use of supramolecular concepts providing enhanced insight into and control of how molecules interact and assemble, exemplified by the two types of supramolecular systems presented herein, represents a successful approach to design materials directly at the molecular level.

5.3. Future Directions

Considering the inherent modularity of systems based upon molecular building units that can be systematically modified and adjusted, application of the supramolecular approach for the design of new materials can be applied to the construction of an even wider range of supramolecular systems.

The modular nature of crystal engineered metal-organic networks, which can be generated from a diverse array of complementary building units and their structural diversity, represented by the range of supramolecular isomers that can be generated from each set of molecular components are of particular interest in the context of fine-tuning the chemical or physical properties. Investigation towards the variation of the metal centers may result in additional properties integrated to the networks and could offer materials possessing catalytical or optical properties. Further investigation towards functionalization of the organic ligands, in an extension to the parallel study of metal-organic structures based upon nicotinate and dinicotinate ligands, may be of interest towards the generation of networks containing specific functions as reactive or binding sites at well-defined and controllable positions within the network topology.

Further use of aliphatic linkers possessing various chain lengths and functionalities should be fully developed. The goal in this regard would be the generation of *flexible* architectures with variable shapes and sizes, and should represent great potential for supramolecular chemistry. Another outcome from the use of this type of ligand is the expectation that the resulting structures may expand the concept of supramolecular isomerism to its conformational counterpart and provide a route to the

generation of a novel class of nanostructures possessing useful properties directely related to the conformational lability of the organic building units.

Finally, in the current context of multi-disciplinary research, it should be interesting to expand the study of pseudo-amphiphilic calixarenes to other derivatives that would incorporate specific functionalities towards the generation of materials possessing additional properties. Such materials could offer opportunities to impact areas as diverse as material and surface sciences or physics. In addition, further study of inclusion properties of self-assembled bilayers generated from calixarenes may reveal significant with a view towards biomimetics since these artificial and controllable systems could possess similar properties as those of biological membranes.

As a last note, it should be emphasized that technological advances in both software and hardware have rendered possible the determination of large complex structures. However, related methods for structural determination of micro- and nano-crystalline materials may represent inestimable advantages with respect to the characterization of special classes of supramolecular materials, *e.g.* large structures possessing broad flexible regions inclined to induce high disorder, and the study of some of their properties, in a similar perspective as porosity can be characterized *via* single crystal structural determination.

References

1. Hauy, R. J. *Essai D'Une Theory Sur La Structure Des Crystaux;* Paris, 1784.
2. Wood, E. A. *Crystals and Light;* 2nd ed. Dover Publications, Inc.: New York, 1977.
3. Ewald, P. P. *Fifty Years of X-Ray Diffraction*; International Union of Crystallography: Utrecht, The Netherlands, 1962.
4. Cohen, M. D. *Angew. Chem., Int. Ed. Engl.* **1975**, *14*, 386-393.
5. Stupp, S. I.; Braun, P. V. *Science* **1997**, *277*, 1242-1248.
6. Ozin, G. A. *Acc. Chem. Res.* **1997**, *30*, 17-27.
7. Green, B. S.; Heller, L. *Science* **1974**, *185*, 525-527.
8. Addadi, L.; Moradian, J.; Shay, E.; Maroudas, N. G.; Weiner, S. *Proc. Natl. Acad. Sci. U. S. A.* **1987**, *84*, 2732-2736.
9. Addadi, L.; Weiner, S. *Proc. Natl. Acad. Sci. U. S. A.* **1985**, *82*, 4110-4114.
10. Addadi, L.; Berkovitchyellin, Z.; Weissbuch, I.; Vanmil, J.; Shimon, L. J. W.; Lahav, M.; Leiserowitz, L. *Angew. Chem., Int. Ed. Engl.* **1985**, *24*, 466-485.
11. Addadi, L.; Vanmil, J.; Gati, E.; Lahav, M. *Origins of Life and Evolution of the Biosphere* **1981**, *11*, 107-118.
12. Addadi, L.; Lahav, M. *J. Am. Chem. Soc.* **1979**, *101*, 2152-2156.

13. Mann, S.; Archibald, D. D.; Didymus, J. M.; Douglas, T.; Heywood, B. R.; Meldrum, F. C.; Reeves, N. J. *Science* **1993**, *261*, 1286-1292.

14. Mann, S.; Heywood, B. R.; Rajam, S.; Walker, J. B. A. *ACS Symp. Ser.* **1991**, *444*, 28-41.

15. Jones, W.; Ramdas, S.; Theocharis, C. R.; Thomas, J. M.; Thomas, N. W. *J. Phys. Chem.* **1981**, *85*, 2594-2597.

16. Thomas, J. M. *Philos. Trans. R. Soc. London, A* **1974**, *277*, 251-287.

17. Davey, R. J.; Black, S. N.; Bromley, L. A.; Cottier, D.; Dobbs, B.; Rout, J. E. *Nature* **1991**, *353*, 549-550.

18. Davey, R. J.; Mullin, J. W. *J. Cryst. Growth* **1974**, *26*, 45-51.

19. Schmidt, G. M. J. *Pure Appl. Chem.* **1971**, *27*, 647-678.

20. Lehn, J. M. *ACS Symp. Ser.* **1991**, *455*, 436-445.

21. Lehn, J. M. *Pure Appl. Chem.* **1978**, *50*, 871-892.

22. Kitaigorodskii, A. I. *Uspekhi Fizicheskikh Nauk* **1979**, *127*, 391-419.

23. Lehn, J. M. *Supramolecular Chemistry: Concepts and Perspectives;* VCH: Weinheim, 1995.

24. Dunitz, J. D. *Pure Appl. Chem.* **1991** , *63*, 177-185.

25. Dunitz, J. D. Wiley: New York, 1996; Vol. 2.

26. Allen, F. H.; Kennard, O. *Chem. Des. Autom. News* **1993**, *8*, 31-37.

27. Kuleshova, L. N.; Antipin, M. Y. *Usp. Khim.* **1999**, *68*, 3-22.

28. Pauling, L. *The Nature of the Chemical Bond*; Cornell University Press: Ithaca, New York, 1948.

29. Bondi, A. *J. Phys. Chem.* **1964**, *68*, 441-451.

30. Desiraju, G. R.; Gavezzotti, A. *Chem. Commun.* **1989**, 621-623.

31. Desiraju, G. R. *Acc. Chem. Res.* **1991**, *24*, 290-296.

32. Desiraju, G. R. *Angew. Chem., Int. Ed. Engl.* **1995**, *34*, 2311-2327.

33. Etter, M. C. *J. Phys. Chem.* **1991**, *95*, 4601-4610.

34. Lehn, J. M. *Science* **1985**, *227*, 849-856.

35. Lehn, J. M. *Science* **1993**, *260*, 1762-1763.

36. Hofmann, K. A.; Kuspert, Z. *Z. Anorg. Allg. Chem.* **1897**, *69*, 204.

37. Powell, H. M. *J. Chem. Soc.* **1948**, 61-73.

38. Powell, H. M.; Rayner, J. H. *Nature* **1949**, *163*, 566-567.

39. Williams, F. V. *J. Am. Chem. Soc.* **1957**, *79*, 5876-5877.

40. Cram, D. J.; Steinberg, H. *J. Am. Chem. Soc.* **1951**, *73*, 5691-5704.

41. Pedersen, C. J. *J. Am. Chem. Soc.* **1967**, *89*, 7017-7036.

42. Dietrich, B.; Lehn, J. M.; Sauvage, J. P. *Tetrahedron Lett.* **1969**, *10*, 2889-2892.

43. Ts'o, P. O. P. *Basic Principles in Nucleic Acid Chemistry, Vols 1 and 2*; Academic Press: London, 1974.

44. Saenger, W. *Principles of Nucleic Acid Structure*; Springler-Verlag: New York, 1984.

45. Jaenicke, R. *Biochemistry* **1991**, *30*, 3147-3161.

46. Alberts, B.; Bray, D.; Lewis, J.; Raff , M.; Roberts, K.; Watson, J. D. *Molecular Biology of the Cell ;* 3rd ed. Garland Publishing: London, 1994.

47. MacGillivray, L. R.; Atwood, J. L. *Nature* **1997**, *389*, 469-472.

48. Gutsche, C. D. *Acc. Chem. Res.* **1983** , *16*, 161-170.

49. Berl, V.; Huc, I.; Khoury, R. G.; Krische, M. J.; Lehn, J. M. *Nature* **2000**, *407*, 720-723.

50. Oda, R.; Huc, I.; Schmutz, M.; Candau, S. J.; Mackintosh, F. C. *Nature* **1999**, *399*, 566-569.

51. Barboiu, M.; Lehn, J. M. *Proc. Natl. Acad. Sci. U. S. A.* **2002**, *99*, 5201-5206.

52. Barboiu, M.; Vaughan, G.; Graff, R.; Lehn, J. M. *J. Am. Chem. Soc.* **2003**, *125*, 10257-10265.

53. Huc, I.; Lehn, J. M. *Proc Natl Acad Sci U S A* **1997**, *94*, 2106-2110.

54. Storhoff, J. J.; Mirkin, C. A. *Chem. Rev.* **1999**, *99*, 1849-1862.

55. Kirby, A. J. *Angew. Chem., Int. Ed. Engl.* **1996**, *35*, 707-724.

56. Rakow, N. A.; Suslick, K. S. *Nature* **2000**, *406*, 710-713.

57. Mirkin, C. A.; Letsinger, R. L.; Mucic, R. C.; Storhoff, J. J. *Nature* **1996**, *382*, 607-609.

58. Pepinsky, R. *Phys. Rev.* **1955**, *100*, 971.

59. Desiraju, G. R. *Crystal Engineering: the Design of Organic Solids;* Elsevier: Amsterdam, 1989.

60. Hoskins, B. F.; Robson, R. *J. Am. Chem. Soc.* **1990**, *112*, 1546-1554.

61. Etter, M. C. *Acc. Chem. Res.* **1990**, *23*, 120-126.

62. Subramanian, S.; Zaworotko, M. J. *Coord. Chem. Rev.* **1994**, *137*, 357-401.

63. Zaworotko, M. J.; Seddon, K. R. *Crystal Engineering: the Design and Application of Functional Solids;* Kluwer: Dordrecht, 1999.

64. Russell, V. A.; Evans, C. C.; Li, W. J.; Ward, M. D. *Science* **1997**, *276*, 575-579.

65. Su, D.; Wang, X.; Simard, M.; Wuest, J. D. *Supramol. Chem.* **1995**, *6* , 171-178.

66. Fujita, M.; Kwon, Y. J.; Washizu, S.; Ogura, K. *J. Am. Chem. Soc.* **1994**, *116*, 1151-1152.

67. Zaworotko, M. J. *Chem. Soc. Rev.* **1994**, *23*, 283-288.

68. Gutsche, C. D. *Calixarenes Revisited, Monographs in Supramolecular Chemistry*; Royal Society of Chemistry: Cambridge, UK, 1998.

69. Gutsche, C. D.; Muthukrishnan, R. *J. Org. Chem.* **1978**, *43*, 4905-4906.

70. Bohmer, V. *Angew. Chem., Int. Ed. Engl.* **1995**, *34*, 713-745.

71. Harvey, P. D. *Coord. Chem. Rev.* **2002**, *233*, 289-309.

72. Leon, S.; Leigh, D. A.; Zerbetto, F. *Chem. Eur. J.* **2002**, *8*, 4854-4866.

73. Asfari, Z.; Bohmer, V.; Harrowfield, J.; Vicens, J. *Calixarenes 2001*; Kluwer Academic Publishers: Dordrecht, The Netherlands, 2001.

74. Hosseini, M. W.; De Cian, A. *Chem. Commun.* **1998**, 727-733.

75. Atwood, J. L.; Barbour, L. J.; Hardie, M. J.; Raston, C. L. *Coord. Chem. Rev.* **2001**, *222*, 3-32.

76. Conn, M. M.; Rebek, J. *Chem. Rev.* **1997**, *97*, 1647-1668.

77. Ikeda, A.; Shinkai, S. *Chem. Rev.* **1997**, *97*, 1713-1734.

78. Harrowfield, J. M.; Richmond, W. R.; Sobolev, A. N.; White, A. H. *Perkin Trans. 2* **1994**, 5-9.

79. Shimizu, K. D.; Rebek, J. *Proc. Natl. Acad. Sci. U. S. A.* **1995**, *92*, 12403-12407.

80. Mogck, O.; Bohmer, V.; Vogt, W. *Tetrahedron* **1996**, *52*, 8489-8496.

81. MacGillivray, L. R.; Atwood, J. L. *Angew. Chem., Int. Ed. Engl.* **1999**, *38*, 1019-1034.

82. Orr, G. W.; Barbour, L. J.; Atwood, J. L. *Science* **1999**, *285*, 1049-1052.

83. Coleman, A. W.; Bott, S. G.; Morley, S. D.; Means, C. M.; Robinson, K. D.; Zhang, H. M.; Atwood, J. L. *Angew. Chem., Int. Ed. Engl.* **1988**, *27*, 1361-1362.

84. Andreetti, G. D.; Ungaro, R.; Pochini, A. *Chem. Commun.* **1979**, 1005-1007.

85. Brouwer, E. B.; Enright, G. D.; Ripmeester, J. A. *J. Am. Chem. Soc.* **1997**, *119*, 5404-5412.

86. Brouwer, E. B.; Udachin, K. A.; Enright, G. D.; Ratcliffe, C. I.; Ripmeester, J. A. *Chem. Commun.* **1998**, 587-588.

87. Brouwer, E. B.; Udachin, K. A.; Enright, G. D.; Ripmeester, J. A.; Ooms, K. J.; Halchuk, P. A. *Chem. Commun.* **2001**, 565-566.

88. Wells, A. F. *Structural Inorganic Chemistry*, 5th ed.; Oxford University Press: Oxford, 1984.

89. MacGillivray, L. R.; Subramanian, S.; Zaworotko, M. J. *Chem. Commun.* **1994**, 1325-1326.

90. Biradha, K.; Domasevitch, K. V.; Moulton, B.; Seward, C.; Zaworotko, M. J. *Chem*. *Commun.* **1999**, 1327-1328.

91. Biradha, K.; Mondal, A.; Moulton, B.; Zaworotko, M. J. *Dalton Trans.* **2000**, 3837-3844.

92. Moulton, B.; Rather, E. B.; Zaworotko, M. J. *Cryst. Eng.* **2001**, *4*, 309-317.

93. Moulton, B.; Zaworotko, M. J. *Chem. Rev.* **2001**, *101*, 1629-1658.

94. Yaghi, O. M.; Li, H. L.; Davis, C.; Richardson, D.; Groy, T. L. *Acc. Chem. Res.* **1998**, *31*, 474-484.

95. Eddaoudi, M.; Moler, D. B.; Li, H. L.; Chen, B. L.; Reineke, T. M.; O'Keeffe, M.; Yaghi, O. M. *Acc. Chem. Res.* **2001**, *34*, 319-330.

96. Barton, T. J.; Bull, L. M.; Klemperer, W. G.; Loy, D. A.; Mcenaney, B.; Misono, M.; Monson, P. A.; Pez, G.; Scherer, G. W.; Vartuli, J. C.; Yaghi, O. M. *Chem. Mater.* **1999**, *11*, 2633-2656.

97. Zaworotko, M. J. *Chem. Commun.* **2001** , 1-9.

98. Huang, S. D.; Xiong, R. G. *Polyhedron* **1997**, *16*, 3929-3939.

99. Lu, J.; Paliwala, T.; Lim, S. C.; Yu, C.; Niu, T. Y.; Jacobson, A. J. *Inorg. Chem.* **1997**, *36*, 923-929.

100. Tong, M. L.; Ye, B. H.; Cai, J. W.; Chen, X. M.; Ng, S. W. *Inorg. Chem.* **1998**, *37*, 2645-2650.

101. Aoyagi, M.; Biradha, K.; Fujita, M. *Bull. Chem. Soc. Jpn.* **2000**, *73*, 1369-1373.

102. Biradha, K.; Fujita, M. *Dalton Trans.* **2000**, 3805-3810.

103. Biradha, K.; Hongo, Y.; Fujita, M. *Angew. Chem., Int. Ed. Engl.* **2000**, *39*, 3843-3845.

104. Soma, T.; Iwamoto, T. *Acta Crystallogr.* **1996**, *C52*, 1200-1203.

105. Kondo, M.; Yoshitomi, T.; Seki, K.; Matsuzaka, H.; Kitagawa, S. *Angew. Chem., Int. Ed. Engl.* **1997**, *36*, 1725-1727.

106. Hagrman, D.; Hammond, R. P.; Haushalter, R.; Zubieta, J. *Chem. Mater.* **1998**, *10*, 2091-2100.

107. Choi, H. J.; Suh, M. P. *J. Am. Chem. Soc.* **1998**, *120*, 10622-10628.

108. Carlucci, L.; Ciani, G.; Proserpio, D. M. *Dalton Trans.* **1999**, 1799-1804.

109. Biradha, K.; Dennis, D.; MacKinnon, V. A.; Seward, C.; Zaworotko, M. J. *Supramolecular Synthesis of Organic and Metal-Organic Laminates With Affinity for Aromatic Guests: Hydrophobic Clay Mimics* Kluwer: Dordrecht, 1999.

110. Gable, R. W.; Hoskins, B. F.; Robson, R. *Chem. Commun.* **1990**, 1677-1678.

111. Batten, S. R.; Hoskins, B. F.; Robson, R. *Chem. Eur. J.* **2000**, *6* , 156-161.

112. Biradha, K.; Domasevitch, K. V.; Hogg, C.; Moulton, B.; Power, K. N.; Zaworotko, M. J. *Cryst. Eng.* **1999**, *2*, 37-45.

113. Noro, S.; Kitaura, R.; Kondo, M.; Kitagawa, S.; Ishii, T.; Matsuzaka, H.; Yamashita, M. *J. Am. Chem. Soc.* **2002**, *124*, 2568-2583.

114. Subramanian, S.; Zaworotko, M. J. *Angew. Chem., Int. Ed. Engl.* **1995**, *34*, 2127-2129.

115. Subramanian, S.; Zaworotko, M. J. *Angew. Chem., Int. Ed. Engl.* **1995**, *34*, 2561.

116. Carlucci, L.; Ciani, G.; Proserpio, D. M.; Sironi, A. *Angew. Chem., Int. Ed. Engl.* **1995**, *34*, 1895-1898.

117. Yaghi, O. M.; Li, H. L. *J. Am. Chem. Soc.* **1996**, *118*, 295-296.

118. Carlucci, L.; Ciani, G.; Proserpio, D. M.; Sironi, A. *Chem. Commun.* **1994**, 2755-2756.

119. Noro, S.; Kitagawa, S.; Kondo, M.; Seki, K. *Angew. Chem., Int. Ed. Engl.* **2000** , *39*, 2082-2084.

120. Dong, Y. B.; Smith, M. D.; Layland, R. C.; Zur Loye, H. C. *Dalton Trans.* **2000**, 775-780.

121. Biradha, K.; Dennis, D.; MacKinnon, V. A.; Sharma, C. V. K.; Zaworotko, M. J. *J. Am. Chem. Soc.* **1998**, *120*, 11894-11903.

122. Batten, S. R.; Robson, R. *Angew. Chem., Int. Ed. Engl.* **1998**, *37*, 1461-1494.

123. Batten, S. R. *CrystEngComm* **2001**, *18*, 1-7.

124. Xu, X. L.; Nieuwenhuyzen, M.; James, S. L. *Angew. Chem., Int. Ed. Engl.* **2002**, *41*, 764-767.

125. Halder, G. J.; Kepert, C. J.; Moubaraki, B.; Murray, K. S.; Cashion, J. D. *Science* **2002**, *298*, 1762-1765.

126. Kitaura, R.; Seki, K.; Akiyama, G.; Kitagawa, S. *Angew. Chem., Int. Ed. Engl.* **2003**, *42*, 428-431.

127. Whitesides, G. M.; Mathias, J. P.; Seto, C. T. *Science* **1991**, *254*, 1312-1319.

128. Rudkevich, D. A. *Bull. Chem. Soc. Jpn.* **2002**, *75*, 393-413.

129. Wieser, C.; Dieleman, C. B.; Matt, D. *Coord. Chem. Rev.* **1997**, *165*, 93-161.

130. Takeuchi, M.; Ikeda, M.; Sugasaki, A.; Shinkai, S. *Acc. Chem. Res.* **2001**, *34*, 865-873.

131. Casnati, A.; Barboso, S.; Rouquette, H.; Schwing-Weill, M. J.; Arnaud-Neu, F.; Dozol, J. F.; Ungaro, R. *J. Am. Chem. Soc.* **2001**, *123*, 12182-12190.

132. Ohnishi, Y.; Fujita, J.; Ochiai, Y.; Matsui, S. *Microelectron. Eng.* **1997**, *35*, 117-120.

133. De Namor, A. F. D.; Cleverley, R. M.; Zapata-Ormachea, M. L. *Chem. Rev.* **1998**, *98*, 2495-2525.

134. Cornforth, J. W.; Hart, P. D.; Nicholls, G. A.; Rees, R. J. W.; Stock, J. A. *Brit. J. Pharmacol. Chemotherapy* **1955** , *10*, 73-86.

135. Gansey Mhbg; De Haan, A. S.; Bos, E. S.; Verboom, W.; Reinhoudt, D. N. *Bioconjugate Chem.* **1999**, *10*, 613-623.

136. Peczuh, M. W.; Hamilton, A. D. *Chem. Rev.* **2000**, *100*, 2479-2493.

137. Kenis, P. J. A.; Noordman, O. F. J.; Schonherr, H.; Kerver, E. G.; Snellink-Ruel, B. H. M.; Van Hummel, G. J.; Harkema, S.; Van Der Vorst Cpjm; Hare, J.; Picken, S. J.; Engbersen, J. F. J.; Van Hulst, N. F.; Vancso, G. J.; Reinhoudt, D. N. *Chem. Eur. J.* **1998**, *4*, 1225-1234.

138. Conner, M.; Janout, V.; Regen, S. L. *J. Am. Chem. Soc.* **1993**, *115*, 1178-1180.

139. Zhang, L. H.; Hendel, R. A.; Cozzi, P. G.; Regen, S. L. *J. Am. Chem. Soc.* **1999**, *121*, 1621-1622.

140. Shahgaldian, P.; Da Silva, E.; Coleman, A. W.; Rather, B.; Zaworotko, M. J. *Int. J. Pharm.* **2003**, *253*, 23-38.

141. Gualbert, J.; Shahgaldian, P.; Coleman, A. W. *Int. J. Pharm.* **2003**, *257*, 69-73.

142. Alivisatos, A. P.; Barbara, P. F.; Castleman, A. W.; Chang, J.; Dixon, D. A.; Klein, M. L.; Mclendon, G. L.; Miller, J. S.; Ratner, M. A.; Rossky, P. J.; Stupp, S. I.; Thompson, M. E. *Adv. Mater.* **1998**, *10*, 1297-1336.

143. Kaskel, S. *Porous Metal-Organic Frameworks*; Wiley VCH: Weinheim, 2002; pp 1190-1249.

144. James, S. L. *Chem. Soc. Rev.* **2003**, *32*, 276-288.

145. Janiak, C. *Dalton Trans.* **2003**, 2781-2804.

146. Braga, D. *Dalton Trans.* **2000**, 3705-3713.

147. Hart, P. D.; Armstrong, J. A.; Brodaty, E. *Infect. Immun.* **1996**, *64*, 1491-1493.

148. Atwood, J. L.; Barbour, L. J.; Jerga, A.; Schottel, B. L. *Science* **2002**, *298*, 1000-1002.

149. Vocanson, F.; Seigle-Ferrand, P.; Lamartine, R.; Fort, A.; Coleman, A. W.; Shahgaldian, P.; Mugnier, J.; Zerroukhi, A. *J. Mater. Chem.* **2003**, *13*, 1596-1602.

150. Rebek, J. *Chem. Commun.* **2000**, 637-643.

151. Shi, Y. H.; Schneider, H. J. *Perkin Trans. 2* **1999**, 1797-1803.

152. Hamuro, Y.; Calama, M. C.; Park, H. S.; Hamilton, A. D. *Angew. Chem., Int. Ed. Engl.* **1997**, *36*, 2680-2683.

153. Lin, Q.; Park, H. S.; Hamuro, Y.; Lee, C. S.; Hamilton, A. D. *Biopolymers* **1998**, *47*, 285-297.

154. Aime, S.; Barge, A.; Botta, M.; Casnati, A.; Fragai, M.; Luchinat, C.; Ungaro, R. *Angew. Chem., Int. Ed. Engl.* **2001**, *40*, 4737-4739.

155. Memmi, L.; Lazar, A.; Brioude, A.; Ball, V.; Coleman, A. W. *Chem. Commun.* **2001**, 2474-2475.

156. Mandolini, L.; Ungaro, R. *Calixarenes in Action*; Imperial College Press: London, UK, 2000.

157. Hatano, T.; Ikeda, A.; Akiyama, T.; Yamada, S.; Sano, M.; Kanekiyo, Y.; Shinkai, S. *Perkin Trans. 2* **2000**, *5*, 909-912.

158. Katz, A.; Da Costa, P.; Lam, A. C. P.; Notestein, J. M. *Chem. Mater.* **2002**, *14*, 3364-3368.

159. Friggeri, A.; Van Veggel Fcjm; Reinhoudt, D. N. *Chem. Eur. J.* **1999**, *5* , 3595-3602.

160. Shahgaldian, P.; Goreloff, P.; Lamartine, R.; Coleman, A. W. *Cryst. Eng.* **2002**, *5*, 47-58.

161. Mlika, R.; Ben Ouada, H.; Hamza, M. A.; Gamoudi, M.; Guillaud, G.; Jaffrezic-Renault, N. *Synth. Met.* **1997**, *90*, 173-179.

162. Mlika, R.; Dumazet, I.; Gamoudi, M.; Lamartine, R.; Benouada, H.; Jaffrezicrenault, N.; Guillaud, G. *Anal. Chim. Acta* **1997**, *354*, 283-289.

163. Mlika, R.; Gamoudi, M.; Guillaud, G.; Charbonnier, M.; Romand, M.; Davenas, J.; Jaffrezic-Renault, N.; Lamartine, R.; Touhami, A. *Mater. Sci. Eng., C* **2000**, *11*, 129-136.

164. Wamme, N.; Ohnishi, Y. *Polym. Mater. Sci. Eng.* **1992**, *67*, 451-452.

165. Epand, R. M. *Biochim. Biophys. Acta* **1998**, *1376*, 353-368.

166. Gutsche, C. D.; Dhawan, B.; No, K. H.; Muthukrishnan, R. *J. Am. Chem. Soc.* **1981**, *103*, 3782-3792.

167. Atwood, J. L.; Barbour, L. J.; Jerga, A. *Science* **2002**, *296*, 2367-2369.

168. Bott, S. G.; Coleman, A. W.; Atwood, J. L. *J. Am. Chem. Soc.* **1988**, *110*, 610-611.

169. Leverd, P. C.; Berthault, P.; Lance, M.; Nierlich, M. *Eur. J. Org. Chem.* **2000**, 133-139.

170. Barbour, L. J.; Damon, A. K.; Orr, G. W.; Atwood, J. L. *Supramol. Chem.* **1996**, *7*, 209-213.

171. Selkti, M.; Coleman, A. W.; Nicolis, I.; Douteau-Guevel, N.; Villain, F.; Tomas, A.; De Rango, C. *Chem. Commun.* **2000**, 161-162.

172. Atwood, J. L.; Ness, T.; Nichols, P. J.; Raston, C. L. *Crystal Growth & Design* **2002**, *2*, 171-176.

173. Nichols, P. J.; Raston, C. L. *Dalton Trans.* **2003**, 2923-2927.

174. Da Silva, E.; Nouar, F.; Coleman, A. W.; Rather, B.; Zaworotko, M. J. *J. Inclusion Phenom.* **2003**, *46*, 161-166.

175. Drljaca, A.; Hardie, M. J.; Johnson, J. A.; Raston, C. L.; Webb, H. R. *Chem. Commun.* **1999**, 1135-1136.

176. Drljaca, A.; Hardie, M. J.; Raston, C. L. *Dalton Trans.* **1999**, 3639-3642.

177. Drljaca, A.; Hardie, M. J.; Raston, C. L.; Spiccia, L. *Chem. Eur. J.* **1999**, *5*, 2295-2299.

178. Ness, T.; Nichols, P. J.; Raston, C. L. *Eur. J. Inorg. Chem.* **2001**, 1993-1997.

179. Rather, B.; Moulton, B.; Zaworotko, M. J.; Perret, F.; Morel-Desrosiers, N.; Da Silva, E.; Coleman, A. W. *Cryst. Eng.* **2003**, *6*, 15-21.

180. Evans, D. R.; Huang, M. S.; Fettinger, J. C.; Williams, T. L. *Inorg. Chem.* **2002**, *41*, 5986-6000.

181. Thondorf, I.; Broda, F.; Rissanen, K.; Vysotsky, M.; Bohmer, V. *Perkin Trans. 2* **2002**, 1796-1800.

182. Vysotsky, M. O.; Bohmer, V.; Wurthner, F.; You, C. C.; Rissanen, K. *Organic Letters* **2002**, *4*, 2901-2904.

183. Lu, G. Y.; Song, W.; Wan, X. B. *Journal of Chemical Crystallography* **2000**, *30*, 185-188.

184. Shahgaldian, P.; Cesario, M.; Goreloff, P.; Coleman, A. W. *Chem. Commun.* **2002**, 326-327.

185. Jain, M. *Introduction to Biological Membranes*, 2nd ed.; John Wiley & Sons: New York, 1988.

186. Hamada, F.; Bott, S. G.; Orr, G. W.; Coleman, A. W.; Zhang, H. M.; Atwood, J. L. *J. Inclusion Phenom.* **1990**, *9*, 195-206.

187. Barbour, L. J.; Orr, G. W.; Atwood, J. L. *Chem. Commun.* **1997**, 1439-1440.

188. Barbour, L. J.; Orr, G. W.; Atwood, J. L. *Chem. Commun.* **1998**, 1901-1902.

189. Soi, A.; Bauer, W.; Mauser, H.; Moll, C.; Hampel, F.; Hirsch, A. *Perkin Trans. 2* **1998**, 1471-1478.

190. Prins, L. J.; De Jong, F.; Timmerman, P.; Reinhoudt, D. N. *Nature* **2000**, *408*, 181-184.

191. Gutsche, C. D.; Pagoria, P. F. *J. Org. Chem.* **1985**, *50*, 5795-5802.

192. Arduini, A.; Casnati, A. *Macrocycle Synthesis;* Oxford University Press: New York, 1996.

193. Harada, T.; Ohseto, F.; Shinkai, S. *Tetrahedron* **1994**, *50*, 13377-13394.

194. Desiraju, G. R.; Parthasarathy, R. *J. Am. Chem. Soc.* **1989**, *111*, 8725-8726.

195. Pedireddi, V. R.; Reddy, D. S.; Goud, B. S.; Craig, D. C.; Rae, A. D.; Desiraju, G. R. *Perkin Trans. 2* **1994**, 2353-2360.

196. Dahl, T.; Hassel, O. *Acta Chem. Scand.* **1968**, *22*, 2851-2866.

197. Walsh, R. B.; Padgett, C. W.; Metrangolo, P.; Resnati, G.; Hanks, T. W.; Pennington, W. T. *Crystal Growth & Design* **2001**, *1*, 165-175.

198. Jaunky, W.; Hosseini, M. W.; Planeix, J. M.; De Cian, A.; Kyritsakas, N.; Fischer, J. *Chem. Commun.* **1999**, 2313-2314.

199. Ferguson, G.; Gallagher, J. F.; Mckervey, M. A. *Acta Crystallogr.* **1993**, *49*, 602-604.

200. Roundhill, D. M. *Prog. Inorg. Chem.* **1995**, *43*, 533-592.

201. Schmidt, C.; Straub, T.; Falabu, D.; Paulus, E. F.; Wegelius, E.; Kolehmainen, E.; Bohmer, V.; Rissanen, K.; Vogt, W. *Eur. J. Org. Chem.* **2000**, 3937-3944.

202. Pascher, I.; Lundmark, M.; Nyholm, P. G.; Sundell, S. *Biochim. Biophys. Acta* **1992**, *1113*, 339-373.

203. De Wall, S. L.; Barbour, L. J.; Gokel, G. W. *J. Phys. Org. Chem.* **2001**, *14*, 383-391.

204. Moulton, B.; Zaworotko, M. J. *Curr. Opin. Solid State Mater. Sci.* **2002**, *6* , 117-123.

205. Eddaoudi, M.; Kim, J.; O'keeffe, M.; Yaghi, O. M. *J. Am. Chem. Soc.* **2002**, *124*, 376-377.

206. Cotton, F. A.; Lin, C.; Murillo, C. A. *Acc. Chem. Res.* **2001**, *34*, 759-771.

207. Fujita, M. *Chem. Soc. Rev*. **1998**, *27*, 417-425.

208. Hennigar, T. L.; Macquarrie, D. C.; Losier, P.; Rogers, R. D.; Zaworotko, M. J. *Angew. Chem., Int. Ed. Engl.* **1997**, *36*, 972-973.

209. Lin, W. B.; Evans, O. R.; Xiong, R. G.; Wang, Z. Y. *J. Am. Chem. Soc.* **1998**, *120*, 13272-13273.

210. Evans, O. R.; Lin, W. B. *Dalton Trans.* **2000**, 3949-3954.

211. Evans, O. R.; Lin, W. B. *Chem. Mater.* **2001**, *13*, 3009-3017.

212. Evans, O. R.; Lin, W. B. *Acc. Chem. Res.* **2002**, *35*, 511-522.

213. Evans, O. R.; Wang, Z. Y.; Xiong, R. G.; Foxman, B. M.; Lin, W. B. *Inorg. Chem.* **1999**, *38*, 2969-2973.

214. Ayyappan, P.; Evans, O. R.; Lin, W. B. *Inorg. Chem.* **2001**, *40*, 4627-4632.

215. Liu, Y. H.; Tsai, H. L.; Lu, Y. L.; Wen, Y. S.; Wang, J. C.; Li, K. L. *Inorg. Chem.* **2001**, *40*, 6426-6431.

216. Xu, H. T.; Zheng, N. W.; Xu, H. H.; Wu, Y. G.; Yang, R. Y.; Ye, E. Y.; Jin, X. L. *J. Mol. Struct.* **2002**, *606*, 117-122.

217. Lin, W. B.; Evans, O. R.; Yee, G. T. *J. Solid State Chem.* **2000**, *152*, 152-158.

218. Chapman, M. E.; Ayyappan, P.; Foxman, B. M.; Yee, G. T.; Lin, W. B. *Crystal Growth & Design* **2001**, *1*, 159-163.

219. Min, D. W.; Yoon, S. S.; Jung, D. Y.; Lee, C. Y.; Kim, Y.; Han, W. S.; Lee, S. W. *Inorg. Chim. Acta* **2001**, *324*, 293-299.

220. Whitfield, T.; Zheng, L. M.; Wang, X. Q.; Jacobson, A. J. *Solid State Sciences* **2001**, *3*, 829-835.

221. Lin, W. B.; Chapman, M. E.; Wang, Z. Y.; Yee, G. T. *Inorg. Chem.* **2000**, *39*, 4169-4173.

222. Yaghi, O. M.; Li, G. M. *Angew. Chem., Int. Ed. Engl.* **1995**, *34*, 207-209.

223. Li, H. L.; Davis, C. E.; Groy, T. L.; Kelley, D. G.; Yaghi, O. M. *J. Am. Chem. Soc.* **1998**, *120*, 2186-2187.

224. Kim, J.; Chen, B. L.; Reineke, T. M.; Li, H. L.; Eddaoudi, M.; Moler, D. B.; O'Keeffe, M.; Yaghi, O. M. *J. Am. Chem. Soc.* **2001**, *123*, 8239-8247.

225. Moulton, B.; Lu, J.; Mondal, A.; Zaworotko, M. J. *Chem. Commun.* **2001**, 863-864.

226. Abourahma, H.; Coleman, A. W.; Moulton, B.; Rather, B.; Shahgaldian, P.; Zaworotko, M. J. *Chem. Commun.* **2001**, 2380-2381.

227. Moulton, B.; Lu, J. J.; Zaworotko, M. J. *J. Am. Chem. Soc.* **2001**, *123*, 9224-9225.

228. Bourne, S. A.; Lu, J. J.; Mondal, A.; Moulton, B.; Zaworotko, M. J. *Angew. Chem., Int. Ed. Engl.* **2001**, *40*, 2111-2113.

229. Lu, J. J.; Mondal, A.; Moulton, B.; Zaworotko, M. J. *Angew. Chem., Int. Ed. Engl.* **2001**, *40*, 2113-2116.

230. Moulton, B.; Lu, J. J.; Hajndl, R.; Hariharan, S.; Zaworotko, M. J. *Angew. Chem., Int. Ed. Engl.* **2002**, *41*, 2821-2824.

231. Abourahma, H.; Bodwell, G. J.; Lu, J. J.; Moulton, B.; Pottie, I. R.; Walsh, R. B.; Zaworotko, M. J. *Crystal Growth & Design* **2003**, *3*, 513-519.

232. Moulton, B.; Abourahma, H.; Bradner, M. W.; Lu, J. J.; Mcmanus, G. J.; Zaworotko, M. J. *Chem. Commun.* **2003**, 1342-1343.

233. Groeneman, R. H.; MacGillivray, L. R.; Atwood, J. L. *Chem. Commun.* **1998**, 2735-2736.

234. Guilera, G.; Steed, J. W. *Chem. Commun.* **1999**, 1563-1564.

235. Chen, X. M.; Liu, G. F. *Chem. Eur. J.* **2002**, *8*, 4811-4817.

236. Li, H.; Eddaoudi, M.; O'Keeffe, M.; Yaghi, O. M. *Nature* **1999**, *402*, 276-279.

237. Eddaoudi, M.; Kim, J.; Rosi, N.; Vodak, D.; Wachter, J.; O'Keeffe, M.; Yaghi, O. M. *Science* **2002**, *295*, 469-472.

238. Lu, J. Y.; Babb, A. M. *Chem. Commun.* **2002**, 1340-1341.

239. Evans, O. R.; Lin, W. B. *Inorg. Chem.* **2000**, *39*, 2189-2198.

240. Lin, W. B.; Evans, O. R.; Cui, Y. *Crystal Growth & Design* **2002**, *2*, 409-414.

241. Lu, J. Y.; Babb, A. M. *Chem. Commun.* **2001**, 821-822.

242. Zheng, S. L.; Tong, M. L.; Yu, X. L.; Chen, X. M. *Dalton Trans.* **2001**, 586-592.

243. Lu, J. Y.; Kohler, E. E. *Inorg. Chem. Commun.* **2002**, *5*, 600-601.

244. Evans, O. R.; Lin, W. B. *Chem. Mater.* **2001**, *13*, 2705-2712.

245. Wells, A. F. *Three-Dimensional Nets and Polyhedra*; Wiley: New York, 1977.

246. Bregeaul, J. M.; Herpin, P. *Bull. Soc. Fr. Mineral. Cristallo.* **1970**, *93*, 37.

247. Hawkins, S. C.; Bishop, R.; Craig, D. C.; Dance, I. G.; Rae, A. D.; Scudder, M. L. *Perkin Trans. 2* **1993**, 1737-1745.

248. Boldog, I.; Rusanov, E. B.; Chernega, A. N.; Sieler, J.; Domasevitch, K. V. *Dalton Trans.* **2001**, 893-897.

249. Evans, O. R.; Xiong, R. G.; Wang, Z. Y.; Wong, G. K.; Lin, W. B. *Angew. Chem., Int. Ed. Engl.* **1999**, *38*, 536-538.

250. Vogel, A. I. *Vogel's Textbook of Practical Organic Chemistry*, 5th ed.; John Wiley & Sons, Inc.: New York, 1989.

251. Rather, B.; Moulton, B.; Walsh, R. D. B.; Zaworotko, M. J. *Chem. Commun.* **2002**, 694-695.

252. Seki, K.; Takamizawa, S.; Mori, W. *Chem. Lett.* **2001**, 122-123.

253. Seki, K.; Takamizawa, S.; Mori, W. *Chem. Lett.* **2001**, 332-333.

254. Mori, W.; Takamizawa, S. *J. Solid State Chem.* **2000**, *152*, 120-129.

255. Kondo, M.; Shimamura, M.; Noro, S.; Minakoshi, S.; Asami, A.; Seki, K.; Kitagawa, S. *Chem. Mater.* **2000**, *12*, 1288-1299.

256. Yang, S. Y.; Long, L. S.; Jiang, Y. B.; Huang, R. B.; Zheng, L. S. *Chem. Mater.* **2002**, *14*, 3229-3231.

257. Bakalbassis, E. G.; Korabik, M.; Michailides, A.; Mrozinski, J.; Raptopoulou, C.; Skoulika, S.; Terzis, A.; Tsaousis, D. *Dalton Trans.* **2001**, 850-857.

258. Hornick, C.; Rabu, P.; Drillon, M. *Polyhedron* **2000**, *19*, 259-266.

259. Kim, Y.; Jung, D. P. *Inorg. Chem.* **2000**, *39*, 1470-1475.

260. Suh, M. P.; Ko, J. W.; Choi, H. J. *J. Am. Chem. Soc.* **2002**, *124*, 10976-10977.

261. Forster, P. M.; Cheetham, A. K. *Angew. Chem., Int. Ed. Engl.* **2002**, *41*, 457-459.

262. Kitaura, R.; Fujimoto, K.; Noro, S.; Kondo, M.; Kitagawa, S. *Angew. Chem., Int. Ed. Engl.* **2002**, *41*, 133-135.

263. Bourne, S. A.; Lu, J. J.; Moulton, B.; Zaworotko, M. J. *Chem. Commun.* **2001**, 861-862.

264. Fu, Z. Y.; Wu, X. T.; Dai, J. C.; Wu, L. M.; Cui, C. P.; Hu, S. M. *Chem. Commun.* **2001**, 1856-1857.

265. Carlucci, L.; Ciani, G.; Moret, M.; Proserpio, D. M.; Rizzato, S. *Angew. Chem., Int. Ed. Engl.* **2000**, *39*, 1506-1510.

266. Kasai, K.; Aoyagi, M.; Fujita, M. *J. Am. Chem. Soc.* **2000**, *122*, 2140-2141.

267. Batten, S. R.; Jeffery, J. C.; Ward, M. D. *Inorg. Chim. Acta* **1999**, *292*, 231-237.

268. Power, K. N.; Hennigar, T. L.; Zaworotko, M. J. *Chem. Commun.* **1998**, 595-596.

269. Losier, P.; Zaworotko, M. J. *Angew. Chem., Int. Ed. Engl.* **1996**, *35*, 2779-2782.

270. Carlucci, L.; Ciani, G.; Macchi, P.; Proserpio, D. M.; Rizzato, S. *Chem. Eur. J.* **1999**, *5*, 237-243.

271. Rueff, J. M.; Masciocchi, N.; Rabu, P.; Sironi, A.; Skoulios, A. *Eur. J. Inorg. Chem.* **2001**, 2843-2848.

272. Hashimoto, M.; Iwamoto, T. *Chem. Lett.* **1990**, 1531-1534.

273. Kim, Y. J.; Jung, D. Y. *Chem. Commun.* **2002**, 1650.

274. Eddaoudi, M.; Kim, J.; Wachter, J. B.; Chae, H. K.; O'Keeffe, M.; Yaghi, O. M. *J. Am. Chem. Soc.* **2001**, *123*, 4368-4369.

275. Chui, S. S. Y.; Lo, S. M. F.; Charmant, J. P. H.; Orpen, A. G.; Williams, I. D. *Science* **1999**, *283*, 1148-1150.

276. Forster, P. M.; Thomas, P. M.; Cheetham, A. K. *Chem. Mater.* **2002**, *14*, 17-20.

277. Michaelides, A.; Skoulika, S.; Kiritsis, V.; Aubry, A. *Chem. Commun.* **1995**, 1415-1416.

278. Batten, S. R. *Curr. Opin. Solid State Mater. Sci.* **2001**, *5*, 107-114.

279. Abrahams, B. F.; Hoskins, B. F.; Robson, R. *J. Am. Chem. Soc.* **1991**, *113*, 3606-3607.

280. Kosal, M. E.; Chou, J. H.; Wilson, S. R.; Suslick, K. S. *Nature Mater.* **2002**, *1*, 118-121.

281. Kitaura, R.; Kitagawa, S.; Kubota, Y.; Kobayashi, T. C.; Kindo, K.; Mita, Y.; Matsuo, A.; Kobayashi, M.; Chang, H. C.; Ozawa, T. C.; Suzuki, M.; Sakata, M.; Takata, M. *Science* **2002**, *298*, 2358-2361.

282. Seo, J. S.; Whang, D.; Lee, H.; Jun, S. I.; Oh, J.; Jeon, Y. J.; Kim, K. *Nature* **2000**, *404*, 982-986.

283. Cheetham, A. K.; Ferey, G.; Loiseau, T. *Angew. Chem., Int. Ed. Engl.* **1999**, *38*, 3269-3292.

284. Kitagawa, S.; Kondo, M. *Bull. Chem. Soc. Jpn.* **1998**, *71*, 1739-1753.

285. Tanaka, T.; Tasaki, T.; Aoyama, Y. *J. Am. Chem. Soc.* **2002**, *124*, 12453-12462.

286. Nangia, A. *Curr. Opin. Solid State Mater. Sci.* **2001**, *5*, 115-122.

287. Aoyama, Y. *Top. Curr. Chem.* **1998**, *198*, 131-161.

288. Brunet, P.; Simard, M.; Wuest, J. D. *J. Am. Chem. Soc.* **1997**, *119*, 2737-2738.

289. Kepert, C. J.; Hesek, D.; Beer, P. D.; Rosseinsky, M. J. *Angew. Chem., Int. Ed. Engl.* **1998**, *37*, 3158-3160.

290. Cussen, E. J.; Claridge, J. B.; Rosseinsky, M. J.; Kepert, C. J. *J. Am. Chem. Soc.* **2002**, *124*, 9574-9581.

291. Kepert, C. J.; Rosseinsky, M. J. *Chem. Commun.* **1999**, 375-376.

292. Eddaoudi, M.; Li, H. L.; Reineke, T.; Fehr, M.; Kelley, D.; Groy, T. L.; Yaghi, O. M. *Topics in Catalysis* **1999**, *9*, 105-111.

293. Blake, A. J.; Champness, N. R.; Khlobystov, A. N.; Parsons, S.; Schroder, M. *Angew. Chem., Int. Ed. Engl.* **2000**, *39*, 2317-2320.

294. Soldatov, D. V.; Grachev, E. V.; Ripmeester, J. A. *Crystal Growth & Design* **2002**, *2*, 401-408.

295. Maji, T. K.; Mukherjee, P. S.; Mostafa, G.; Zangrando, E.; Chaudhuri, N. R. *Chem. Commun.* **2001**, 1368-1369.

296. Biradha, K.; Fujita, M. *Angew. Chem., Int. Ed. Engl.* **2002**, *41*, 3392-3395.

297. Olejnik, Z.; Lis, T.; Vogt, A.; Wolowiec, S.; Skarzewski, J. *J. Inclusion Phenom.* **2000**, *38*, 221-232.

298. Chen, B. L.; Eddaoudi, M.; Reineke, T. M.; Kampf, J. W.; O'keeffe, M.; Yaghi, O. M. *J. Am. Chem. Soc.* **2000**, *122*, 11559-11560.

299. Eddaoudi, M.; Li, H. L.; Yaghi, O. M. *J. Am. Chem. Soc.* **2000**, *122*, 1391-1397.

300. Reineke, T. M.; Eddaoudi, M.; Fehr, M.; Kelley, D.; Yaghi, O. M. *J. Am. Chem. Soc.* **1999**, *121*, 1651-1657.

301. Min, K. S.; Suh, M. P. *Chem. Eur. J.* **2001**, *7*, 303-313.

302. Rather, B.; Zaworotko, M. J. *Chem. Commun.* **2003**, 830-831.

303. Subramanian, S.; Zaworotko, M. J. *Chem. Commun.* **1993**, 952-954.

304. Abrahams, B. F.; Hardie, M. J.; Hoskins, B. F.; Robson, R.; Sutherland, E. E. *Chem. Commun.* **1994**, 1049-1050.

305. Kuznicki, S. M.; Bell, V. A.; Nair, S.; Hillhouse, H. W.; Jacubinas, R. M.; Braunbarth, C. M.; Toby, B. H.; Tsapatsis, M. *Nature* **2001**, *412*, 720-724.

Appendices

Appendix A. AFM studies for compound 10.

Non-contact mode AFM images of compound **10** on glass after annealing for 24 hours at 37 °C and 25 °C (and corresponding zoom) representative of the variation in self-organization of this compound at different temperatures

Drying Temperatures

37ºC

25ºC

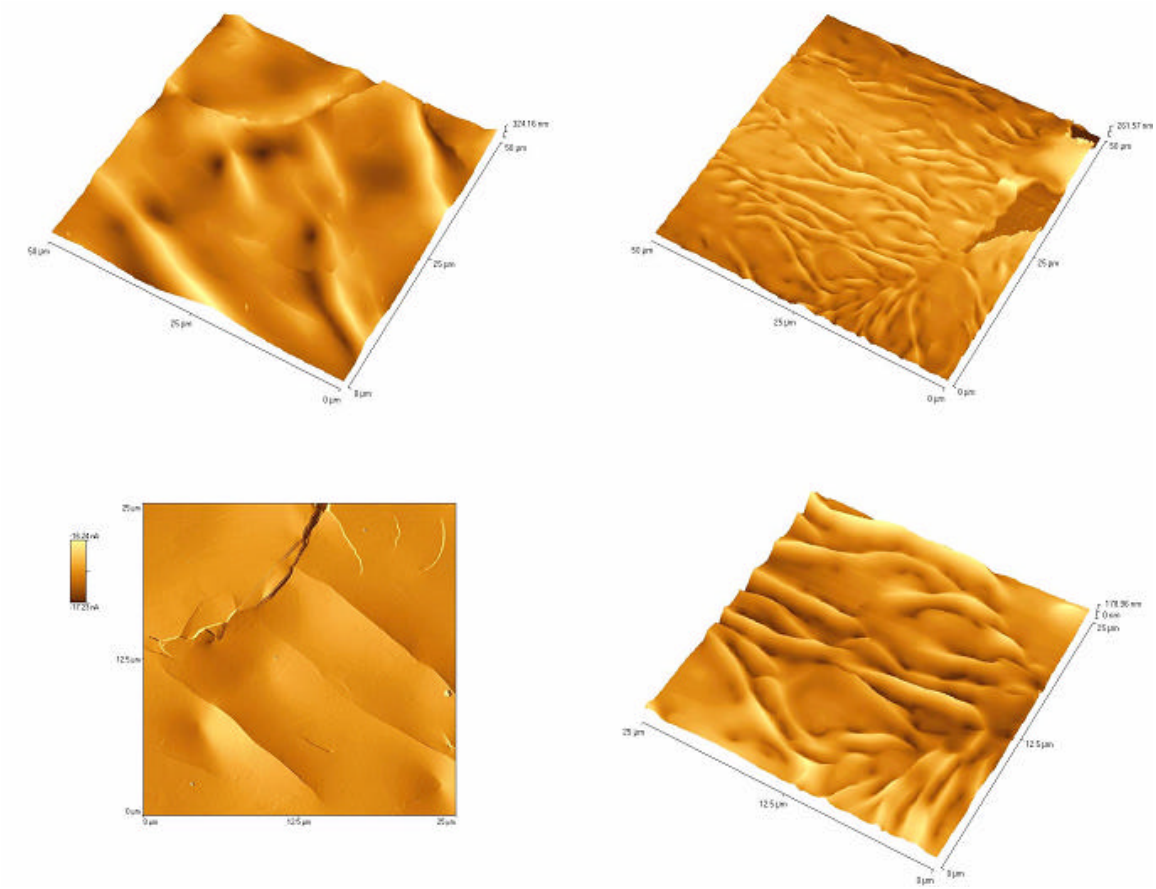

Appendix B. Histogram showing the distribution of Cu-O distances among the structures found in the CSD search of the chromophores of mononuclear Cu 4-, 5- and 6-coordinate containing two functionalities N-donor and carboxylate

Cu 4-coordinate

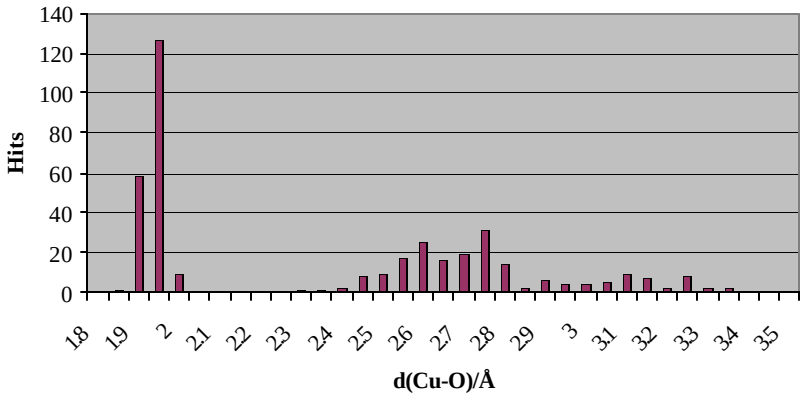

Cu 5-coordinate

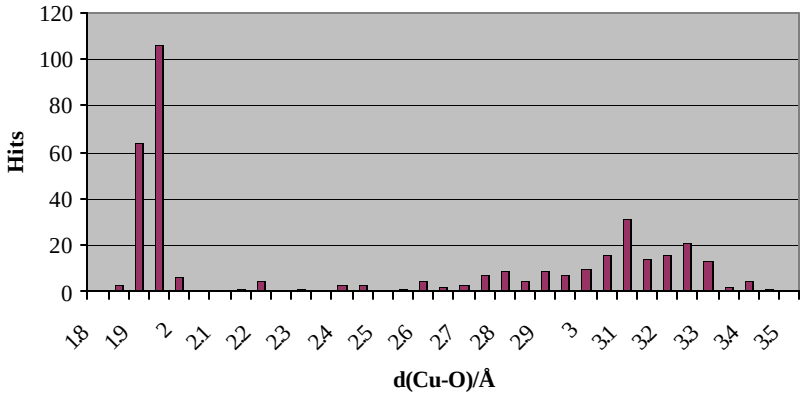

Cu 6-coordinate

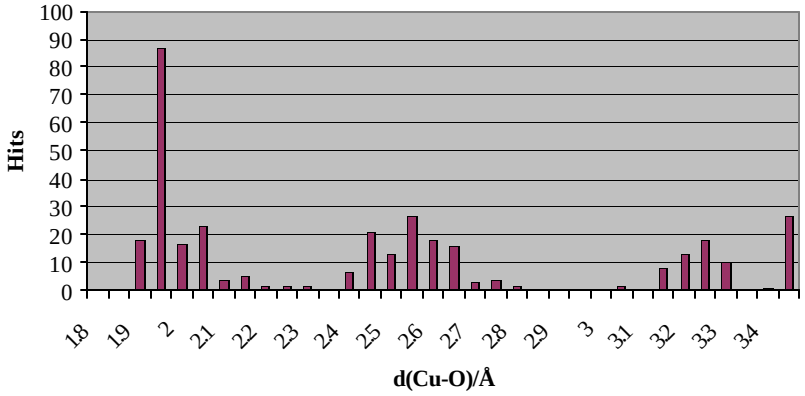

Appendix C-1. Experimental data for compound 13

FT-IR spectrum, TGA trace and X-ray powder diffraction patterns of fresh sample and calculated from the single crystal structure

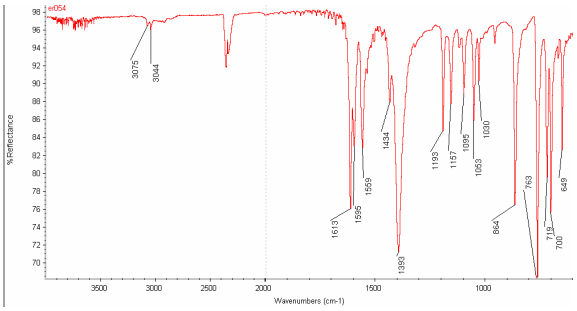

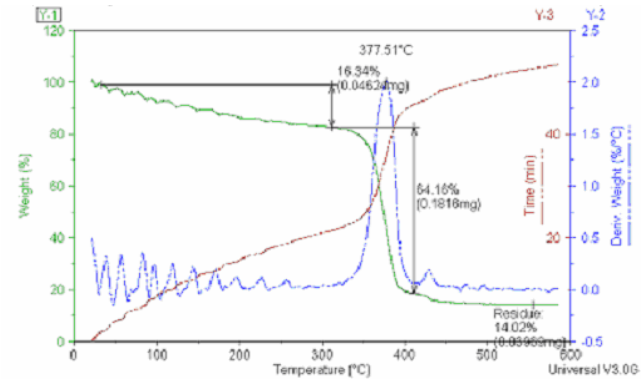

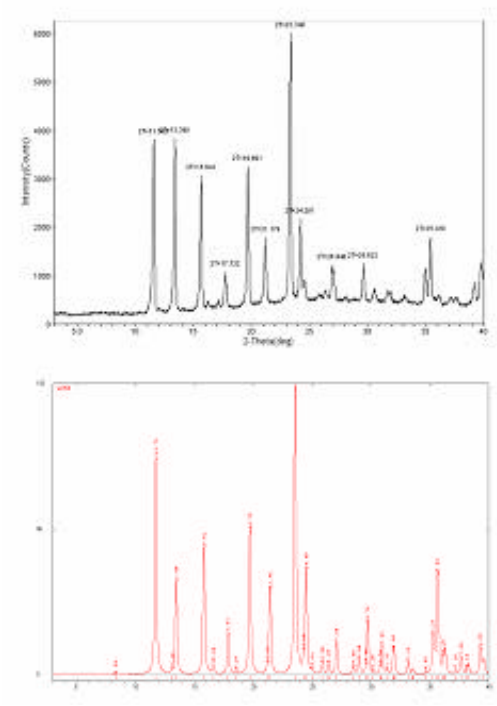

Appendix C-2. Experimental data for compound 14

FT-IR spectrum, TGA trace and X-ray powder diffraction patterns of fresh sample and calculated from the single crystal structure

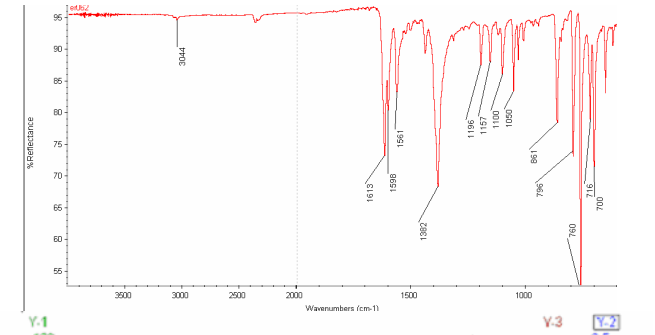

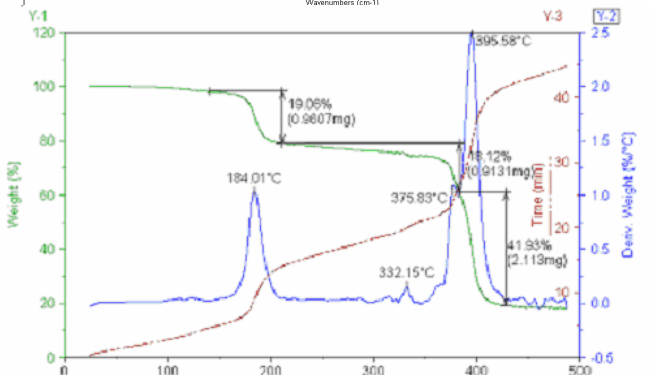

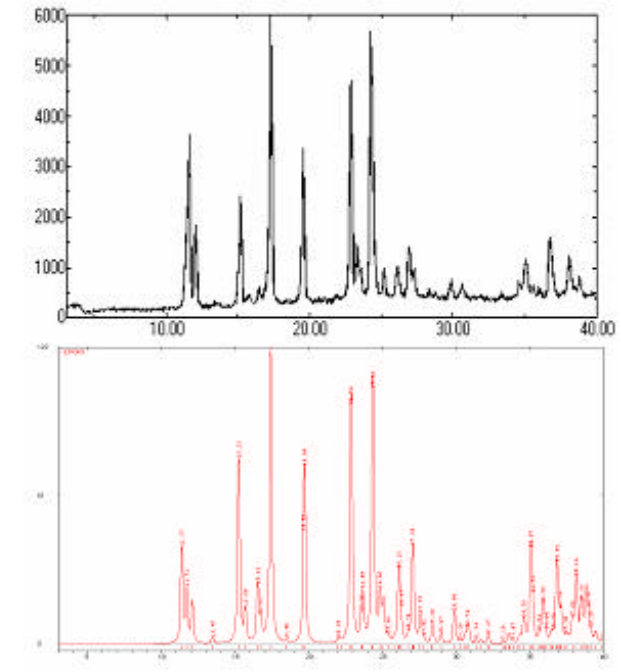

Appendix C-3. Experimental data for compound 15

FT-IR spectrum, TGA trace and X-ray powder diffraction patterns of fresh sample and calculated from the single crystal structure

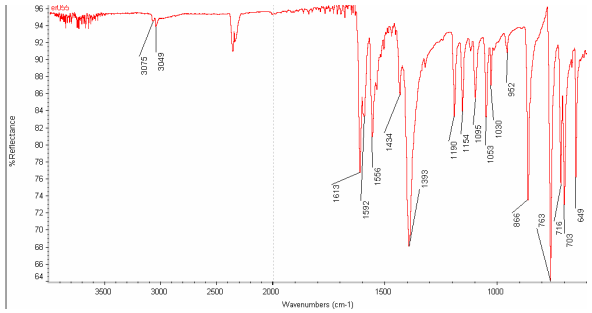

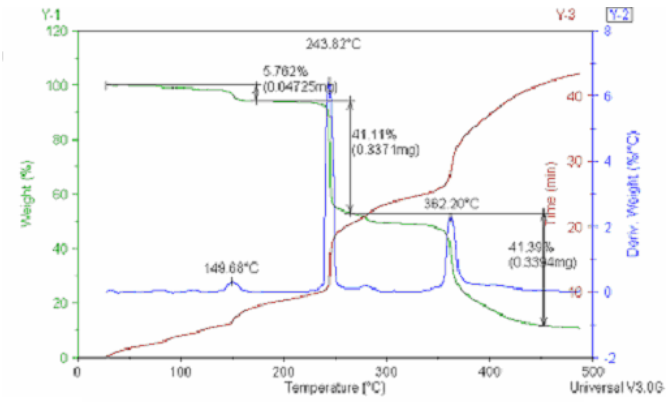

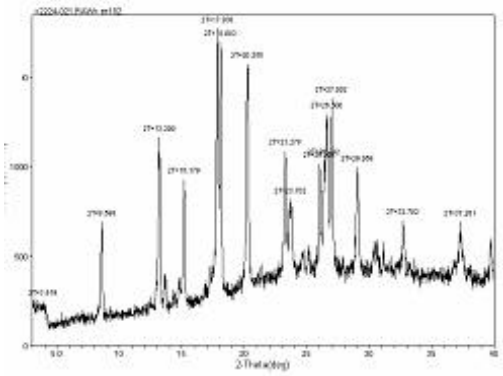

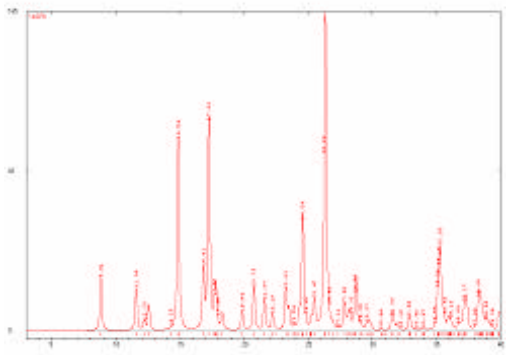

Appendix C-4. Experimental data for compound 16

FT-IR spectrum and TGA traces (after several minutes and one hour of exposure to atmosphere)

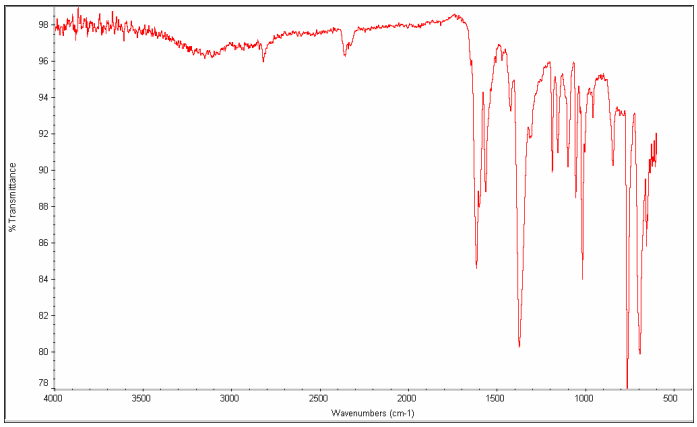

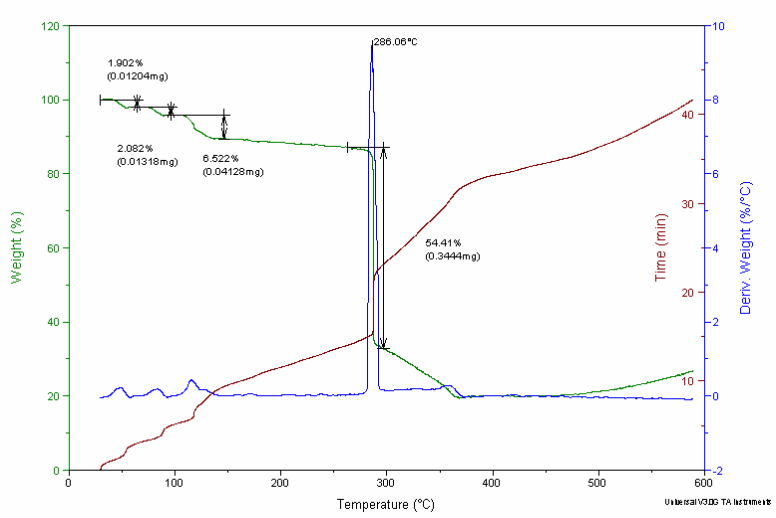

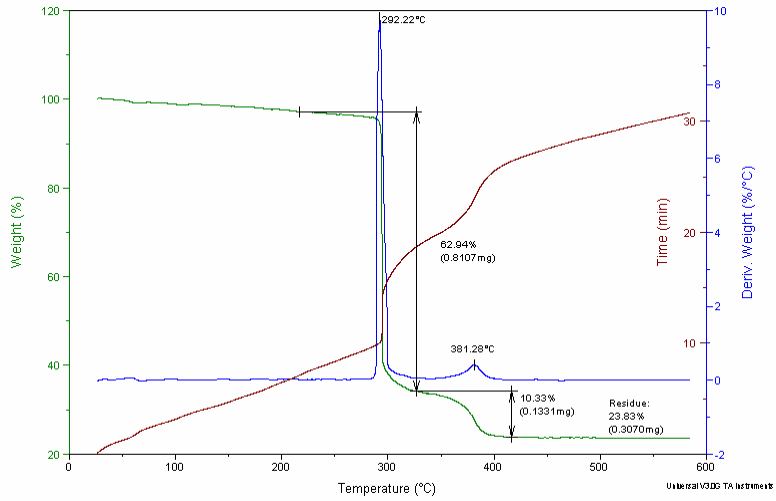

Appendix C-4. (continued)

X-ray powder diffraction patterns of fresh sample and calculated from the single crystal structure

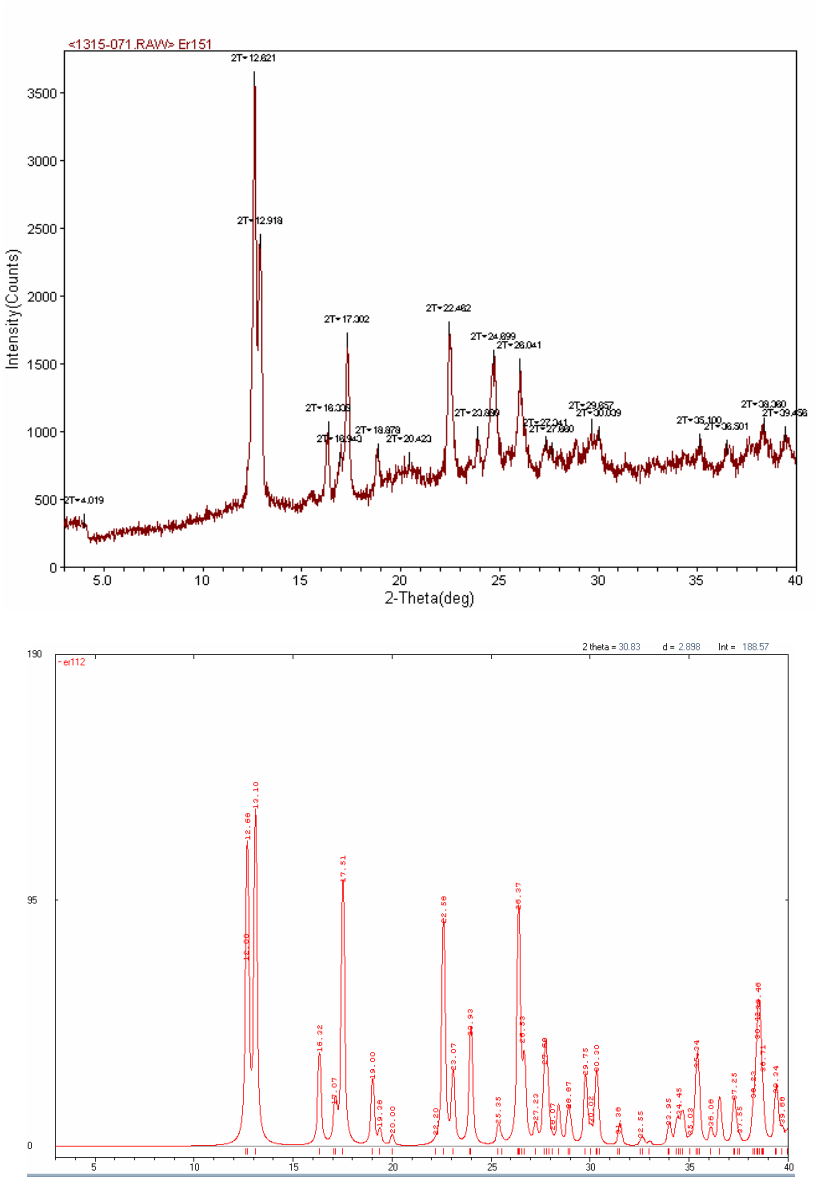

Appendix C-5. Experimental data for compound 17

FT-IR spectrum and X-ray powder diffraction patterns of fresh sample and calculated from the single crystal structure

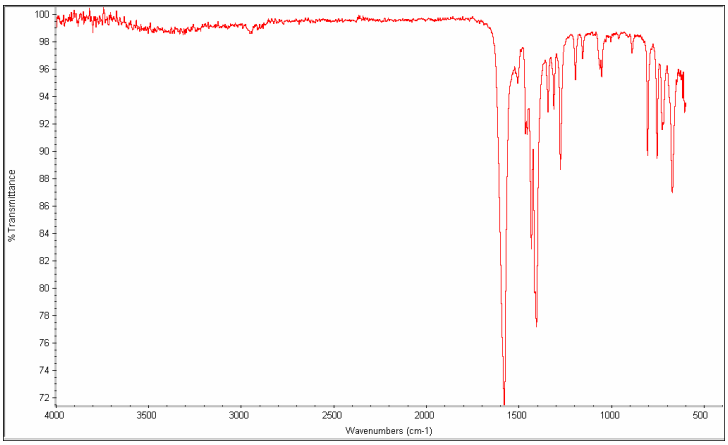

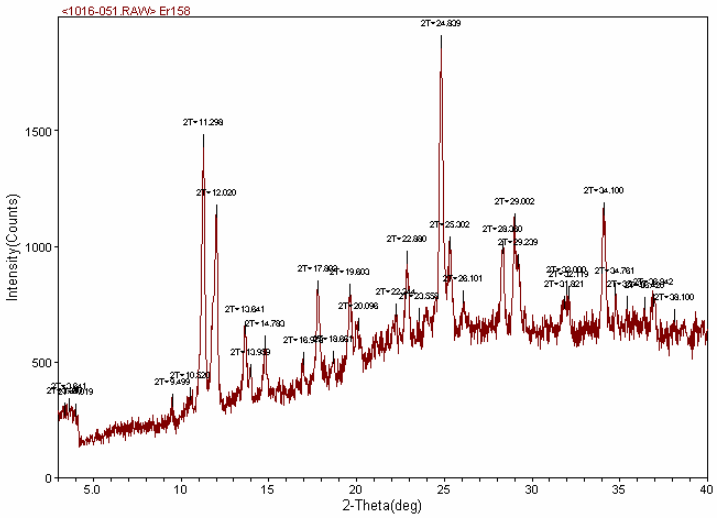

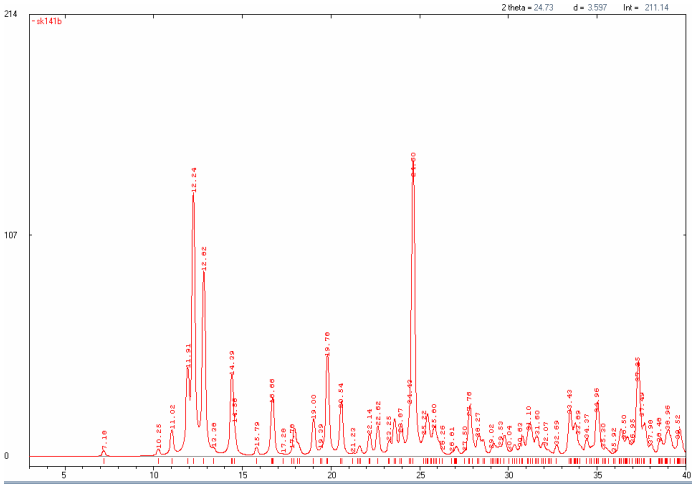

Appendix C-6. Experimental data for compound 18

FT-IR spectrum and X-ray powder diffraction patterns of fresh sample and calculated from the single crystal structure

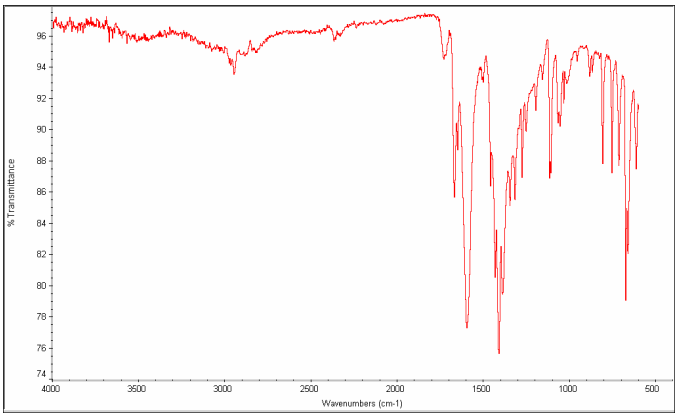

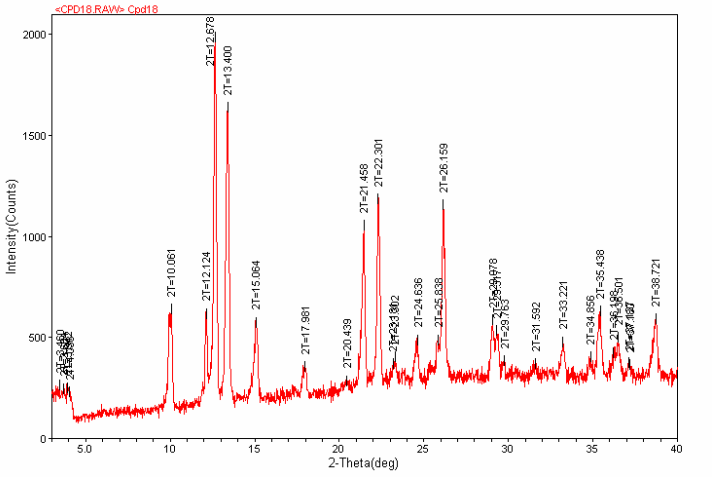

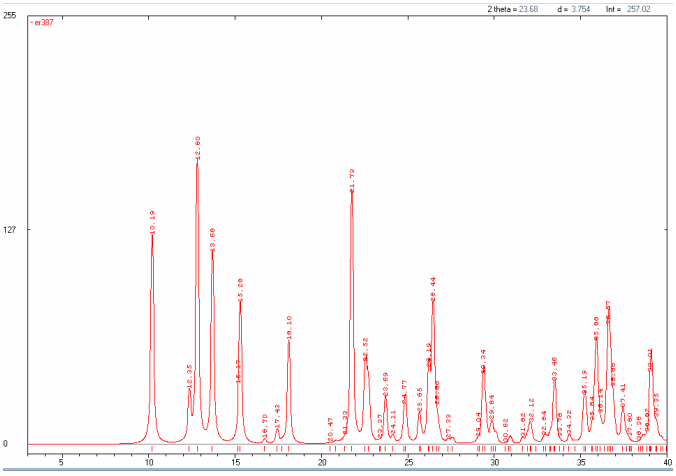

Appendix C-7. Experimental data for compound 19

FT-IR spectrum and X-ray powder diffraction patterns of fresh sample and calculated from the single crystal structure

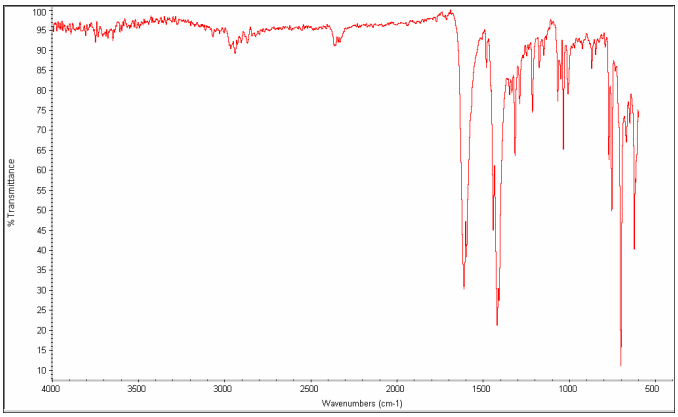

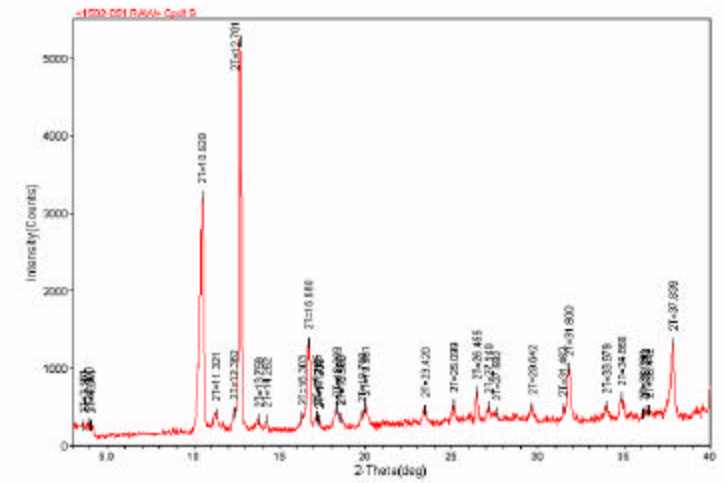

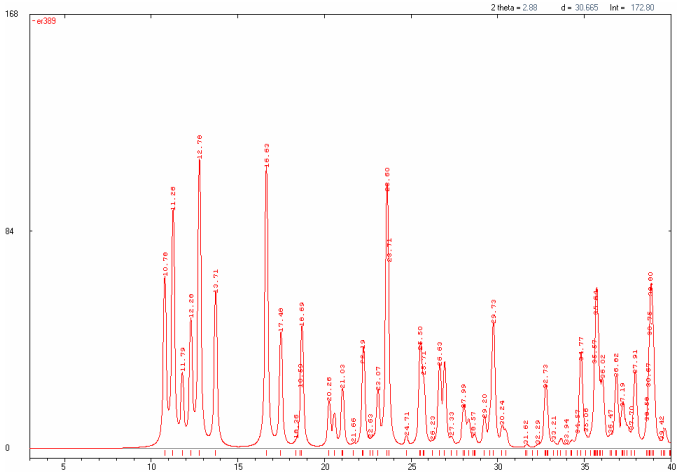

Appendix C-8. Experimental data for compound 20

FT-IR spectrum and X-ray powder diffraction patterns of fresh sample and calculated from the single crystal structure

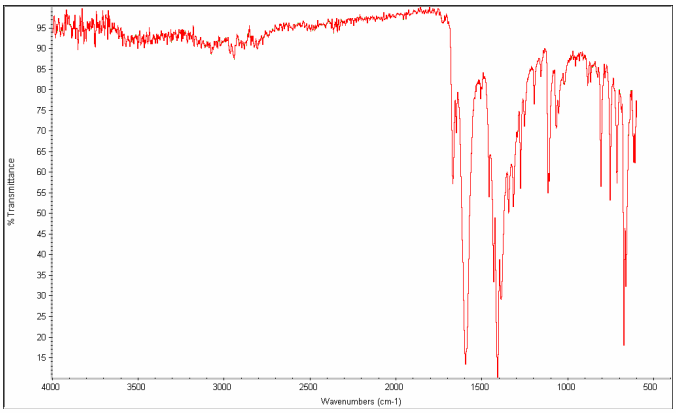

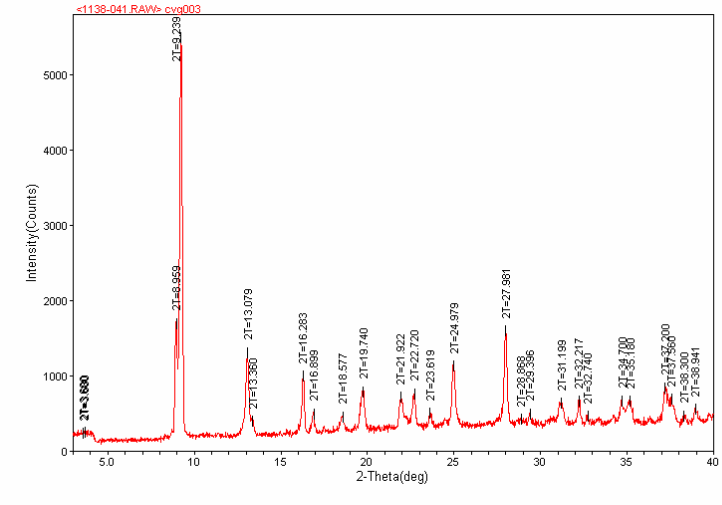

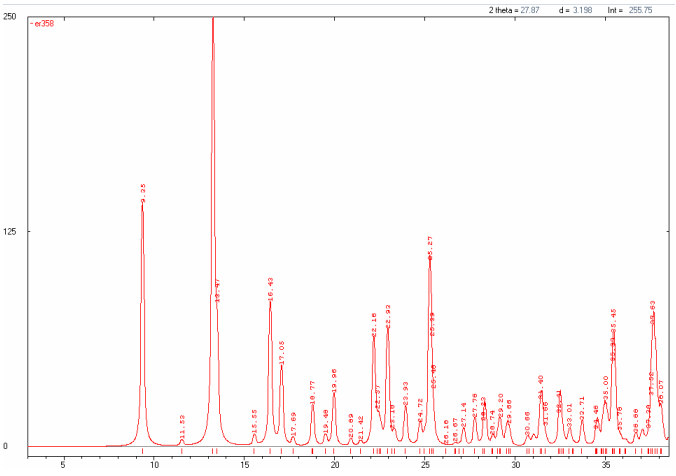

Appendix C-9. Experimental data for compound 21

FT-IR spectra of compounds **21a**, **21b** and **21b** let in MeOH (HPLC grade H2O = 0.009%) for 1 night

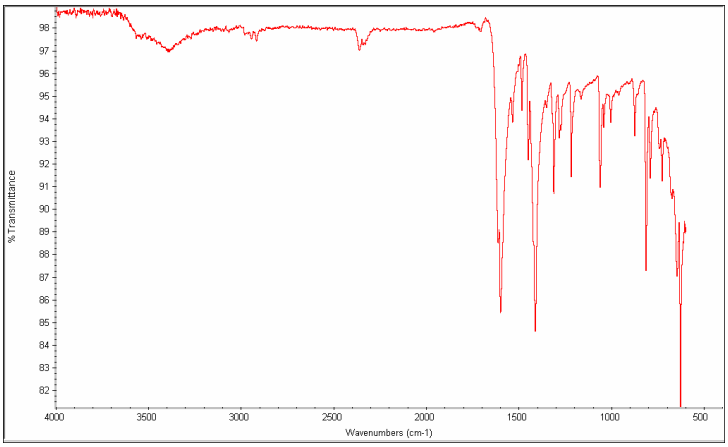

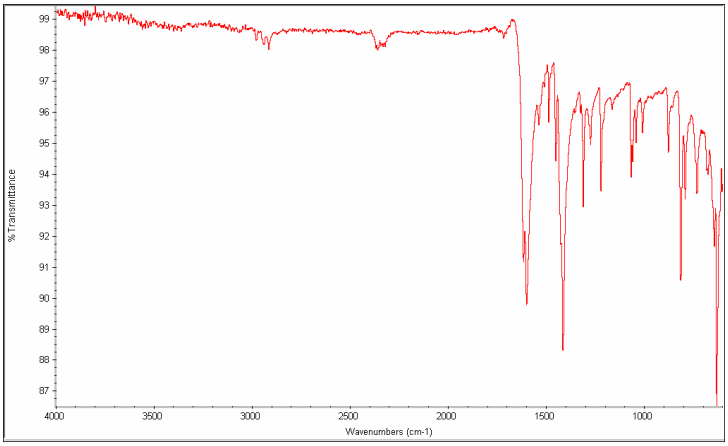

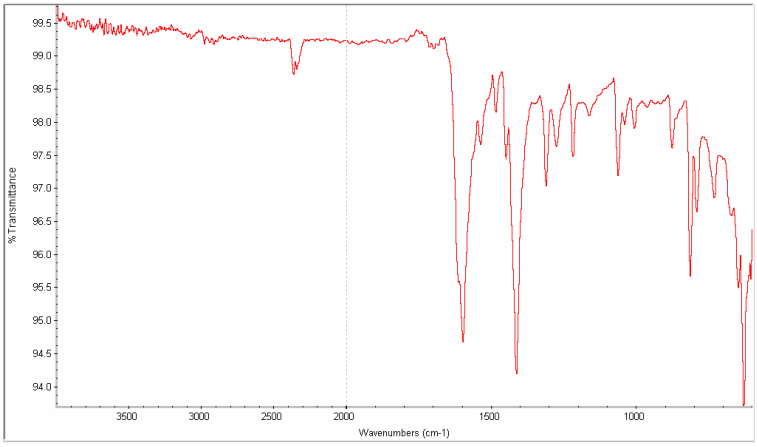

Appendix C-9. (continued)

TGA traces of **21a** and **21b** let in atmosphere for <1hour

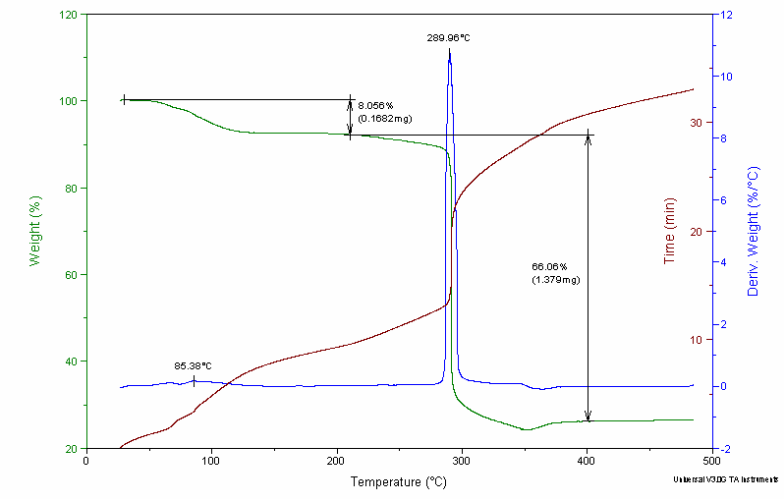

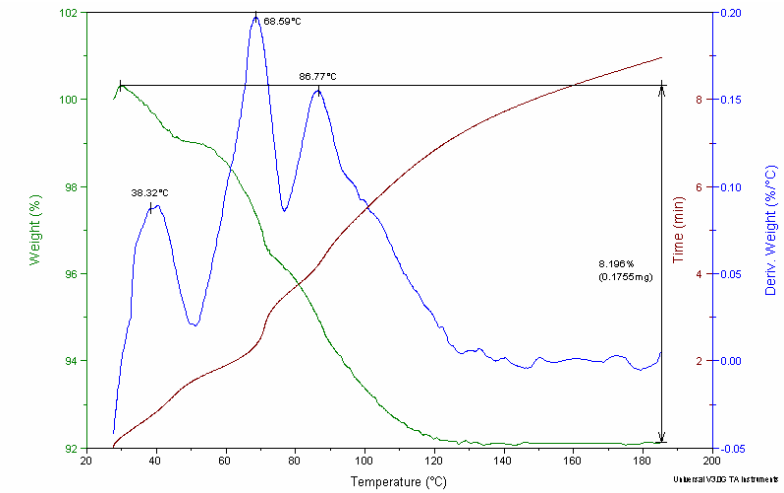

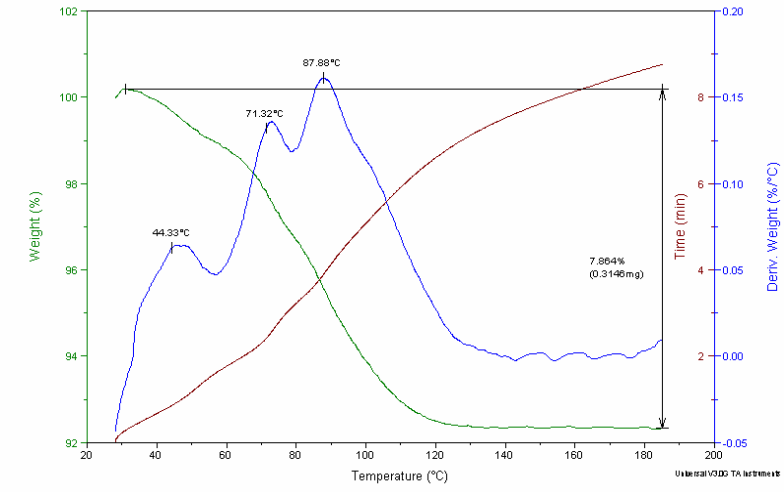

Appendix C-9. (continued)

X-ray powder diffraction patterns of fresh sample and calculated from the single crystal structure for compounds **21a** (left) and **21b** (right) and inclusion of apohost solid **21b** with various guests from GC experiments

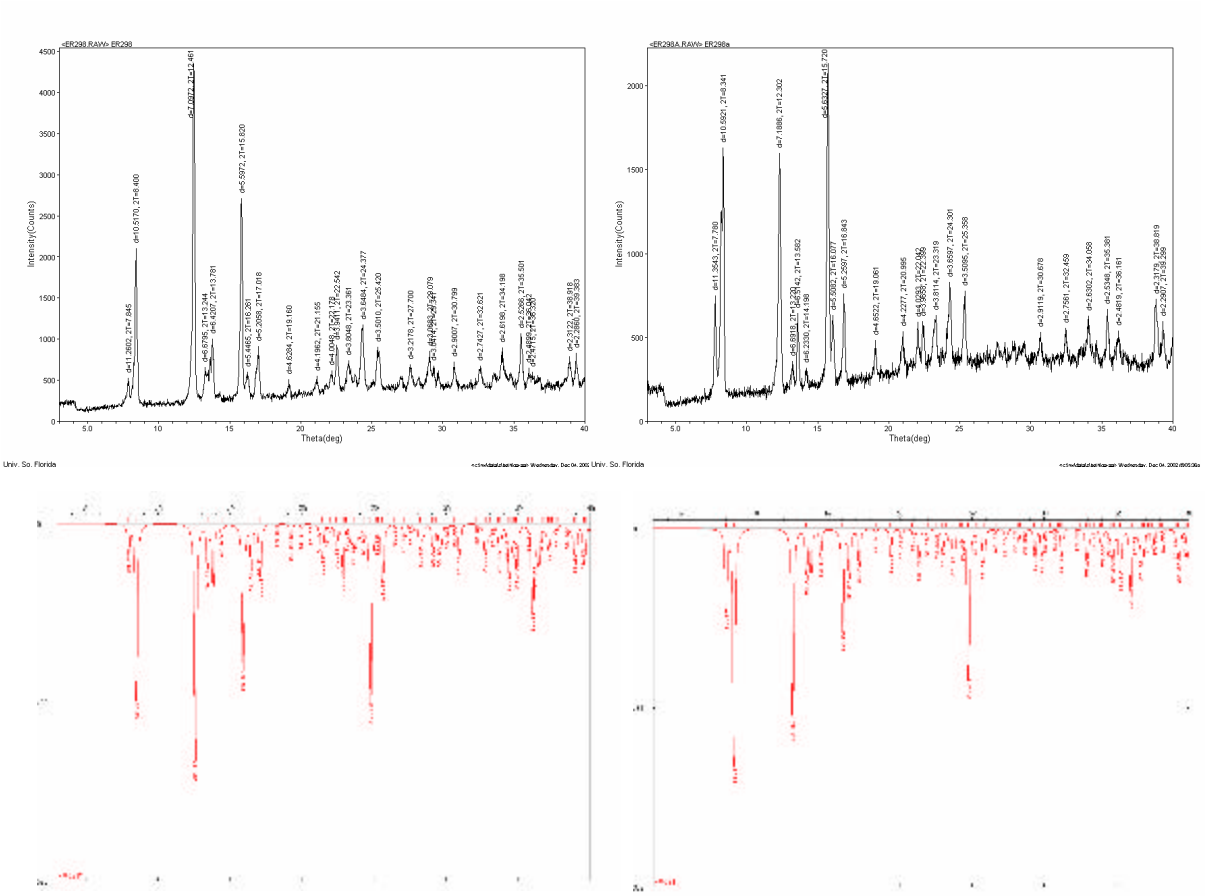

Guest G	Guest (mol) included per unit formula of **1b**
MeOH	$\mathbf{5.00.10^{-9}}$
EtOH	$\mathbf{3.94.10^{-7}}$
CH_3CN	$\mathbf{6.70.10^{-7}}$
n-hexane	$\mathbf{1.21.10^{-8}}$

Appendix C-9. (continued)

X-ray powder diffraction patterns of the blue powder formed during the synthesis of **21a** and simulation from the structure of $[Co(4,4'\text{-bipyridine})_{1.5}(NO_3)_2]_n$ (CSD code REJVUX)

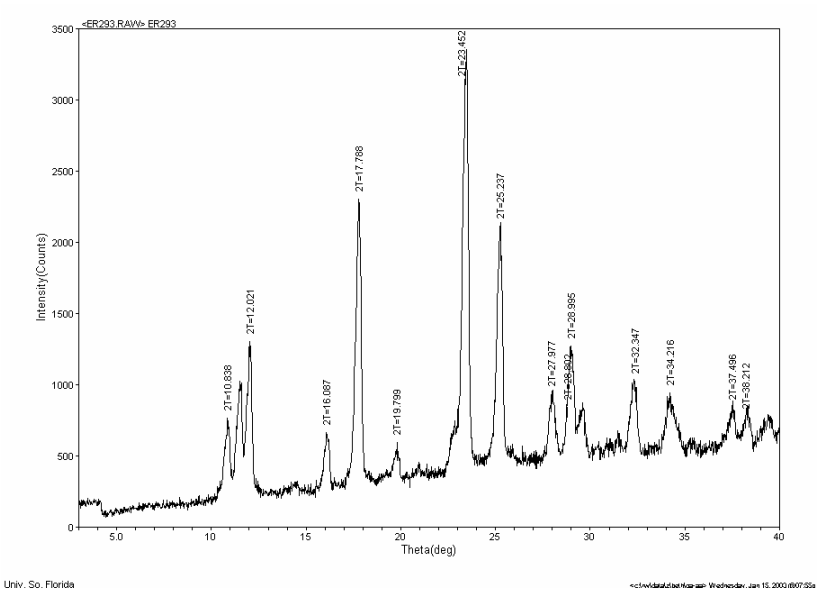

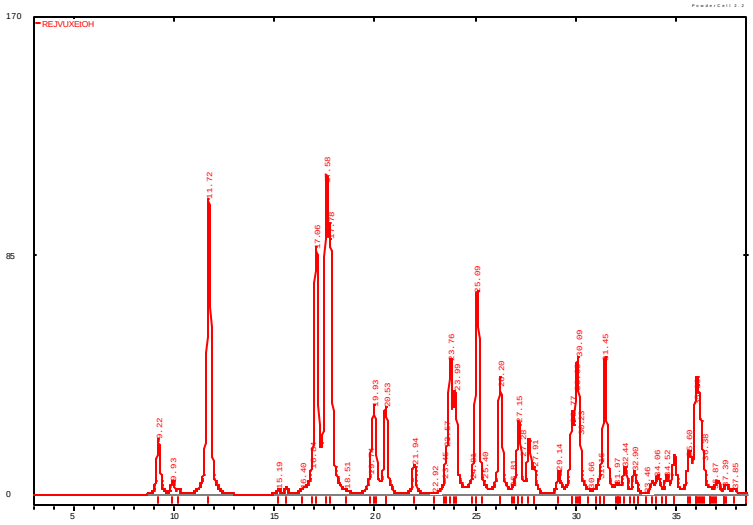

Appendix C-10. Experimental data for compound 22

FT-IR spectra of compounds **22a**, **22b** and **22c**

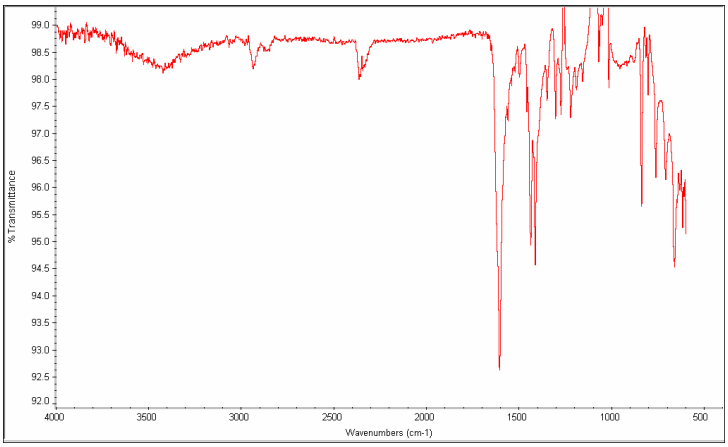

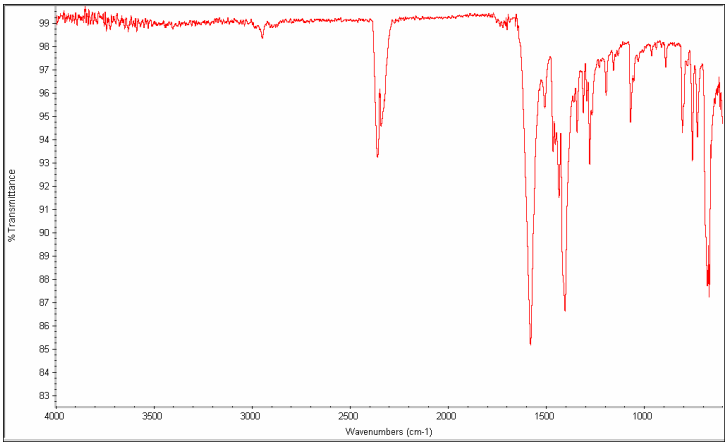

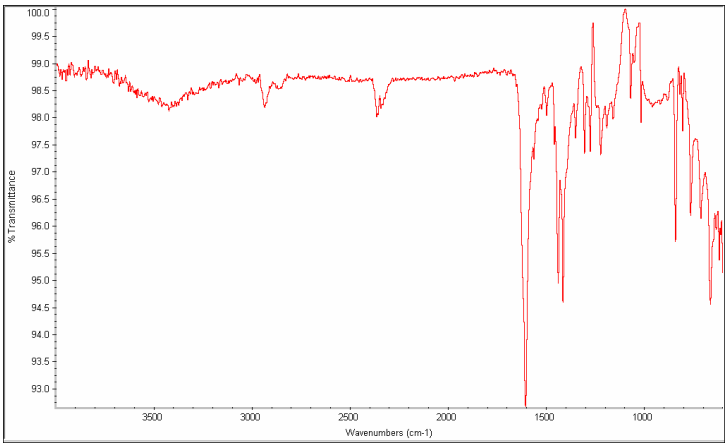

Appendix C-10. (continued)

TGA traces of **22a**, **22b** and **22c**

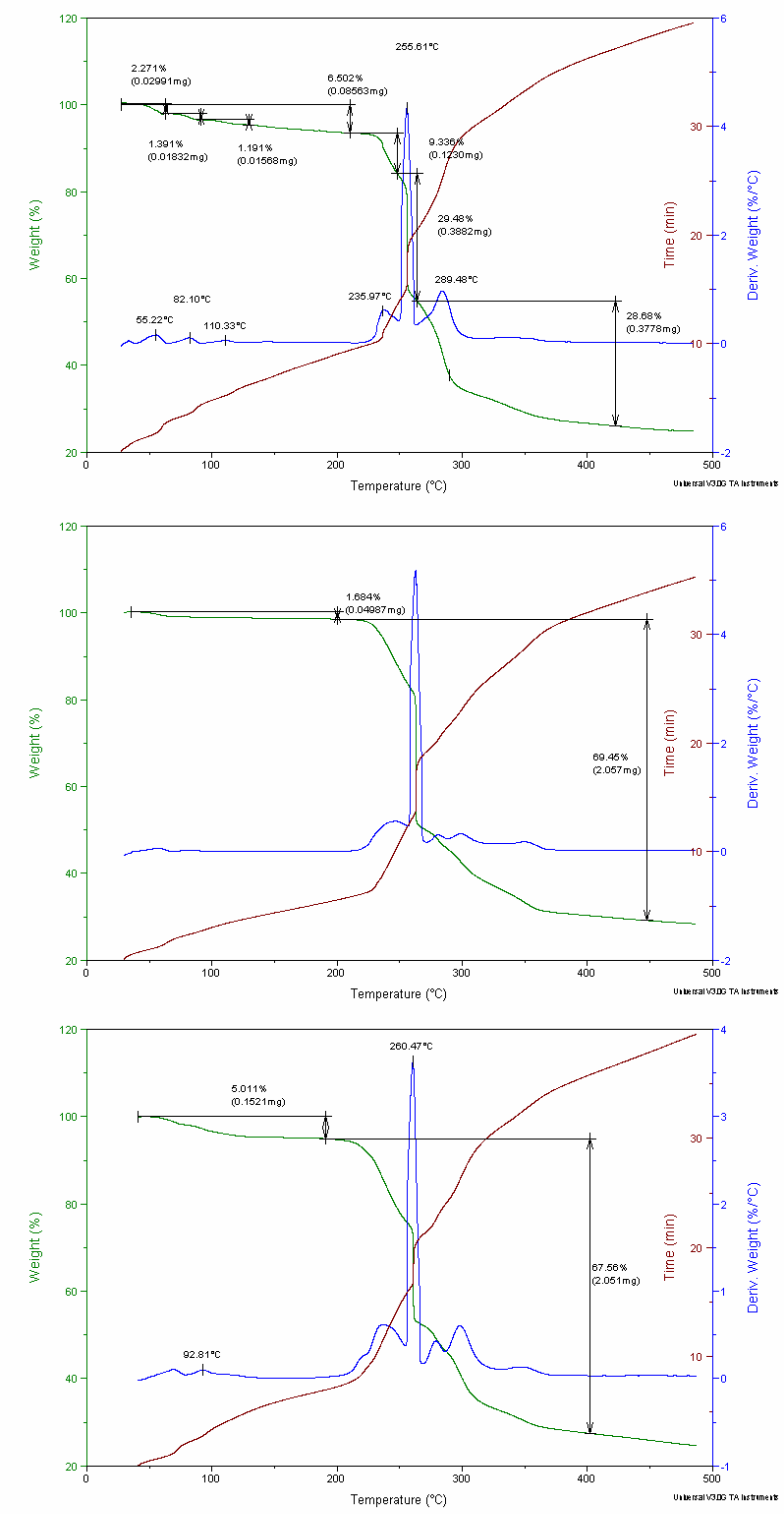

Appendix C-10. (continued)

X-ray powder diffraction patterns of fresh sample and calculated from the single crystal structure

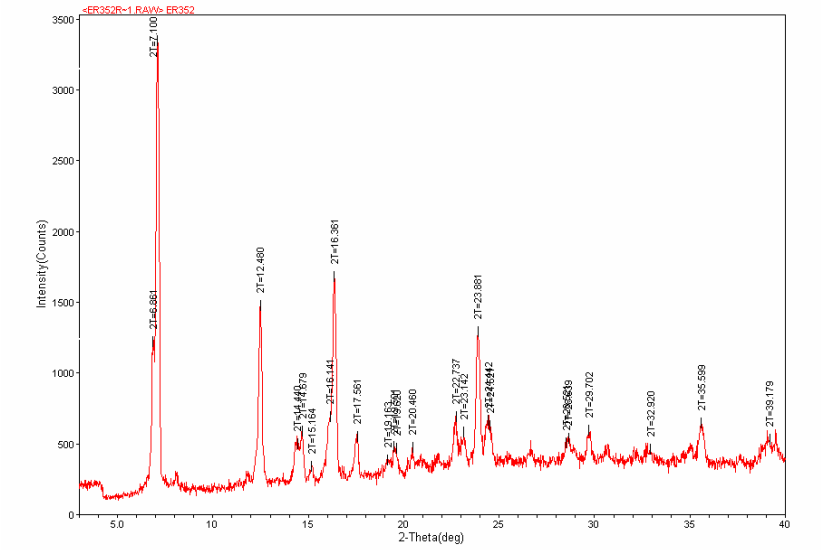

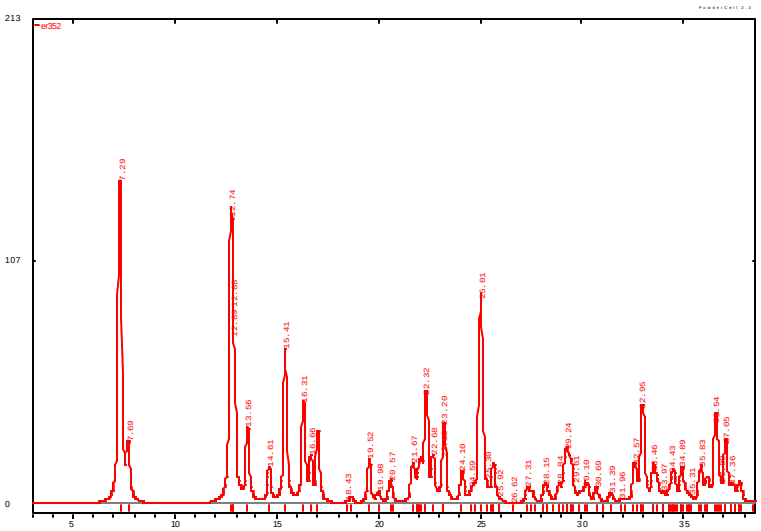

Appendix C-10. (continued)

X-ray powder diffraction patterns of blue crystals formed during the synthesis of **22** and simulation from the structure of bilayer $[Co(4,4'\text{-bipyridine})_{1.5}(NO_3)_2]_n$ (CSD code NAMSEZ)

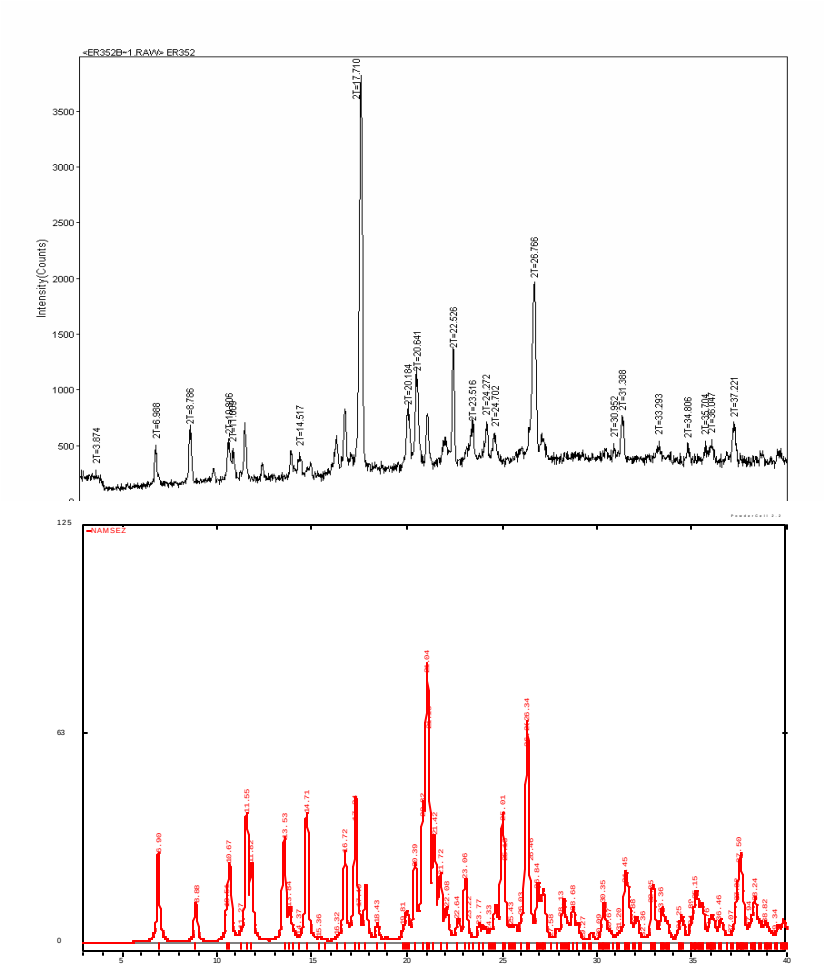

Appendix C-11. Experimental data for compound 23

FT-IR spectrum and X-ray powder diffraction patterns of fresh sample and calculated from the single crystal structure

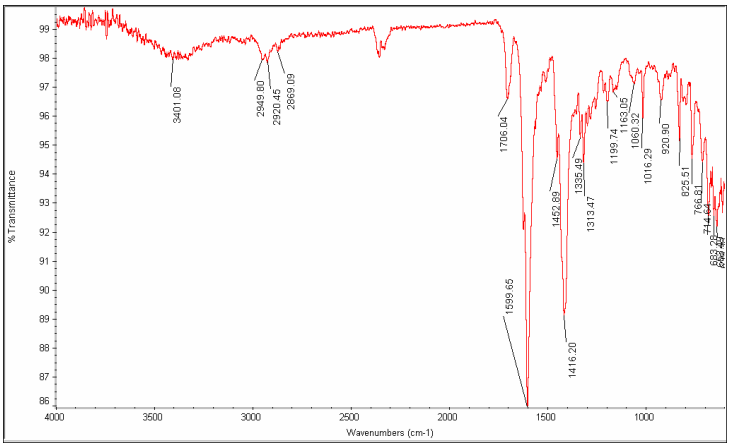

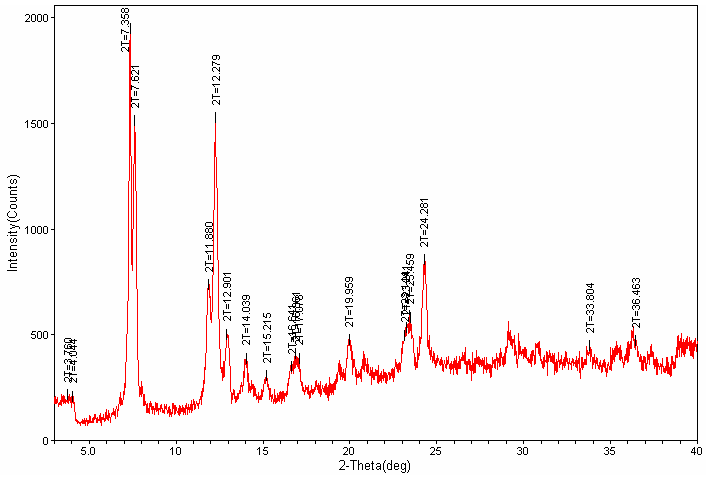

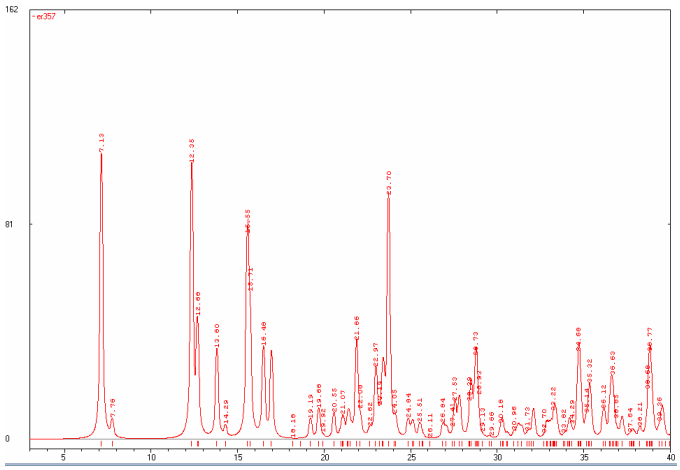

About the Author

Elisabeth Rather received a DEA degree in organic chemistry from Université Claude Bernard, Lyon I, in France in 1999, where she worked on the synthesis of a series of macrocycles *via* olefin metathesis.

In 2000, Elisabeth entered the Ph.D. program at the University of South Florida and joined Dr. Michael J. Zaworotko's research group. While in the Ph.D. program, she was honored with a Chemistry Outstanding Teaching Award in 2001 and the Shembekar Scholarship Award in 2002. She has also coauthored eight publications in chemical journals and made several paper presentations at regional and national scientific meetings of the American Chemical Society and the American Crystallographic Association.